Scuola di Architettura Urbanistica e Ingegneria Delle Costruzioni

Master of Science in Building and Architectural Engineering

Track - Building Engineering

POLITECNICO

MILANO 1863

FAÇADES AND URBAN ENVIRONMENT.
A framework for the assessment of the influence of façade design on the
indoor and outdoor comfort of the users.

Supervisor: Prof. Gabriele Masera
Co-supervisor: Prof. Andrea Giovanni Mainini

Thesis work by:
Francesca Carla Codazzi
920686

Academic year 2019/2020

ABSTRACT

Due to the developments in climate change and urbanization trends, the outdoor thermal comfort of citizens has become an important parameter for assessing the quality of the urban microclimate. While the research has focused considerably on the Urban Heat Island mitigation strategies, like the refurbishment of public spaces with vegetation and the use of cool materials, minor attention has been paid to how high reflective materials applied to building façades might affect the external comfort, , and in particular to the combined effect of materials and facade geometry.

In the context of n-ZEB buildings, the envelope has been studied and evolved to obtain the best energy performance of the indoor environment while ensuring thermal and daylight comfort for users, this thesis aims to develop a workflow aimed at assessing how a design focused on guaranteeing internal daylight comfort can influence the conditions of users in the surrounding.

The Reference Index for the evaluation of the influence of the façade on urban comfort is the Universal Thermal Climate Index (UTCI). The simulation process to compute it is based on the evaluation of the Mean Radiant Temperature (MRT), one of the most critical parameters influencing outdoor thermal comfort, that indicates how human beings experience radiation in their surrounding environment.

The resulting method will be applied to study the effect of different materials, geometries, and their combinations on the urban microclimate, keeping the parallel goal to reach the LEED standards for Indoor Daylight Comfort.

The thesis work will be divided into a first part that describes the development of the method and the theoretical context in which it is inserted and a second section in which the method will be applied to the case study of the south façade of the office building, ex Uffici Tecnici Comunali (UTC), in via Pirelli 39 in Milan.

KEYWORDS

Outdoor Thermal Comfort, Outdoor Thermal Simulation, Mean Radiant Temperature, Universal Thermal Climate Index, Annual Sunlight Exposure, Spatial Daylight Autonomy, Indoor Daylight Comfort, Daylight Simulations, Grasshopper, Parametric Modeling, Building Envelope.

ABSTRACT (Italian Lenguage)

A causa degli sviluppi del cambiamento climatico e delle tendenze di urbanizzazione, il comfort termico nell'ambiente esterno è diventato un parametro importante per valutare la qualità del microclima urbano. Mentre la ricerca si è concentrata principalmente sulle strategie di mitigazione dell'effetto dell'Isola di Calore, come il rifacimento di spazi pubblici con vegetazione e tramite l'uso di cool materials, minore attenzione è stata prestata a come i materiali altamente riflettenti applicati alle facciate degli edifici potrebbero influenzare il comfort esterno, e in particolare all'effetto combinato di materiali e geometria di facciata.

Nell'ambito degli edifici n-ZEB, l'involucro è stato studiato ed evoluto per ottenere la migliore prestazione energetica dell'ambiente interno garantendo il comfort termico e illuminotecnico per gli utenti, l'obiettivo di questa tesi è sviluppare un workflow finalizzato allo studio di come un design incentrato sulla garanzia del comfort visivo interno può influenzare le condizioni degli utenti nell'ambiente circostante.

L'Indice di riferimento per la valutazione dell'influenza è lo Universal Thermal Climate Index (UTCI). Il processo di simulazione per calcolarlo si basa sulla valutazione della Temperatura Radiante Media (TMR), uno dei parametri più critici che influenzano il comfort termico esterno, che indica come percepiscono gli utenti le radiazioni provenienti dall'ambiente circostante.

Il metodo risultante sarà applicato per studiare l'effetto di diversi materiali, geometrie e delle loro combinazioni sul microclima urbano, mantenendo come obiettivo il raggiungimento degli standard LEED per il comfort illuminotecnico interno.

Il lavoro di tesi sarà suddiviso in una prima parte che descrive lo sviluppo del metodo e il contesto teorico in cui è inserito e una seconda sezione in cui il metodo verrà applicato al caso studio della facciata sud dell'edificio per uffici, ex Uffici Tecnici Comunali (UTC), in via Pirelli 39 a Milano.

ACKNOWLEDGMENTS

TABLE OF CONTENTS

List of Figures

List of Tables

List of Graphs

1

INTRODUCTION

1.   INTRODUCTION

This thesis finds its origins in the union of the topics that most fascinated me during the two years of the Master of Science Degree with those encountered and deepened during my experience at the University of New South Wales of Sydney with the Erasmus KA107 project. In particular, starting from the more general topic of the study of facades using parametric tools with a particular focus on the study of daylight comfort, the research work has found an interesting outlet in the study of the impact of the façade on the outdoor thermal comfort.

In recent years, a considerable part of the European Union (EU) policy has focused on addressing and supporting effective strategies to deal with the long-term challenges of climate change and resource constraints. These challenges involve and will increasingly involve the built environment in the future[1]. Currently, the energy consumption of buildings accounts for almost one-third of the total primary energy demand of industrialized countries [2]. To meet the energy demand and the goal of reducing carbon emissions envisaged by the EU directives, intensive and strategic renovation and transformation actions need to be carried out, following the principles and goals of Roadmap to 2050 to support the transition of the built environment to low carbon.

For this reason during the last decade, the design of buildings has been focussed on the objective of reducing the energy consumption of buildings, reaching the requirements imposed by the European energy policies, with particular reference to nearly-Zero Energy Buildings (n-ZEBs). Innovative technological solutions, and retrofit strategies, aimed at improving the quality and performance of new and existing buildings, integrate a range of active and passive techniques to facilitate energy consumption reduction.

On the other hand, the topic of climate change and energy demand has also an important branch related to urban scale design, which may lead to phenomena such as Urban Heat Islands (UHI). The urban heat island is a well-established phenomenon characterized by anthropogenic heating of an urban area, compared to its surrounding rural areas [3]. As already said, it leads to higher energy demand and can also have a significant impact on human health.

Despite the wide research on how the urban environment affects the microclimate [4][5] and many validated strategies [6][7] to mitigate UHI are mainly focused on the use of reflective materials on horizontal surfaces, few studies are addressing reflective materials applied to walls[8][9]. Vertical facades receive direct sun for a longer period in summer, compared to roofs, and this indicates the potential of facades in contributing to the local heat islands [10].

The solar radiation incident daily in the urban environment is reflected or absorbed by the surfaces exposed to the sun. According to the characteristics of the surface, solar radiation is divided into radiative, sensible, latent, or accumulated heat flows. Radiative and sensible heat flows dominate the surface energy balance, in absence of humidity. The sensible heat, that corresponds to the perceptible increase in air temperature, is amplified when the difference between the surface and ambient temperatures is high. A reduction in the surface temperature of the building envelope, which is achieved by shading or increasing the reflectance of the surface, limits the convective heat transfer to the surrounding air and simultaneously reduces the cooling needs of the building.

Conversely, surfaces with lower solar reflectance absorb more energy, thereby heating the surface, through enhanced convective transfer, heats the adjacent volume of air, and at the same time increase the energy demand for cooling. Also, through long wave radiation transfer, the hottest surfaces emit infrared radiation towards colder objects within sight. In summary, the increase in surface reflectance, or albedo, potentially reduces the surface temperature of the surface, the cooling energy demand, the intensity of the convective transfer to the air, and the infrared radiation emitted to the exposed surfaces[11].

However, higher solar reflectance within cities can also increase solar radiation reflected on the area near the surface and to people, with a significant impact on human Outdoor Thermal Comfort.

The attention to the conditions of comfort and liveability of cities is one of the current hot topics in the construction field, and not only. It is well known that outdoor thermal comfort conditions and the consequent satisfaction will affect how residents use public spaces for daily interaction and entertainment. High albedo and reflective materials, largely used on façades for the exposed reasons, have been applied to numerous recent cases that demonstrate that a wrong design with these materials can lead to increasing temperature in the neighbourhood and glare that results in a general discomfort condition in the urban environment for people[12].

The scientific literature provides some studies about the assessment of the impacts of building envelope design on outdoor microclimate and thermal comfort, with a strong focus on canyons and finishing materials[13][14]. The available studies, however, do not consider the geometry of the façade as a variable input in the design process, mostly because applied to already built areas[15][16]. The available research works consider the form and the materials applied to the façade as two different stages of the envelop project, and therefore, neglect the effect of their combination in the decision making.

To design a building that captures the positive benefits of the mitigation strategy without itself negatively impacting the surrounding urban comfort, the envelope should be studied and designed applying a multiple-prospective approach, coupling tools, and strategies that may come from different sectors or design stages.

This thesis aims to develop a robust and reliable workflow to analyse how a façade design focussed on indoor comfort affects the microclimate of the surrounding area, considering multiple geometry and material combinations. The developed framework will provide the required engineering approach to the theme of the impact of the building vertical envelope on outdoor comfort and can be incorporated as a design-decision support tool for the first stages of the design to evaluate the effect of the form-finding ideas directly combined with different materials.

The indoor parameter that guides the geometry design procedure evolved in this research is Daylight Comfort. The choice of internal visual comfort is guided by the importance of this factor for the well-being of the occupants and many other aspects which are inherently considered in the study of daylight, including its influence on energy consumption. A smart daylighting-based design ensures a good energy performance too since light is strictly related to solar radiation: a façade geometry that limits as much as possible the annual glare, ensure also a small amount of direct solar radiation within the same space.

The simulation tool is developed as a Grasshopper script, the visual scripting environment integrated into the software Rhino 6 (by Robert McNeel & Associates, 2018), which allows incorporating three aspects of the workflow:

- the parametric nature of the software, both for the geometry definition and for the simulation settings;

- the chance to perform both indoor daylight and outdoor thermal simulations in the same environment;

- the ease of use even for designers with limited knowledge in the microclimate simulation topic.

The framework is applied to the ex Uffici Tecnici Comunali (UTC) building, in via Pirelli 39 in Milan. The south facade of the building and the adjacent green area are considered and a limited number of cases, combining the modules geometries defined to guarantee the indoor daylight comfort and different materials, are tested for different seasons, time of the day, and subjects.

The thesis is divided into two main sections. The first one regards the definition of the environmental parameters, the physical models behind them and of their application in

the software to perform the simulations, and the methodology to follow for the analysis. The second section includes the application of the previously defined workflow, with a pre-analysis to define the simulation matrix and the Case Study analysis.

2

ENVIRONMENTAL PARAMETERS

THEORETICAL PRINCIPLES AND SIMULATION APPLICATION

2. ENVIRONMENTAL PARAMETERS

The comfort, indoor and outdoor, of users is the focus and objective of this work, but to be able to evaluate it, it is necessary to define some environmental parameters that synthesize the numerous factors, both linked to the ambient conditions and to those of the individual, that interact and influence the well-being of the subjects.

For this reason, this first chapter represents a presentation of the comfort indicators that will guide the whole analysis during the thesis.

In particular, the first part focuses on the used software and indexes simulation methods. It explains how the physical principles, explained previously, are applied and/or translated into a programming language.

The second part is a theoretical excursus on the Indoor Daylight Comfort and Outdoor Thermal Comfort, on their impact on the users' well-being, on the indexes that quantify them, and on the physical and mathematical models on which are based.

Lastly, in the third section, the application of the theoretical concepts to perform the simulations, basis of the reseach work, is exposed.

The methodology for carrying out the simulations of this research work, with the list of properties and boundary conditions for the simulations, will then be further explored in the next chapter.

2.1. Outdoor thermal comfort

According to the ANSI/ASHRAE Standard, Thermal Comfort is defined as the condition of mind that expresses satisfaction with the thermal environment and is assessed by subjective evaluation.

The comfort models are based on the heat exchange between the human body and the surrounding environment. It can be described by the heat balance equation, which involves independent environmental variables, related physiological factors, and properties of the boundary between the human body and the environment.

The heat balance equation describing the thermal exchange between the body and its environment takes the classic form:

$$M + W^* + R^* + C^* + E^* + J^* = 0 \qquad (1)$$

Where M is the rate of metabolic energy production, W* the rate of work, J* is the rate of storage of body heat, E* the rate of evaporative heat transfer, R* the rate of radiant heat exchange, and C* the rate of convective heat transfer[17].

In urban areas, heat transfer by radiation is the most important factor in the energy exchange process between the human body and its environment.

An artificial measure to express the degree of exposure to environmental radiation is the Mean Radiant Temperature. It is an important index of human thermal comfort, and is an important input to other models of thermal comfort, and, in particular, the current most comprehensive and mostly used human thermal indices: the physiologically equivalent temperature (PET), Predicted Mean Vote (PMV), Universal Thermal Climate Index (UTCI) and Standard Effective Temperature (SET*)[18].

2.1.1.   Mean Radiant Temperature

The Mean Radiant Temperature is a key variable in evaluating thermal sensation outdoors regardless of the comfort index used, thus, there is a need to measure or estimate MRT accurately.

It is defined by the ASHRAE society as "the uniform surface temperature of an imaginary black enclosure in which an occupant would exchange the same amount of radiant heat as in the actual non-uniform space". It represents a suitable measure for the stress of the human organism due to the heat effect of the radiation from the whole surrounding sphere as it is influenced by the solar shortwave radiation (direct, diffuse, and reflected components), and by the terrestrial longwave radiation (atmospheric and

environmental). It is a key variable in evaluating thermal sensation outdoors regardless of the comfort index used, thus, there is a need to measure or estimate MRT accurately.

Measuring MRT directly has been the subject of numerous studies, but two main approaches were obtained: the six-direction method and the globe temperature method [14]. In the first method, short and long wave radiative fluxes, in the six directions, are measured and these are used in an equation to solve for MRT. In the globe temperature approach, the required inputs are the measurements made with a globe thermometer, a dry bulb thermometer, and an anemometer[19].

The comparison between these two methods shows that the globe thermometer method may overestimate the MRT since wind velocity is a key variable in the estimation based on this method. For better estimation, MRT measured by the globe-thermometer method should be corrected by the imported wind speed (stable, low, and assuming wind speed) and validated by the six-direction radiation method.

The determination of MRT by the integral radiation measurements can be done if the mean radiant flux density (S_{str}) of the human body is known. To calculate S_{str}, the six individual measurements of the short wave radiation and long wave radiation fluxes have to be multiplied by the angular factors $F_{i(i=1-6)}$ between a person and the surrounding surfaces according to Equation (2)[19]:

$$S_{str} = \alpha_k \sum_{i=1}^{6} K_i F_i + \varepsilon_p \sum_{i=1}^{6} L_i F_i \qquad (2)$$

K_i = the short-wave radiation fluxes (i=1–6).

L_i = the long-wave radiation fluxes (i=1–6).

F_i = the angular factors between a person and the surrounding surfaces (i=1–6). F_i depends on the position and orientation of the person. The calculation of F_i is complicated for complex urban forms and simplifications are thus necessary.

α_k = the absorption coefficient for short-wave radiation (standard value 0.7).

ε_p = the emissivity of the human body. According to Kirchhoff's laws ε_p is equal to the absorption coefficient for long-wave radiation (standard value 0.97).

If S_{str} is known, the MRT (°C) can be calculated from the Stefan–Boltzmann law:

$$MRT = \sqrt[4]{S_{str}/(\varepsilon_p \sigma)} - 273.15 \qquad (3)$$

Where:

σ = the Stefan–Boltzmann constant ($5.67 \cdot 10^{-8}$ Wm^{-2} K^{-4}).

As regards the determination of MRT by globe temperature measurements, the starting point is the ASHRAE definition that states that the temperature assumed by the globe

thermometer at equilibrium results from a balance between the heat gained and lost by radiation and through convection. The globe temperature represents the weighted average of radiant and ambient temperatures. If the globe temperature, air temperature, and air velocity are known then the MRT can be calculated according to Equation (4):

$$MRT = \left[(T_g + 273.15)^4 + \frac{1.1\times10^8 V_a^{0.6}}{\varepsilon D^{0.4}} \times (T_g - T_a)\right]^{1/4} - 273.15 \quad (4)$$

Where:

V_a = the air velocity (ms^{-1}).

T_g = the globe temperature (°C).

T_a = the air temperature (°C).

D = the globe diameter (mm).

ε = the globe emissivity.

Without sophisticated and time-consuming on-site measurement procedures, the MRT can be obtained by modelling the whole radiation field with simulation models approaches.

The challenge in the MRT computation is that it requires considering different contributions in the heat transfer that require knowledge of its principles. In particular, it depends on the contribution of the long wave radiation, caused by a difference in temperature between the subject and the surrounding surfaces, and on the short wave one, that is the one produced by direct, diffuse, or reflected solar radiation reaching the subject.

The method for the MRT evaluation without the use of on-site measurements following described is based on the models exposed in two different papers, in particular, "*A Framework for Outdoor Mean Radiant Temperature Simulation: Towards Spatially Resolved Thermal Comfort Mapping in Urban Spaces*" by Tarek Rakha, Pouya Zhand and Christoph Reinhart, for the long wave contribution [20], and "*Modelling The Comfort Effects Of Short-Wave Solar Radiation Indoors*" by Arens et al., for the short wave one [21].

Long Wave Mean Radiant Temperature Model

According to the traditional method of simulation the lw MR evaluation depends on three main factors [20]:

1. surrounding surface temperatures,
2. view factors,
3. climatic conditions.

The first step of the computation requires the evaluation of the surface temperature (T_{sup}) of the urban environment under analysis.

The method applied is the Thermal Admittance Method, based on the Heat Diffusion Equation.

The conduction through the surfaces can be simplified as one-dimensional heat transfer with the Heat Diffusion Equation. The simplified heat transfer process is here shown, the three equations that define heat transfer inside the wall, the external boundary condition, and the internal boundary condition are reported.

$$\begin{cases} \dfrac{\partial t}{\partial \tau} = \alpha \dfrac{\partial^2 t}{\partial x^2} \\ -\lambda \dfrac{\partial t|_{x=0}}{\partial x} = h_{out}(t_{out} - t|_{x=0}) + aQ \\ -\lambda \dfrac{\partial t|_{x=\delta}}{\partial x} = h_{in}(t|_{x=\delta} - t_{in}) \end{cases}$$

5)
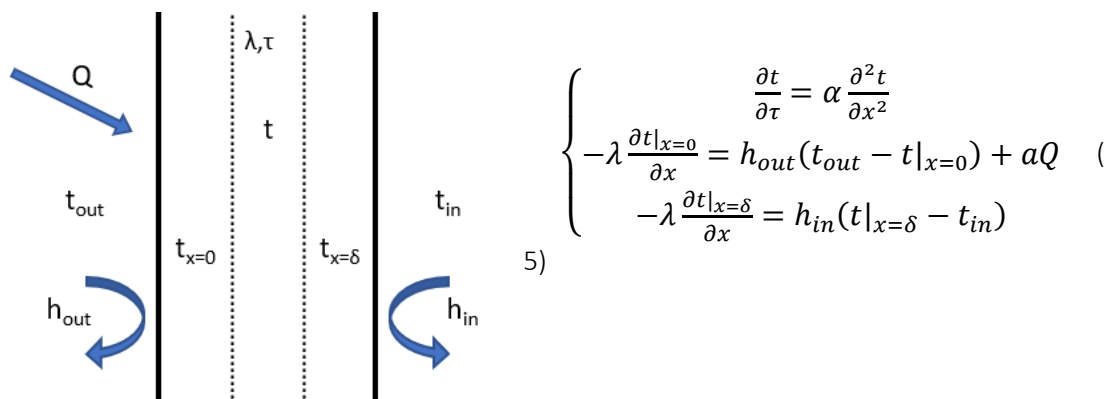
Figure 1 Heat Diffusion Equation and equilibrium equations at the boundaries.
Where: Q = Solar Radiation (W/m2) h = convection coefficient (W/m2K) t_{out} = External Temperature (°C) t_{in} = Internal Temperature (°C) τ = Time (s) λ = Conductivity (W/mK) α = Diffusivity (m²/s) L = Depth (m) a = solar absorbance.

The three equations are derived from the energy balances within the wall and with the indoor and outdoor conditions.

To be able to calculate the external surface temperatures, it is necessary to know the materials that compose the building envelope and all the urban surfaces and their characteristics, in particular:

- the thickness,
- the conductivity,
- the density,
- the specific heat capacity,
- the solar absorbance.

These data, together with the climatic factors of a predetermined period of analysis, allows to calculate the surfaces' temperature.

For the ground surface temperature calculation, the same principles are applied, but different boundary conditions must be imposed. The ground temperature at 0.5 m is provided by the EPW file of the location object of the study, therefore on the surface exposed to the outdoor environment the equilibrium equation does not change but the other boundary has an imposed temperature, and the equations become:

$$\begin{cases} \frac{\partial t}{\partial \tau} = \alpha \frac{\partial^2 t}{\partial x^2} \\ -\lambda \frac{\partial t|_{x=0}}{\partial x} = h_{out}(t_{out} - t|_{x=0}) + aQ \\ \frac{\partial t|_{x=0.5}}{\partial x} = T_g \end{cases} \tag{6}$$

The last contribution to consider is the Temperature of the sky and the consequent long wave loss. The long wave temperature of the sky (T_{sky}) is defined following the Man-Environment Heat Exchange Model [22] and it is estimated using the horizontal infrared radiation provided by the EPW file.

In particular, the model describes the net long wave radiation as a balance of heat exchange by thermal radiation between the human body and the atmosphere as well as between the human body and the ground. From this definition the temperature of the sky is derived:

$$Ls = \varepsilon_p \sigma (T_{sky} + 273.15)^4 \tag{7}$$

$$T_{sky} = \sqrt[4]{\frac{L_s}{\varepsilon_p \sigma}} - 273.15 \tag{8}$$

Where:

T_{sky} = the temperature of the sky (°C).
σ = the Stefan-Boltzmann constant (5.667×10^{-8}).
ε_p = the human emissivity (assumed to be 0.95).
L_a = the downwelling long wave radiation from the sky in W/m^2 (assumed equal to the horizontal infrared radiation).

In the second stage, the long wave part of the Mean Radiant Temperature can be computed. For performing this calculation is necessary, in addition to the surface temperatures, to know the View Factor (VF) referred to the Test Point for which the radiant temperature is calculated.
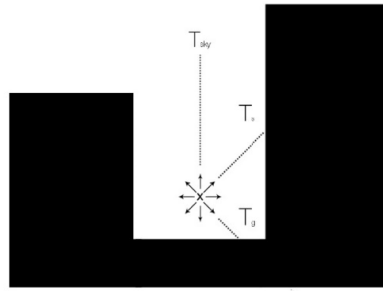
Figure 2 Test point and long wave contributions in an urban model.[20]

With such information it is possible to calculate the long wave contribution in the Mean Radiant Temperature for each Test Point:

$$MTR_{lw} = \sqrt[4]{T_1^4 F_{p-1} + \cdots + T_n^4 F_{p-n}} \qquad (9)$$

Where:

T_n = the surface temperature for the surface n (K).

F_{p-n} = the view factor between the test point p and the surface n.

Short Wave Mean Radiant Temperature Model

For the indoor environment computation, a method is reported in the ANSI/ASHRAE Standard 55-2017 "*Thermal Environmental Conditions for Human Occupancy*", more specifically in the appendix C a "*Procedure For Calculating Comfort Impact Of Solar Gain On Occupants*" [23].

This appendix describes a full calculation of MRT based on the work of Arens et al. [21] that consists of computing and then summing up the long and short wave contributions.

The model, for the short wave part calculation, is based on the Effective Radiant Field (ERF), a measure of the net radiant energy flux to or from the human body. ERF is used to describe the additional (positive or negative) long wave radiation energy at the body surface when surrounding surface temperatures are different from the air temperature. It is in W/m², where the area refers to body surface area, and the surrounding surface temperature is expressed as MRT.

The ERF on the human body from long wave exchange with surfaces is related to MRT by:

$$ERF = f_{eff} h_r (MRT - T_a) \qquad (10)$$

Where:

f_{eff} = fraction of the body surface exposed to radiation from the environment.

h_r = radiation heat transfer coefficient (W/m^{2}K).

T_a = the air temperature (°C).

The energy flux absorbed by the body is ERF times the long wave emissivity/absorptivity α_{LW}. The solar radiation absorbed on the body's surface can be equated to an additional amount of long wave flux, ERF$_{solar}$, and it is possible to state:

$$\propto_{LW} ERF_{solar} = \propto_{SW} E_{solar} \tag{11}$$

Where:

E_{solar} = short wave solar radiant flux on the body surface (W/m^2).

α_{SW} = short-wave absorptivity.

The short wave radiant flux is the sum of three radiant fluxes (direct, diffused, and reflected) that can be found, starting from the normal solar radiation (W/m^2), through the definitions of Arens et al. as functions of surrounding surfaces, fenestration system, occupant position and posture, solar position, body exposure, and clothing insulation. For the outdoor environment, the calculation is simplified as the incident radiation is not filtered by the windows, moreover, if the radiation incident on the Test Point is derived with a software, that already takes into account the surrounding context, in the E$_{solar}$ calculation only the parameters related to the user. Again this can be simplified if the software uses a mannequin to compute the incident radiation, in this case, the result of the simulation would correspond with the short wave solar radiant flux on the body surface.

In the model developed for the indoor, the only reflected component considered is the one coming from the floor. It is calculated starting from the total outdoor solar radiation on the horizontal, it is filtered by both T$_{sol}$ (total solar transmittance of the windows) and f$_{svv}$ (fraction of sky vault in occupant's view) and multiplied by the reflectance (albedo) of the floor and lower furnishings (R$_{floor}$). Besides, the short wave reflected to the lower half of the body will be accompanied by increased long wave radiation from floor surfaces warmed by the non-reflected portion of the solar radiation, this long-wave flux was approximated by increasing the value of R$_{floor}$.

$$E_{refl} = 0.5 f_{eff} f_{svv} T_{sol} I_{TH} R_{floor} \tag{12}$$

Considering the urban environment, this approximation can not be applied, and the radiation reflected by the surrounding surfaces must be included. However, considering to derive this information by the software it is important to consider the reflected portion of radiation coming from the ground. As it may not be considered in the simulation tool here is reported the adaptation of Equation (12) to the outdoor.

In this case, the filters imposed by the windows are not present, and the component 0.5 x f_{eff} is substituted with the actual calculation of the View Factor of the ground from the point of view of the user (Test Point). As regards the reflectance of the ground the common albedo values are between 0.2-0.3, in this case, it is not increased to consider the long wave influence, which has already been considered in the previous calculations. The equation became, therefore:

$$E_{ground} = FV E_{solContext} R_{ground} \tag{13}$$

Where $E_{solContext}$ is the cumulative radiation reaching the Test Point, that includes the direct and diffuse portions and the radiation reflected by the surroundings.

When the reflectivity of the ground is not considered in the simulations, this value is summed with the aforementioned cumulative radiation and the obtained total E_{solar} is used to find ERF_{solar}.

With the previously reported formulas (10) and (11) the Effective Radiant Field and the Delta Mean Radiant Temperature (ΔMRT) can be determined, representing the potential increment of MRT caused by solar radiation.

$$ERF_{solar} = \frac{\propto_{SW}}{\propto_{LW}} E_{solar} \tag{14}$$

$$\Delta MTR = \frac{ERF_{solar}}{f_{eff} h_r} \tag{15}$$

Mean Radiant Temperature Combination

Finally, the results from the two branches are summed to obtain the total value of Mean Radian Temperature that will be used to evaluate the comfort indices in an accurate way.

2.1.2.   Definition of Parameters

The Thermal indices are based on the human being's energy balance, showing the interrelation between metabolic activities, clothing, and environmental parameters on the user's thermal perception. A complete review of the available indices to assess outdoor human comfort and thermal stress, together with an explanation of the physical equations that drive these models, is provided by S. Coccolo et al. in *"Outdoor human comfort and thermal stress: A comprehensive review on models and standards"*, this document has been a very useful reference to understand the models on which the indices are based [18].

The first subdivision that must be done between the existing models to quantify human comfort is between those applicable to indoor and outdoor environments.

While indoor comfort has been already largely studied, and its quantification is well-established thanks to the relative stability of the closed environment, it is still a challenge to quantitatively describe the outdoor environment in terms of human comfort. Mostly because it is largely influenced by the rapid variability of the conditions (especially in terms of solar exposure and wind speed) and by the time of exposure, which can vary from minutes to several hours.

However, some outdoor models are available, well described in literature, and have been validated. These are divided into three categories Thermal indices, Empirical indices, and Indices based on linear equations. For the purpose of this work, only the thermal indices have been considered, as anticipated at the beginning of the paragraph.

In this short review, the most used thermal indices for outdoor thermal comfort are presented, and the physical principles on which are based are explained.

Physiologically Equivalent Temperature (PET)

The Physiologically Equivalent Temperature (PET) is defined as the "air temperature at which the heat balance of the human body is maintained with core and skin temperature equal to those under the conditions being assessed". PET is based on the Munich Energy-Balance Model for Individuals (MEMI) that defines the balance equation of the human body.

Further development of PET is mPET (modified PET) that improves the capacity of the model to react to the change of relative humidity (by a simple multi-segment body model) and clothing insulation (by a multi-layer clothing model). PET has been used in several climates around the world, and the results obtained through simulation have positive significance compared with on-site monitoring. Furthermore, it is essential to know that the PET thermal scale can vary according to the climate: if the scale is not yet defined, the simulations need to be validated with onsite monitoring and questionnaires.

Predicted Mean Vote (PMV)

The Predicted Mean Vote (PMV), based on Fanger's heat balance model, is defined as the average thermal sensation vote of a group of people (from −3 = cold to +3 = hot) and is related to the Predicted Percentage of Dissatisfied (PPD) that describes the number of people unsatisfied with the thermal environment. A detailed description of the model is given in ISO7730.

PMV and PPD were firstly defined for the indoor environment, then, under the name "Klima-Michel-Modell" adapted to outdoor conditions, by using weather data as input, adding the short and long wave radiations fluxes, and assuming typical activity and clothing. This model was later improved by the Perceived Temperature.

New Standard Effective Temperature (SET*) and Outdoor Effective Temperature (OUT_SET*)

New Standard Effective Temperature (SET*) is a later development of the Effective Temperature (ET*) and is defined as the equivalent temperature of an isothermal environment (RH = 50%, wind speed lower than 1.5 ms^{-1}, and air temperature equals to mean radiant temperature) where a person (standard clothing according to the metabolic activity) would have the same heat stress and thermo-regulatory strain as in the actual environment. Outdoor Effective Temperature (OUT_SET*) corresponds to the outdoor adaptation of the Standard Effective Temperature (SET*) by adding the Mean Radiant Temperature.

Universal Thermal Climate Index (UTCI)

The Universal Thermal Climate Index (UTCI) was developed in 1999 by a group of multidisciplinary experts (thermo-physiology, occupational medicine, physics, meteorology, biometeorological and environmental sciences), designed by the International Society of Biometeorology and later by COST Action730 (Cooperation in Science and Technical Development). UTCI is defined as the reference air temperature that elicits the same thermal strain as the actual condition. A 10-point thermal scale expresses the thermal perception from +46°C (extreme heat stress) to −40 °C (extreme cold stress); the neutral sensation is between 9°C to 26°C. UTCI is based on the multi-node dynamic thermal physiological UTCI-Fiala model, this model defines the thermal effects (active and passive) on the human body (for the whole body and individual parts) over a wide range of climates and is validated with measured data.

Clothing insulation is automatically calculated as function of the actual air temperature and wind speed, using an adaptive clothing model.

The UTCI model can express the thermal perception in all climates (artic, moderate, dry and wet subtropical) and has been compared with other thermal indices (as PET, PMV, and SET*), showing a large correlation factor (average R^2=0.95).

2.1.3.   Choice of parameter

In conclusion, the choice of the metrics fell on the Universal Thermal Climate Index.

The UTCI, as explained on the project's website (www.utci.org), has been developed satisfying the following requirements:

- Thermo-physiologically significant in the whole range of heat exchange,

- Valid in all climates, seasons, and scales,

- Useful for key applications in human biometeorology (e.g. daily forecasts, warnings, regional and global bioclimatic mapping, epidemiological studies, and climate impact research),

- Independent of person's characteristics (age, gender, specific activities, and clothing, etc.).

The concept of UTCI was then developed as an equivalent temperature[24]. This involves the definition of reference conditions (air temperature equal to MRT, wind speed = 0.5 ms^{-1} at 10 m, relative humidity = 50 % up to a constant water vapour pressure of 20hPa, and metabolic rate = 135 Wm^{-2}) to which all other climatic conditions will be compared. The equivalence between actual conditions and reference conditions is based on the equivalence of dynamic physiological responses between the two. As this dynamic physiological response is multidimensional (body core temperature, sweat rate, skin wittedness, etc at different time points), a single-dimensional strain index was calculated based on principal component analysis.

The basic equation to describe UTCI is:

$$UTCI(T_a, \text{MRT}, va, pa) = T_a + Offset(T_a, \text{MTR}, va, pa) \qquad (16)$$

Where:

T_a = air temperature (°C)

MRT = mean radiant temperature (°C)

v_a = wind speed(m·s^{-1})

p_a = water vapour pressure (hPa)

Offset = deviation from air temperature

The UTCI as an equivalent temperature for a given combination of wind, radiation, humidity, and air temperature is then defined as the air temperature in the reference condition of humidity, radiation, and wind speed, which produces the same strain index value. The associated assessment scale was developed from the simulated physiological responses and comprises 10 categories. As reported in the scale description on the official

website "Stress is appropriate in this instance since it refers to the insult to the body; strain is the resultant consequence due to exposure". Because the stress-strain concept may not be understood by the general public also a sensation scale is used (Figure 3).
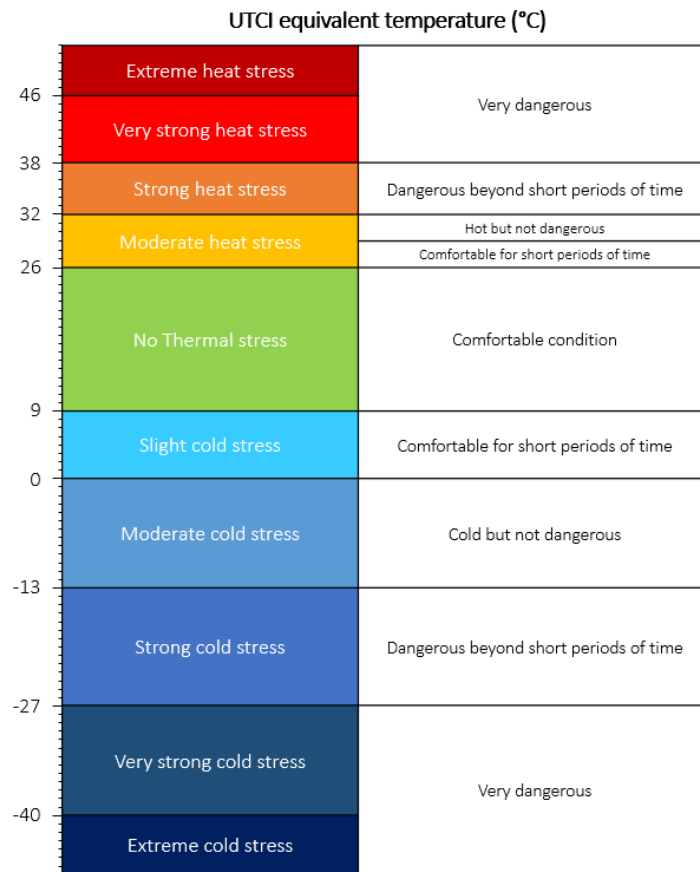
Figure 3 UTCI assessment scale of heat stress categories and sensation scale comparison.

2.2. Indoor Daylight Comfort

The lighting design has always been aimed at optimizing the visual performance required but is fundamental to remember that light has a strong implication also for health and well-being. With reference to the paper by ENEA "*Studio per la valutazione degli effetti della luce sugli esseri umani*" by Barbalace et al., this aspect of daylight comfort has been deepened [25]. Two main aspects about the influence of lightning on people are highlighted in the document: the relationship with physiology and the one with psychology.

It has been demonstrated the presence of a link between light and the circadian rhythm. The human biorhythm is based on the alternation of day and night along the day, due to the earth rotation, which consequently activates the production of hormones: cortisol and melatonin. Besides many elements, such as the time of the meals, the sound, temperature, social interactions, and caffeine influence this cycle, the light is the main one.

There are different aspects of the exposition to the light which contribute to the shift of circadian rhythm:

- light quantity/type

- spectral composition (different wavelengths)

- time of application of a light source

- direction of application of a light source.

This is the reason why the design of lightning in a closed space should be carefully developed. The relationship between psychology and light is a more complex issue to investigate than that between physiology and light, but equally important. In 2009, preliminary evidence was provided that the red monochromatic light, generally considered a rest element for the circadian system, can at the same time activate the psychological alert reaction. This discovery raises serious doubts about the current practice linked to the use of light with particular spectral distributions to optimize the circadian alignment, without taking into account possible psychological side effects.

2.2.1.   Definition of Parameters

As mentioned in the previous paragraph lighting has significant relevance on comfort and human life, with direct and indirect effects on the human body. The direct effects are related to visual performance and visual comfort; the indirect effects are related to the possible consequences on safety and health. Traditionally, lighting assessment is limited to the assessment of illuminance in the task areas, however, there is a growing awareness of the effects of light on both health and the quality of human life.

At European level, the Directive 89/654/EEC [26] includes an indication about lighting, and provides the requirements to guarantee health and safety in the workplaces, it is indicated that "Workplaces must as far as possible receive sufficient natural light and be equipped with artificial lighting adequate for the protection of workers' safety and health", but as in local directives only rather general instructions, without specific limit values, are provided.

For this reason, the consequences on safety and health are generally assessed in a qualitative way or through the parameters defined for the evaluation of visual comfort.

The indicators for the visual comfort evaluation can be separated into four groups: amount of light, colour rendering, daylight availability, and glare [27]. For the aim of this thesis, only indexes in daylight availability and glare fields will be considered as possible control parameters in the analysis.

Daylight Factor (DF)

The Daylight Factor (DF) is the most widely used performance measure for daylighting as it has the advantage that predictions are intuitive and easy to share within a design team.

It is a percentage defined as "the ratio of the internal illuminance at a point in a building to the unshaded, external horizontal illuminance under a CIE overcast sky" [28].

Building geometry, surrounding landscape and buildings, as well as surface properties have an impact on the daylight factor, but at the same time, it does not consider seasons, time of day, direct solar ingress, variable sky conditions, building orientation, or building location. Due to this DF analysis cannot provide any information about the appearance of glare problems.

For this reason, it can be used as a measure for the minimum lightning requirement, but it cannot provide enough design recommendations to reach visual comfort.

Daylight Autonomy (DA)

Daylight Autonomy (DA) uses work plane illuminance as an indicator of whether there is sufficient daylight in a space so that an occupant can work by daylight alone. The definition of this parameter is "the percentage of the year when a minimum illuminance threshold is met by daylit alone" [28].

It is therefore clear that this parameter is strictly linked to the minimum illuminance levels required by the reference standards. At European level, the reference standard is the BS EN 12464-1:2011 "*Light and lighting — Lighting of workplaces Part 1: Indoor workplaces*", which provides the required illuminance threshold for every destination of use of the analysed zone and the specific activity of the people inside it.

Since in this measure a lower limit is defined, but not an upper one, there is still no indication about the glare in this analysis.

Useful Daylight Index (UDI)

In 2005 Mardaljevic and Nabil proposed the Useful Daylight Index (UDI) as an evolution of the DA concept. In place of a threshold value, they propose that a measure of the occurrence of a range of illuminances that can be said to constitute useful levels of illumination provides a more informative metric [29].

This index is a step forward in considering visual comfort in the analysis and not only the light availability. Since there are no conclusive studies that correlate daylighting provision and occupant satisfaction the definition of "comfort range" is based on a review of the published papers on occupant preferences and behaviour.

As result the UDI defines three ranges of illuminances:

- Useful daylight illuminance (between 100 and 2000 lux)

- Below the useful daylight illuminance (lower than 100 lux)

- Exceeding the useful range (over 2000 lux).

Daylight Glare Probability (DGP)

The Daily Glare Probability (DPG) is a metric for evaluating glare that improves the correlation with user assessments, it was proposed by Wienold and Christoffersen in 2006 [30]. DGP evaluates the risk of glare inside the space at a certain hour of a certain day. It requires a proper setting of all the elements that can influence the visual comfort in the analysed space. For the analysis, it is needed that all the boundary conditions are set in the right way, and to place also the furniture inside the analysed space, since they are going to reflect the light in the same way as walls/roofs/ceilings do.

DGP is classified according to different classes, as it follows:

- IMPERCEPTIBLE: DGP < 0.3

- PERCEPTIBLE: 0.3 < DGP < 0.35

- DISTURBING: 0.35 < DGP < 0.40

- INTOLERABLE: DGP > 0.40

Spatial Daylight Autonomy (sDA)

Spatial Daylight Autonomy (sDA) measures daylight illuminance sufficiency for a given area. It is defined as the percentage of floor area, that meets or exceeds a specified illuminance level (recommended 300 lux on horizontal surfaces, 0.8m above finished floor) for a specified amount of annual hours (recommendation: 50% of the hours from 8:00 to 18:00)[31].

This is index is part of the Climate Based Daylight Modelling (CBDM), which is an IES (Illuminating Engineering Society) approved approach for daylight evaluation developed to overcome the disadvantages of the Daylight Factor. This method is based on two metrics (sDA and ASE) using daylight conditions from typical meteorological years as its basis.

Annual Sunlight Exposure

Annual Sunlight Exposure (ASE) assesses the potential visual discomfort using as an indicator an illuminance value (>=1000 lux) caused by direct sunlight on the working surface ASE is defined as the percentage of the analysis area which exceeds 1000lux for more than 250h per year without the use of any blinds and assuming the operational period between 8:00 and 18:00.

ASE is the second parameter considered in the CBDM, while the sDA provides information on the daylight availability this metric evaluates the possible presence of glare and therefore discomfort.

Although climate-based daylight modelling may be more accurate than daylight factor evaluation and combines the quality of light (i.e. potentially glary sunlight) with qualitative parameters, the disadvantage of this method is that the evaluation method is much more complicated.

2.2.2.   Choice of parameter

In conclusion, after the most used control parameters for daylight analysis have been examined, sDA and ASE have been selected.

This choice is led by two main reasons: the possibility to perform a complete and dynamic analysis considering these two metrics together, and the fact that are considered in the options suggested for assessing the LEED Daylight Credit.

Leadership in Energy & Environmental Design (LEED) is a green building certification program that recognizes sustainable building strategies and practices. To receive LEED certification, building projects should satisfy prerequisites and earn points towards one of the five rating systems – Building Design and Construction; Interior Design and Construction; Building Operations and Maintenance; Neighbourhood Development; and Homes. Each rating system is made up of a combination of credit categories [32].

To assess the Daylight credits required by the LEED v4, Illuminating Engineering Society has developed a method titled "*IES Spatial Daylight Autonomy (sDA) and Annual Sunlight Exposure (ASE)*" (IES LM-83-12) [33]. These two metrics have been developed to describe multiple important dimensions of daylighting performance in an existing building and a new design. The purpose of these new climate-based indicators is to define a consistent calculation method that will allow multiple design options of proposed designs, daylight buildings, and/or climate locations to be compared in a consistent way[33].

Both metrics use the same building information and simulation methodology to analyse hourly illumination patterns, summed for an annual period, across an analysis area.

They should be reported together to evaluate properly building designs considering both the sufficiency of daylight illuminance and the potential risk of excessive sunlight penetration. On one side sDA is preferred when it has a high value, usually, the limit to be exceeded is 50%, while ASE should be kept lower than 10%, to limit the potential risks coming from glare and solar gains.

Daylight Factor (DF) was previously used for assessing LEED Daylight Credit for buildings. The new version, LEED v4, however, accounts for the annual hourly measurement of daylight in a space. This is, as highlighted previously, more effective in capturing the dynamic characteristic of interior daylight illumination throughout the year.

The one described is the first of three options suggested for assessing the LEED Daylight Credit. The first and second options are based on a computer simulation, while the third one has an experimental approach involving two illuminance measurements. These

options are exposed in the paper "*LEED v4.1 BD+C rating system*" by the U.S. Green Building Council [34]:

- *Option 1: Spatial Daylight Autonomy and Annual Sunlight Exposure*

  "Perform annual computer simulations for spatial daylight autonomy$_{300/50\%}$ (sDA$_{300/50\%}$), and annual sunlight exposure$_{1000,250}$ (ASE$_{1000,250}$) as defined in IES LM-83-12 for each regularly occupied space. Healthcare projects must use each regularly occupied space located in the perimeter area determined under EQ Credit Quality Views. Additionally, calculate the average sDA$_{300/50\%}$ value for the total regularly occupied floor area. For any regularly occupied spaces with ASE1000,250 greater than 10%, identify how the space is designed to address glare."

- *Option 2: Illuminance calculation*

  "Perform computer simulations for illuminance at 9 a.m. and 3 p.m. on a clear-sky day at the equinox for each regularly occupied space. Healthcare projects should use the regularly occupied spaces located in the perimeter area determined under EQ Credit Quality Views.

  Demonstrate illuminance levels are between 300 lux and 3,000 lux at both 9 a.m. and 3 p.m. Spaces with view-preserving automatic (with manual override) glare-control devices may demonstrate compliance for only the minimum 300 lux illuminance level."

- *Option 3: Measurement*

  "Measure illuminance in each regularly occupied space. Healthcare projects should use the regularly occupied spaces located in the perimeter area determined under EQ Credit Quality Views. Achieve illuminance levels between 300 lux and 3,000 lux. Spaces with view-preserving automatic (with manual override) glare-control devices may demonstrate compliance for only the minimum 300 lux illuminance level."

The first option has been considered in this work since it adopts the Climate Based Daylight Modelling (CBDM) approach, predicting hourly daylight quantity on an annual basis through the previously described parameters. In fact, it provides the most accurate estimate of daylighting performance in space.

CBDM includes the use of sun and sky conditions from meteorological data sets to predict various luminous quantities, so in addition to building configuration and composition, it also depends on location and direction [35].

For the LEED rating system, the points for Option 1 are awarded according to Table 1.

The average $sDA_{300/50\%}$ value for the regularly occupied floor area is at least 40%	1 point
The average $sDA_{300/50\%}$ value for the regularly occupied floor area is at least 55%	2 points
The average $sDA_{300/50\%}$ value for the regularly occupied floor area is at least 75%	3 points
Each regularly occupied space achieves $sDA_{300/50\%}$ value of at least 55%	Exemplary performance or 1 additional point if only 1 or 2 points achieved above

Table 1 Points for Option 1 in the LEED v4 rating system.

2.3. Simulation process

2.3.1.   Software definition

While for the Indoor daylight comfort simulation the software choice was guided from my personal experience and previous works, for the outdoor thermal comfort I had limited experience in urban microclimate modelling.

The approach I wanted to apply was to study and understand the physical models for calculating MRT, a key parameter for all the Outdoor Thermal Comfort models, and then translate them into a programming language for the actual computation. To do this I needed an environment that could allow me to integrate the developed script and with some tools able to manage and elaborate the parameters needed as input.

The Grasshopper visual scripting environment, integrated in the software Rhino 6 (by Robert McNeel & Associates, 2018), not only gave me this chance but allows also to integrate both the indoor and outdoor simulations in the same software and to manage parametrically the urban geometry and the simulation itself. Moreover, once the customized components are ready, the designer does not need a thorough knowledge of the principles behind the code but can easily build the script following the workflow developed, providing the required inputs, and use it to evaluate every Case Study.

Among the numerous plugins available for Grasshopper, Ladybug provides the tools necessary to evaluate the Mean Radiant Temperature applying the described models. However, the component's code that adapts the Arens model to the outdoor does not include solar radiation reflected by buildings and free-standing objects in its calculations, at the moment. For this reason, the ERF model modified for the outdoor has been developed as a Python script and then implemented as a custom component in the script.

At this point also the lw MRT simulation model has been applied with a custom procedure, described in the following pages, improving the assumptions used in the Ladybug code.

This procedure to calculate the MTR made the provided component for the UTCI calculation not applicable. Therefore, as explained in detail in the following pages, the original Fortran code for calculating the index has been adapted and used in a custom component.

In the Grasshopper environment, the script merges the custom components and the available components, the used plugins are here reported:

- Ladybug 0.0.69 and Honeybee 0.0.66 [Legacy Plugins] (by M. Roudsari, 08/2020). Two open-source plug-ins, that help explore and evaluate environmental performance. While the first imports standard EnergyPlus weather files (.epw) and provides a variety of 3D interactive graphics, Honeybee joins together four validated simulation engines - specifically, EnergyPlus, Radiance, Daysim, and OpenStudio - which evaluate building energy consumption, comfort, and daylighting.

- DIVA 4.0 (by Solemma, 2019).
  A plugin that runs thermal, daylight, solar radiation, and glare simulations, in this thesis, is used for the indoor daylight simulation. It enables users to perform dynamic daylighting analyses. The solver behind DIVA components is DAYSIM, a dynamic solar simulation software developed by C. Reinhardt et al.

To implement the custom codes in the script there is no need for an external plugin, the "GhPython Script" component acts as a Python interpreter in Grasshopper. Along with its access to IronPython 2.7, the GhPython component can also access the easy-to-use RhinoScritSyntax.

2.3.2.   Outdoor simulation

As exposed in the first part of the chapter the key parameter for the UTCI assessment is the Mean Radiant Temperature. Therefore, before describing the actual process applied to calculate the index it is necessary to explain the simulation procedure for the radiant temperature.

Mean Radiant Temperature Simulation Process

As already explained, the MRT sums up all short and long wave radiation fluxes to which the human body is exposed to. The simulation method was therefore developed following two different streams for the two contributions, each referred to the models exposed in the previous section, then combined in the end to compute the total Mean Radiant Temperature.

The first stage of simulation to assess the lw MRT requires calculating the surrounding surface temperatures.

The 3D geometry is modelled first in Rhino for the fixed elements and integrated with the parametrically changing elements defined in Grasshopper. Every significant surface is converted into a mesh through Grasshopper components so that a grid of points is

created and can be used as an input in the Radiance-based Honeybee component to calculate the hourly incident radiation values.

These radiation values hitting the exterior surfaces are then used as input to compute surfaces' temperature using the Thermal Admittance Method previously described. The conduction through the surfaces is simplified as one-dimensional heat transfer with the Heat Diffusion Equation, described in Figure 1 and Equation (5). To apply this model, it is necessary to discretize the equations with reference to the space.

Considering a generic wall of depth L and made by a uniform material the procedure to derive the previously mentioned equations and their discretization is here reported:

1. Division of the wall in **n** layers, all at equal distance **Δx**. The layers are numerated starting from 0 according to the programming convention.
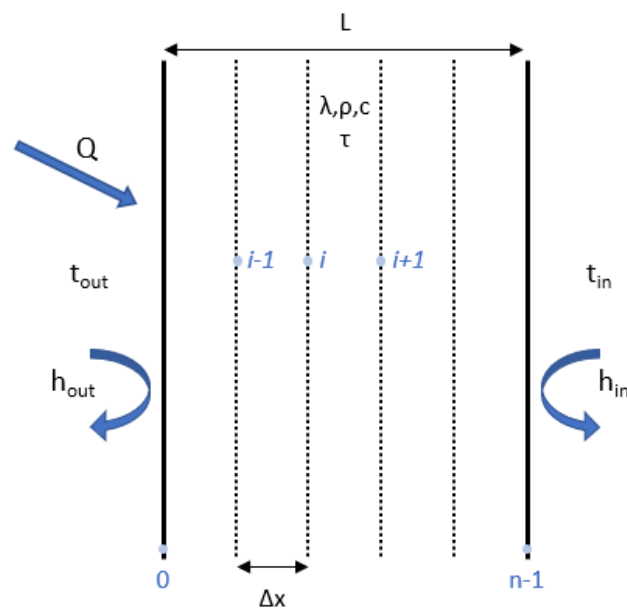
Figure 4 Generic wall starting condition.
Where: Q = Solar Radiation (W/m²) h = convection coefficient (W/m²K) t_{out}= External Temperature (℃) t_{in}=Internal Temperature (℃) τ = Time (s) λ = Conductivity (W/mK) a = Diffusivity (m²/s) L = Depth (m)

2. Balance for the **i-th** layer inside the wall.
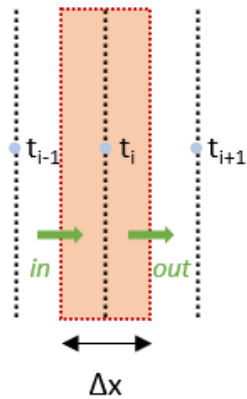
Figure 5 Control Volume for the i-th layer inside the wall.

$$\underline{Accumulation} \qquad \underline{in} \qquad \underline{out}$$

$$\rho c \Delta x \frac{dt}{d\tau} \quad = \quad q_x^H|_x \quad -q_x^H|_{x+\Delta x}$$

$$\rho c \Delta x \frac{dt}{d\tau} = -\lambda \frac{dt}{dx}|_x - \left(-\lambda \frac{dt}{dx}|_{x+\Delta x}\right)$$

Discretization:

$$\rho c \Delta x \frac{dt}{d\tau} = -\lambda \frac{t_i - t_{i-1}}{\Delta x} + \lambda \frac{t_{i+1} - t_i}{\Delta x} \tag{17}$$

3. Balance for layer **0,** surface in contact with the outdoor environment, with a solar absorbance value a.
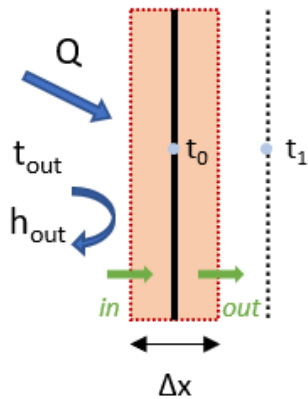
Figure 6 Control Volume for layer 0, in contact with the outdoor environment.

$$\underline{Accumulation} \qquad \underline{in} \qquad \underline{out}$$

$$\rho c \frac{\Delta x}{2} \frac{dt}{d\tau} \quad = \quad h_{out}(t_0 - t_{out}) + Qa \quad -q_x^H|_{\Delta x}$$

$$\rho c \frac{\Delta x}{2} \frac{dt}{d\tau} = h_{out}(t_0 - t_{out}) + Qa - \left(-\lambda \frac{dt}{dx}|_{x+\Delta x}\right)$$

Discretization:

$$\rho c \frac{\Delta x}{2} \frac{dt}{d\tau} = h_{out}(t_0 - t_{out}) + Qa + \lambda \frac{t_1 - t_0}{\Delta x} \tag{18}$$

4. Balance for layer **n-1**, surface in contact with the indoor environment.
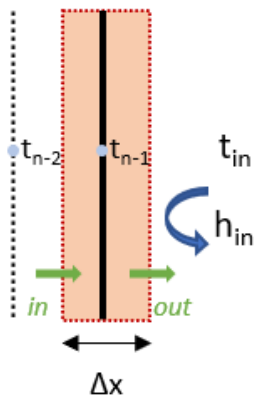
Figure 7 Control Volume for layer 1, in contact with the indoor environment.

$$\underline{Accumulation} \qquad \underline{in} \qquad \underline{out}$$

$$\rho c \frac{\Delta x}{2} \frac{dt}{d\tau} \quad = \quad q_x^H|_{L-\Delta x} \quad -h_{in}(t_{in} - t_{n-1})$$

$$\rho c \frac{\Delta x}{2} \frac{dt}{d\tau} = -\lambda \frac{dt}{dx}|_{x+\Delta x} - h_{in}(t_{in} - t_{n-1})$$

Discretization:

$$\rho c \frac{\Delta x}{2} \frac{dt}{d\tau} = -\lambda \frac{t_{n-1} - t_{n-2}}{\Delta x} - h_{in}(t_{in} - t_{n-1}) \tag{19}$$

The ground surface temperature calculation must follow a different procedure as the boundary conditions are different from the ones of a wall. In this case, as an approximation, the ground is considered as a uniform material for a depth of 0.5 m, where the temperature is provided in the EPW file of the selected location.

The heat transfer mechanisms within the material and at the outdoor boundary are the same as the ones previously described, while the other boundary balance is a conduction heat transfer with a known surface temperature.

4. Balance for layer **n-2**, with layer n-1 at the imposed temperature T_g.
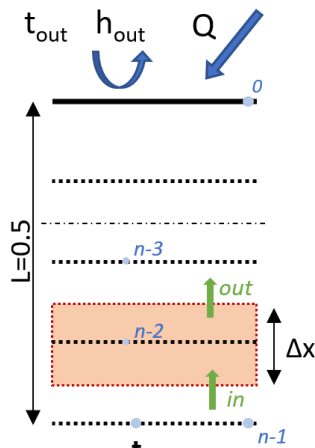
$$\underline{Accumulation} \qquad \underline{in} \qquad \underline{out}$$

$$\rho c \frac{\Delta x}{2} \frac{dt}{d\tau} \quad = \quad q_x^H|_{L-\Delta x} \qquad -q_x^H|_{L-2\Delta x}$$

$$\rho c \Delta x \frac{dt}{d\tau} = -\lambda \frac{dt}{dx}|_{L-\Delta x} - \left(-\lambda \frac{dt}{dx}|_{L-2\Delta x}\right)$$

Discretization:

$$\rho c \Delta x \frac{dt}{d\tau} = -\lambda \frac{t_{n-2}-t_{n-3}}{\Delta x} + \lambda \frac{t_g-t_{n-2}}{\Delta x} \qquad (20)$$

Figure 8 Control Volume for the layer n-2.

The heat diffusion equation is then solved in one dimension using a Python script based on the forward Euler method. It is a first-order numerical procedure for solving ordinary differential equations with a given initial value, after the discretization, this is applicable to the heat transfer problem, as the indoor and outdoor temperatures are known. The resulting solver is time dependant, but as an approximation, it was set to reach a steady-state condition.

The code is integrated in the Grasshopper environment using the GhPyton component, the resulting component requires as input the indoor and outdoor air temperature and convective coefficient, the incident radiation, and the material properties.

For the T_{sky} calculation, the horizontal infrared radiation provided by the EPW file is extracted using the Ladybug components as function of the analysis period and used as input in a second custom component (together with the emissivity ε_p) based on a Python script that applies the Equation (8).

In the second stage of the simulation, the View Factors for the selected Test Point must be computed. To do so, each point is considered as a sensor and the surrounding surfaces are raytraced, with zero bounces. In this way, it is possible to identify the first surface

each ray hits. A database is created in reference to each Test Point and the number of surfaces traced. Using this database View Factors are computed considering the number of rays that hit each surface over the total number of rays, which is controlled by the user as an accuracy level input.

In the View Factor calculation, the human body must be simplified, but the complexity of the human morphology makes a geometrical investigation very difficult, for this reason in most of the available tools for the VF calculation in the thermal comfort analysis field a spheric approximation is used, including the Ladybug tool. In this thesis work the model used is taken from the study of the effect of radiofrequency radiation on human health[36].

An ellipsoid model describes more accurately the human body characteristics and therefore is more suitable as a non-realistic phantom for the determination of the VF. The mass of each ellipsoid coincides with the mass of the corresponding human model.

Four different homogeneous ellipsoidal models of human bodies are available[37], i.e. the average man, the average woman, the 10 year old child, and the 5 year old child, and thanks to the parametric nature of the script the reference model can be easily changed.

A picture of the tri-axial ellipsoid model is shown in Figure 10. The three axes are denoted as a, b, and c with $a \geqslant b \geqslant c$.
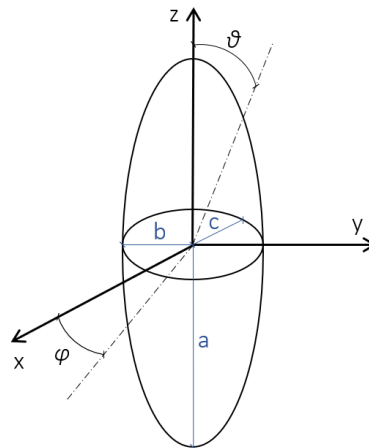
Figure 9 An ellipsoid model for human body approximation. a, b and c are the axes of the ellipsoid. φ and ϑ represent the azimuth and the elevation, respectively.

Phantoms	Average mass (kg)	Height 2a (m)	Length 2b (m)	Width 2c (m)
Average man	70.00	2 x 0.875	2 x 0.195	2 x 0.098
Average woman	61.14	2 x 0.805	2 x 0.200	2 x 0.091
10 year-old child	32.20	2 x 0.690	2 x 0.143	2 x 0.078
5 year-old child	19.50	2 x 0.560	2 x 0.120	2 x 0.069

Table 2 Characteristics of the ellipsoids used as human phantoms.

With such information it is possible to calculate the long wave contribution in the Mean Radiant Temperature for each Test Point combining them in Grasshopper applying the equation previously described:

$$MTR_{lw} = \sqrt[4]{T_1^4 F_{p-1} + \cdots + T_n^4 F_{p-n}} \qquad (21)$$

The first part of the simulation, regarding the long wave contribution is summarized in Figure 11.
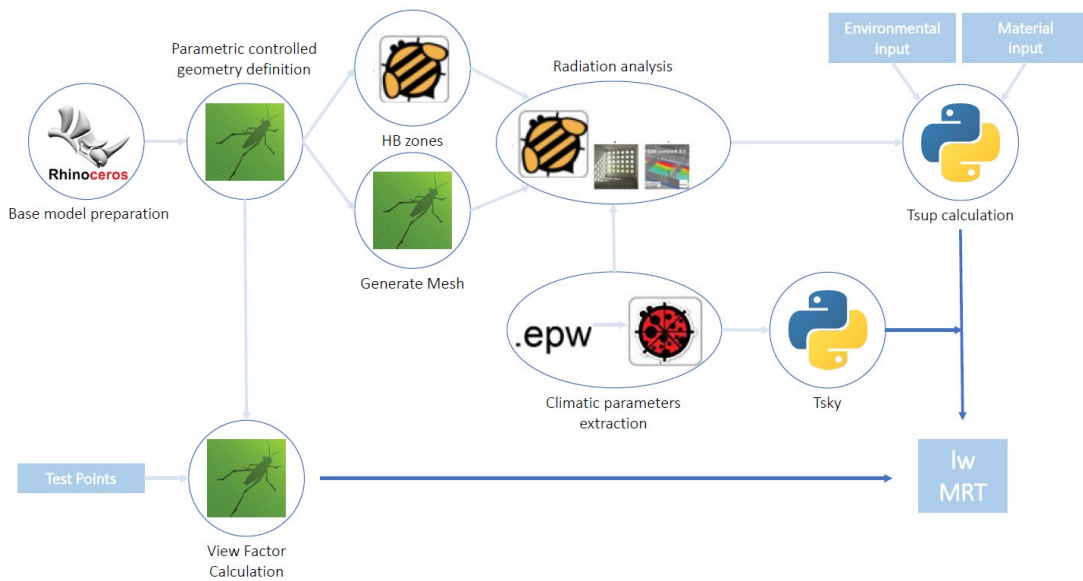
Figure 10 Schematic representation of the lwMRT simulation process.

The second branch of the simulation consists of the calculation of the short wave MRT, which is the contribution in the MRT of the direct, diffuse, and reflected solar radiation directly hitting the human body.

As in the first stage of the simulation, for the radiation evaluation, the tool used is the Grasshopper's Honeybee plug-in, but in this case to obtain a radiation analysis only on the selected Test Points and not on all the urban environment surfaces. The resulting cumulative radiation value, that is in kWh/m^2, is converted in W/m^2 with respect to the analysis period, and the $E_{solContext}$ is derived to be able to apply the ERF method.

This value, which represents the total incident radiation from the sky and reflected by the buildings is used to find the approximate radiation reflected by the ground, through a generic value of albedo and the calculated View Factor for each Test Point.

The two values are then summed, and the obtained total short wave radiant flux (E_{solar}) is used to find ERF$_{solar}$. The Python-based script was written to automatically apply the method and calculate the ΔMRT, which from now on will be called MRT$_{sw}$.

The inputs required by the resulting component, besides the total E_{solar}, are all related to the user: long wave absorptivity (α_{lw}), short wave absorptivity (α_{sw}), radiation heat transfer coefficient (h_r), and the model subject and posture.

The described process to assess the short wave contribution in the MRT is schematized and reported following in Figure 12.
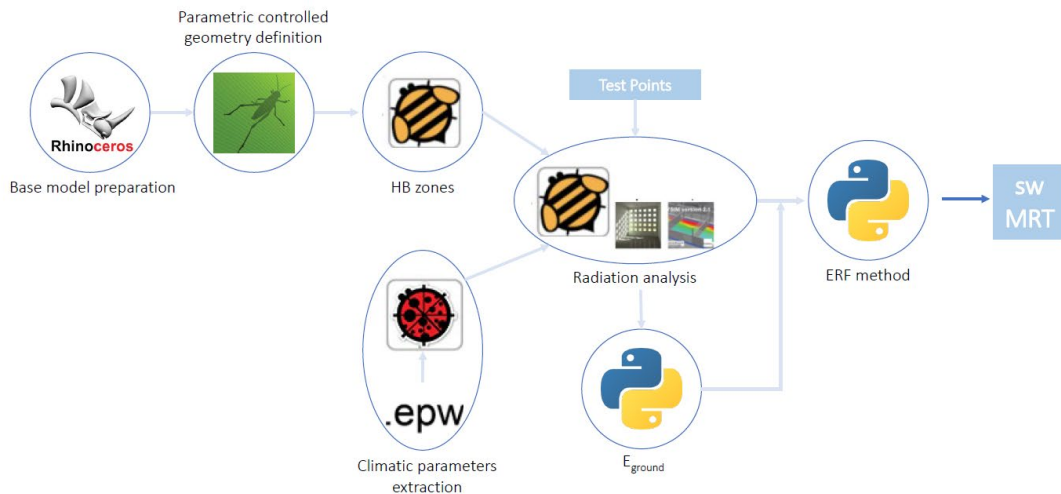
Figure 11 Schematic representation of the swMRT simulation process.

Finally, the results from the two branches of the simulation are summed to obtain the total value of Mean Radian Temperature that will be used to evaluate the comfort indices.
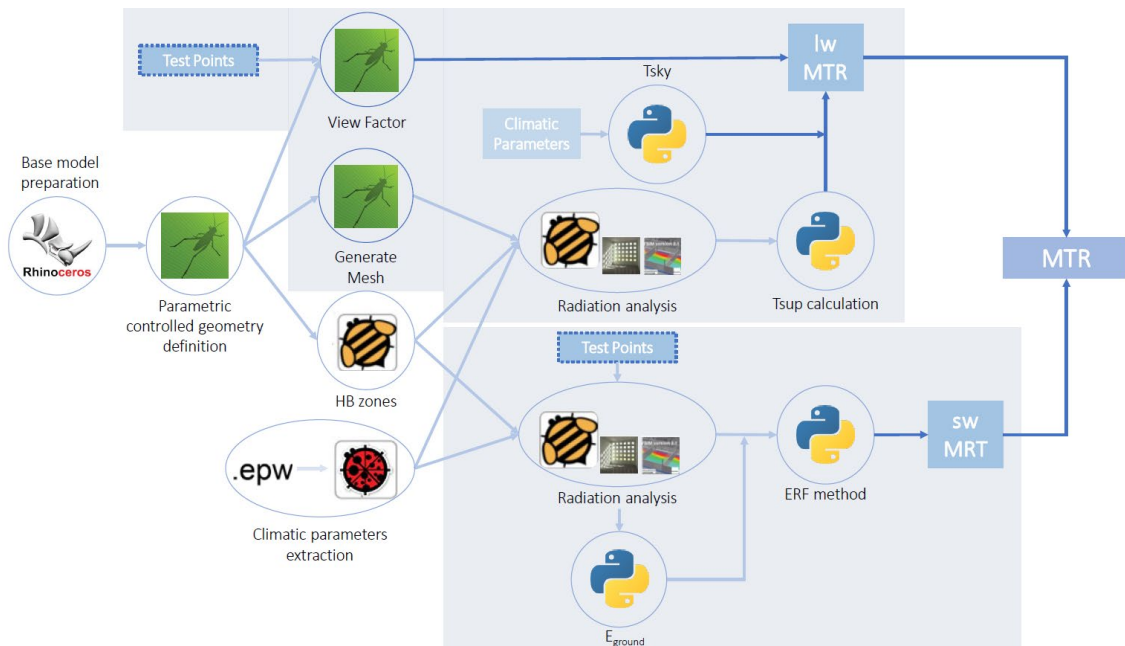
Figure 12 Schematic representation of the complete MRT simulation process.

UTCI simulation process

As previously mentioned, the UTCI was firstly developed in 1999, but since 2005 the COST Action 730 worked on this index with the main objective of "develop, and make easily available, a physiologically relevant assessment model of the thermal environment to significantly enhance applications related to human health and well-being" [38].

The model should take into account all the mechanisms of heat exchange and after an extensive validation of accessible models of human thermoregulation, the advanced multi-node "Fiala" model was adopted.
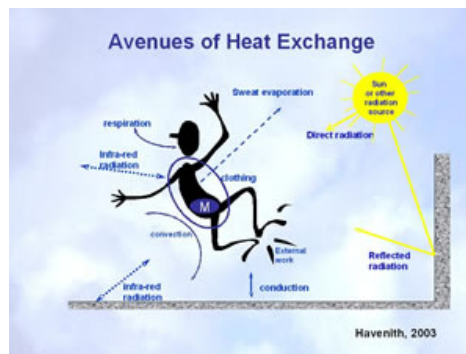
Figure 13 Heat Exchange possible mechanisms (from ww.utci.org).

This model was coupled with a state-of-the-art clothing model considering the behavioural adaptation of clothing insulation by the general urban population to actual environmental temperature.

The Universal Thermal Climate Index (UTCI) was developed conceptually as an Equivalent Temperature (ET). Thus, for any combination of air temperature, wind, radiation, and humidity, UTCI is defined as the air temperature in the reference condition which would elicit the same dynamic response of the physiological model.

The last subroutine (UTCI_approx) version was released in 2009, it calculates UTCI values approximated by a 6th order polynomial from the input.

The input parameters are limited as follows:

- Air temperature, from −50°C to +50°C,

- Mean Radiant Temperature, from 30°C below air temperature to 70°C above it,

- Wind speed at 10 m above the ground, from 0.5 to 1.7 ms^{-1},

- Water vapour pressure in hPa, range of validity until 50 hPa or 100% relative humidity.

Incorporated in the main script there is also a subroutine calculating saturation vapour pressure (es), used for converting relative humidity to vapour pressure and vice versa, that is based on the work of Bob Hardy on the need for new temperature-dependent equations to predict saturation vapor pressure over water and ice, enhancement factor over water and ice, frost point temperature, and dewpoint temperature as a consequence of the change in the temperature scale of ITS-90 [39].

The program is available on the previously mentioned UTCI official site in a FORTRAN source file.

To integrate the UTCI calculation in the Grasshopper model already built to calculate the MRT, a new component has been developed translating the Fortran script into a Python-based script.
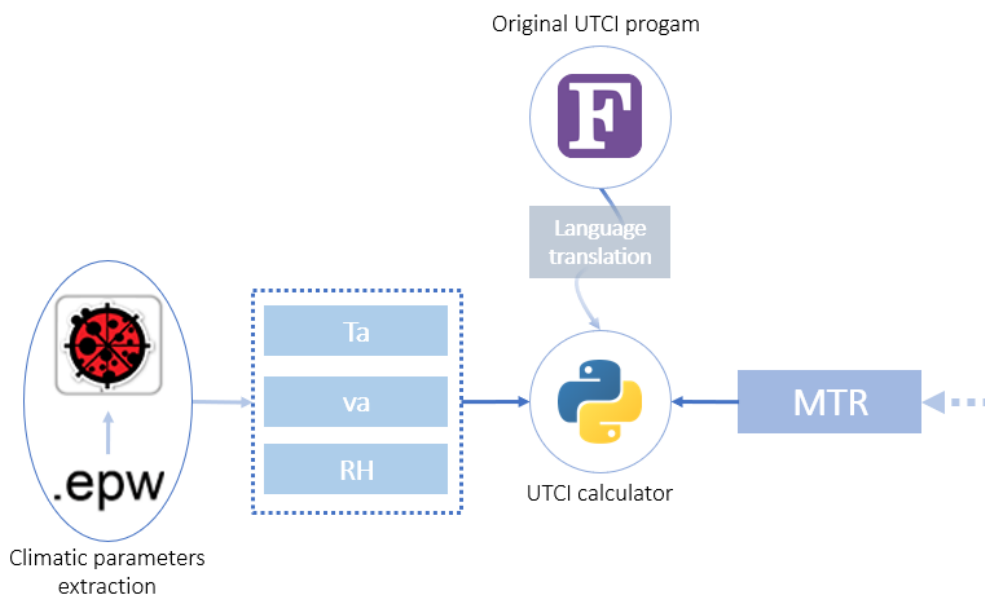
Figure 14 Schematic representation of the UTCI simulation process

This component requires as inputs the climatic factors, already available thanks to the Ladybug plug-in, and the MRT, derived from the previous simulations, relating to the considered period.

This allows to calculate the UTCI value for each Test Point considered for the definition of the MRT, and consequently to represent it on the geometric model.

2.3.3. Indoor simulation

As explained in the software choice paragraph the selected tool for the daylight simulation is Solemma's plug-in DIVA 4. The solver behind its components is DAYSIM, a dynamic solar simulation software developed by C. Reinhardt et al., and it is commonly used by researchers for its precise and reliable outputs.

The ASE and sDA values are computed with an already available and validated component for the Annual Daylight Simulation, the procedure for the simulation will be deepened in the Methodology chapter, however here a summary of the required inputs is reported.
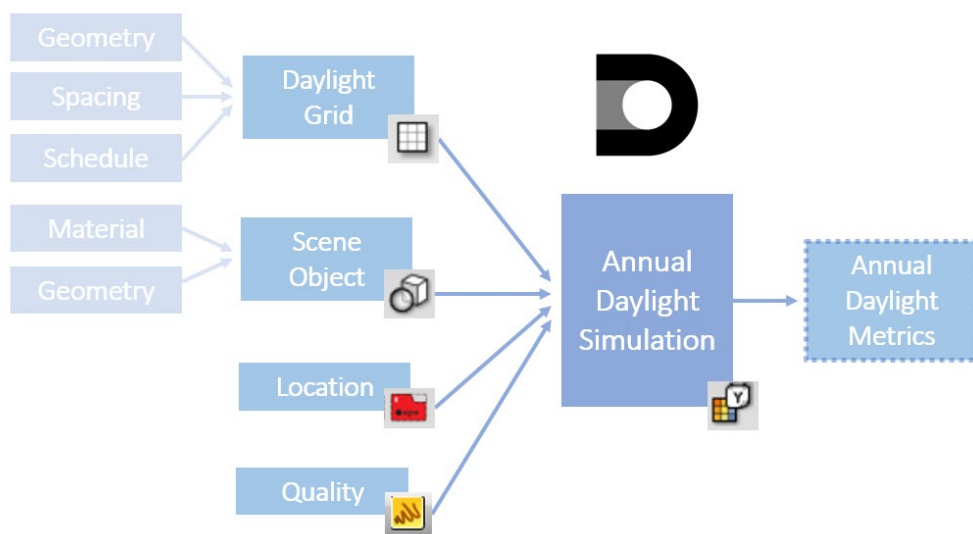
Figure 15 Schematic representation of the Annual Daylight simulation process.

An Annual Daylight Simulation is performed to compute annual climate-based daylight metrics. The first input required is the scene, in this work the geometry and materials are defined in Grasshopper to be able to exploit the parametric nature of the software. Then the analysis grid has to be defined, though the number and position of the ideal sensor are determined. With the grid also the schedule is set according to the destination of use of the space. The last two inputs required are the location, through an EPW file, and the quality of the simulation.

As previously mentioned, the DIVA's components are based on DAYSIM, which is a validated daylighting analysis software that calculates the annual daylight availability in arbitrary buildings based on the RADIANCE backward raytracer. Thus, both the materials of the scene and the quality of the simulation need to be in the Radiance standard format.

3

METHODOLOGY

GENERAL RULES FOR THE SIMULATIONS

3.   METHODOLOGY

As introduced in the previous chapter, now is the time to list the properties and boundary conditions for the simulations. In this section, those boundary conditions and those common properties for all the next simulations of this research project are defined, together with the rules that define the variations that must be evaluated for their impact on indoor and outdoor comfort.

The project of the modules is characterized by two main points: geometry and material.

For the geometry, three main rules are defined and the method to test them in terms of Indoor Daylight Comfort, to find the best cases to apply to the case study, is exposed. The methodology will follow the prescriptions of the LEED v4 standard for all the indoor settings.

In the second section, there is a focus on the materials for the opaque elements, their definition and behaviour, both for their thermal and optical properties. There is not a standard to follow to choose the finishing material according to its effect on the outdoor conditions, and therefore also a fixed methodology is absent. They will be evaluated, in the next chapter, according to the amount of radiation that they reflect on the adjacent area, and the selection is done to represent all the possible architectural choices.

A brief summary of the steps to follow for the application of the simulation to the outdoor is also reported, but this theme will be deepened in detail in the chapter related to the Case Study.

In conclusion, a sensitivity analysis to validate the quality of the parameters chosen for the indoor and outdoor simulations.

3.1. Façade Configurations

Within this subchapter, the geometric configurations of the façade that will be the object of the analysis are introduced and described together with the simulation methodology that will be applied to evaluate them.

The starting point of the workflow is a south-facing generic module with a plane unitized glazed façade. Since the configurations will be evaluated for their effect on the outdoor comfort, no shading systems internal or external are considered, to avoid any influence on the surrounding microclimate. For this reason, in the daylight analysis, the ASE limit is increased to 30%, higher than the standard 10% value for LEED.

The first level of classification is therefore based on the geometry and divides the configurations into three main groups of analysis:

- Plane façade _ Opaque - transparent ratio

- 3D façade _ Type 1

- 3D façade _ Type 2
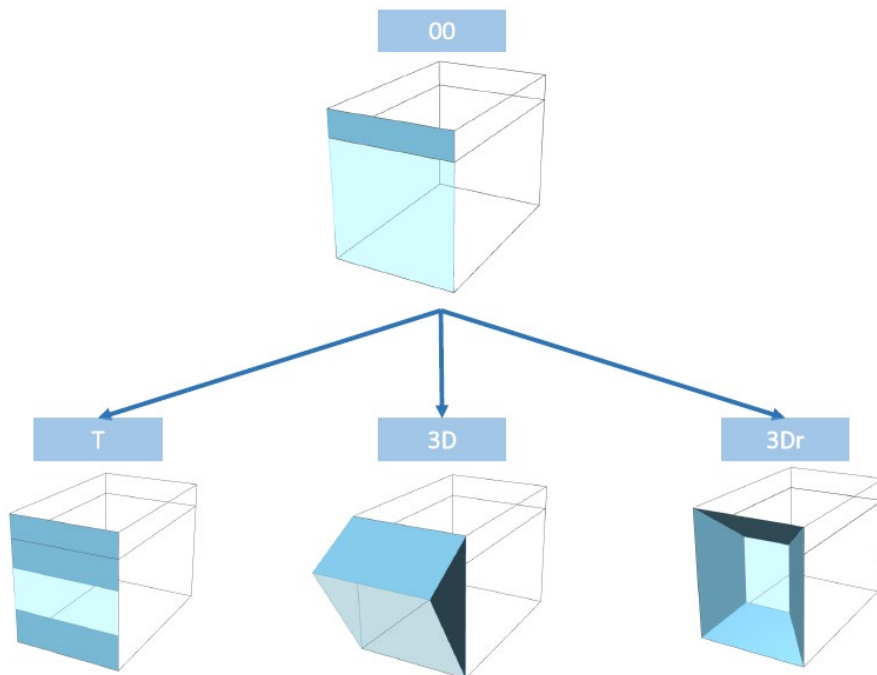
Figure 16 Façade Geometric Classification

3.1.1.   Module Dimensions

The definition of the geometry for the typical room for the indoor daylight analysis is driven by two main factors: the destination of use of the room itself and the geometric limitation arising from the façade system.

For this preliminary analysis, a generic unitized façade is considered, and therefore also the dimensions of the single-cell are not specific to a case study, but one of the measures used on the market. One room corresponds to two cells of the façade.
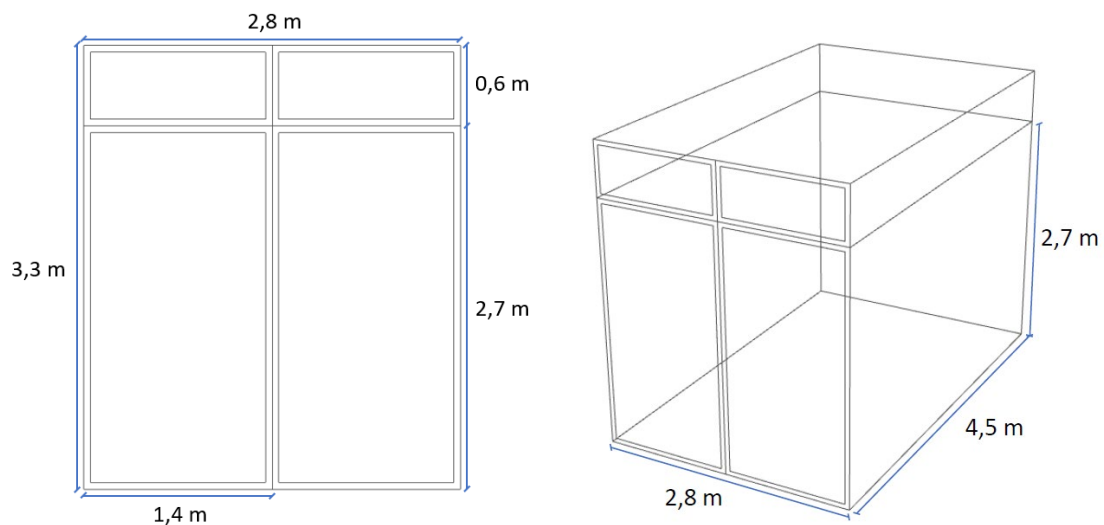
Figure 17 Unitized façade and module dimensions.

The other dimensions of the room were defined in order to comply with the regulation according to the destination of use, in this case, offices. In the absence of more stringent prescriptions by municipal or sector-specific regulations, the minimum measures for the working environments are a net height of 2.70 m and a minimum surface of 10/12 m², with at least 5 m² for each user.

The plan of the room is simple and regular in order to be uniform with most of the literature cases.

3.1.2.   Analysis grid

A fundamental aspect that needs to be defined in preparing a model for daylight analysis is the base grid for the simulations. It is a grid of points, virtual sensors, that correspond to a "real-world" positioning of measurement instruments in the space. The grid is built on a horizontal plane at a height related to the task that is performed in that space.

According to the LEED specifications "*the sDA and ASE calculation grids should be no more than 2 feet square and laid out across the regularly occupied area at a work plane height of 30 inches above finished floor (unless otherwise defined)*" [40].

Therefore, the analysis grid is placed at 0.8 m of height from the floor, as a typical working plane, and the nodes are 0.5 m apart. A minimum distance between the edge of the sensor grid and the boundaries have been specified to about 0.50 m, as recommended by CISBE (Chartered Institution of Building Services Engineers). In the grid area close to walls and windows the illuminance data can provide false results.
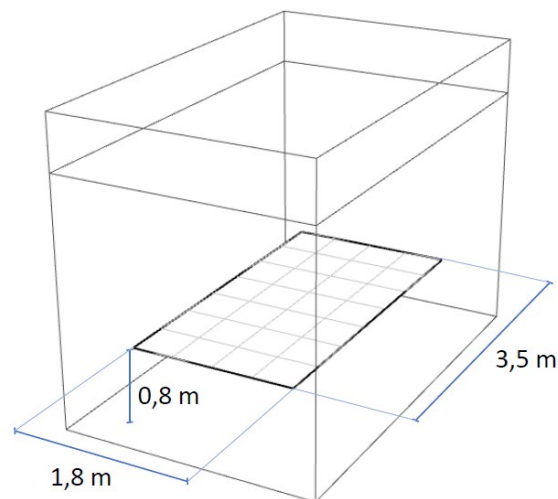
Figure 18 Analysis grid placing and dimensions.

Together with the grid, the schedule is defined, it concerns the occupancy for the daylight simulations only. The chosen one is set according to the Office destination of use previously described. It is based on the occupancy of a typical office: the workers occupy the building only during the working days, from Monday to Friday, each day from the morning at 8.00 till the late afternoon 18.00; with a lunch break from 13.00 to 14.00, and the occupancy is set to zero during these breaks.

3.1.3.   Internal boundaries

As the internal space under analysis is just hypothetic and not based on an existing office, also for the properties of the internal surfaces the LEED specifications are taken as reference.

"CS only if the finishes in the space will not be completed, use the following default surface reflectances: 80% for ceilings, 20% for floors, and 50% for walls" [34].

As reported in the specific paragraph the solver behind DIVA daylight components is DAYSIM, a validated daylighting analysis software based on the RADIANCE backward raytracer. Therefore, the materials are defined through the Radiance primitives format.

The materials Radiance strings used to follow the prescriptions were taken from the DIVA library and are here reported:

- Ceiling: It is a purely diffuse reflector with a standard ceiling reflectance of 80%.

```
void plastic GenericCeiling_80
0
0
5 0.8 0.8 0.8 0 0
```

- Floor: It is a purely diffuse reflector with a standard floor reflectivity of 20%.

```
void plastic GenericFloor_20
0
0
5 0.2 0.2 0.2 0 0
```

- Walls: It is a purely diffuse reflector with a standard grey wall reflectivity of 50%.

```
void plastic GenericInteriorWall_50
0
0
5 0.5 0.5 0.5 0 0
```

The choice of the glazing material was led by the location and orientation of the module, which is deepened in the following paragraph. One of the options presents in the library has been chosen, in particular, it is a Low-e double glazing with argon in the cavity:

```
# Glazing_DoublePane_LowE_Argon:
#Tau_vis = 0.65; SHGC= 0.27;
#U-Value= 1.32W/m2K
# visual transmittance: 65%
# visual transmissivity: 71%

void glass Glazing_DoublePane_LowE_Argon_65
0
0
3 0.71 0.71 0.71
```

3.1.4.   Location and orientation

The whole script of the simulation refers to an EPW file for the weather data of the selected location. Therefore, the workflow can be applied to any location just by changing the reference file.

The location chosen is Milan, in Italy, since the Case Study that will be analysed in the following chapters is here located.

As previously mentioned, the considered module is facing south, despite thanks to the parametric nature of the geometry definition it is easy to change it as the location, follows the representation of the sun-path and the sun positions during the Solstices and Equinoxes at 12:00.

The pictures are taken from the DIVA tool, which provides also the solar altitude.
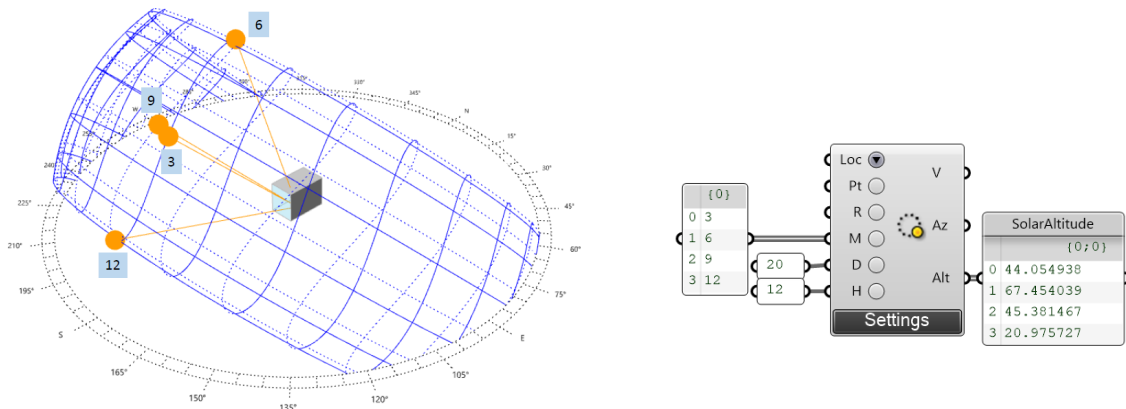
Figure 19 Module orientation and exposition to the sun path.

3.1.5.   Simulation quality

The quality of the simulation is defined by setting the Radiance parameters, this point will be deepened in the Sensitivity Analysis subchapter. However here are reported the settings for the Indoor simulations:

RADIANCE PARAMETER	VALUE
-ab	5
-ad	1000
-ar	300
-as	20
-aa	0.1

Table 3 Indoor simulation Radiance Parameter.

3.1.6.   Plane façade _ Opaque-transparency ratio

The first stage of simulation considers the effect of the variation of the ratio between the transparent and the opaque portions in a plane façade. In particular, the configuration is based on ribbon windows, starting from considering only the spandrel made with an opaque material and with the lower opaque portion that will increase until the height of about 1m to guarantee a clear vision on the outside.
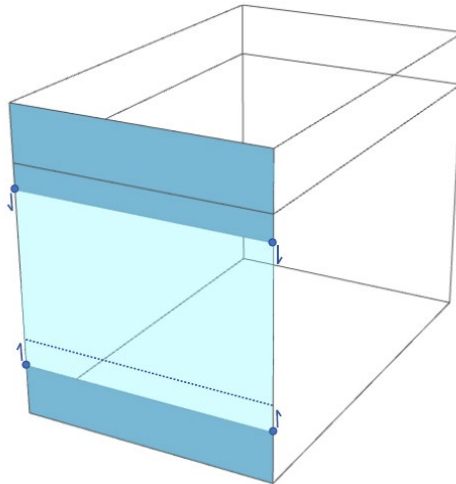
Figure 20 Plane façade _ Opaque-transparency ratio geometry.

3.1.7.   3D façade _ Type 1

The second case takes in consideration a different aspect of the façade system: its 3D geometry. The starting point for the definition of these geometries was the thesis work of Pietro Pavesi titled "*A Parametric Design Workflow Applied To A Responsive Curtain Wall System For Daylight Optimization Of An Existing Building*".

The possible façade shapes would be an infinite number, characterized by different numbers of surfaces and angles. The thesis work is limited to a particular family of geometries, characterized by two control points that can move orthogonally to the façade plane.

Two different rules have been defined for the movement of the control points:

1. The first subfamily is characterized by a fixed-length (L) of the upper panel; therefore, the control points can move along an arc of circumference with radius equal to L.
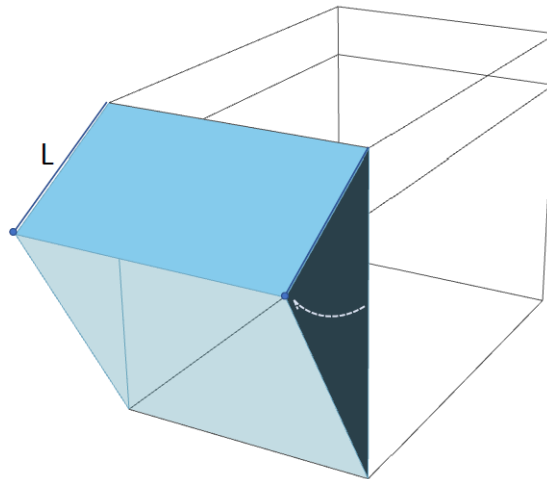
Figure 21 3D façade _ Type 1 subfamily L geometry.

2. In the second group, the fixed parameter is the angle α between the plane of the façade and the upper panel. In this case, the control points are free to move on the lines starting from the vertices of the cell and inclined of α with respect to the vertical.
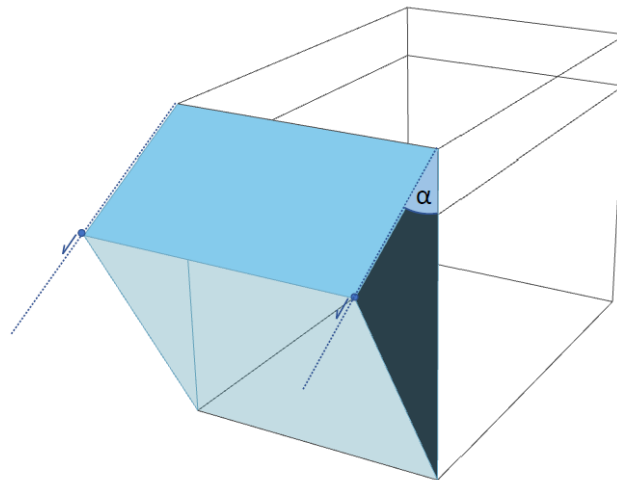
Figure 22 3D façade _ Type 1 subfamily α geometry.

The definition of this geometry can generate some doubts regarding its effect on the surrounding microclimate, especially as concern the areas closer to the façade because the solar radiation reflected by the glazed portion may be concentred and cause local discomfort. For this reason, another subfamily has been introduced:
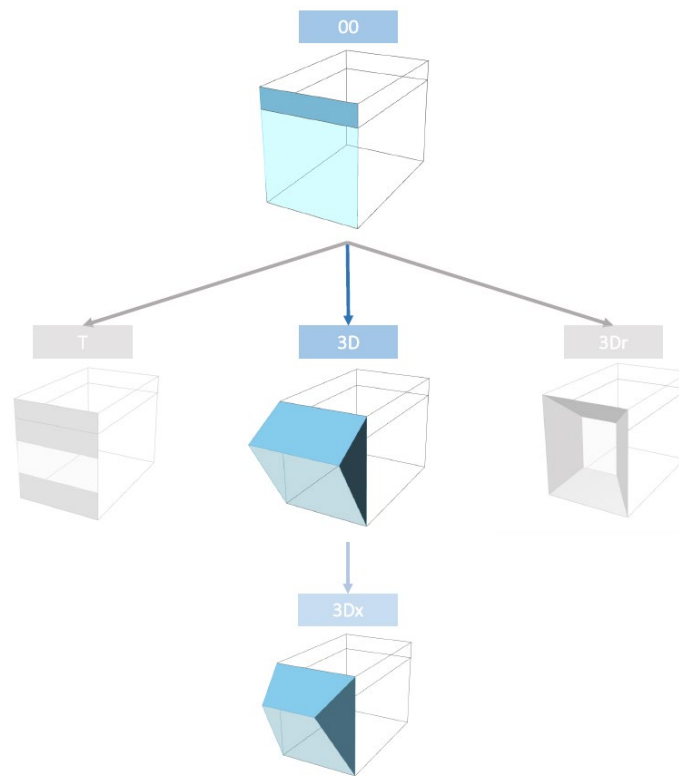
Figure 23 New Façade Geometric Classification.

3. In this third subfamily, the starting point is one of the cases already defined with one of the first two rules. Once the position of the points is fixed in the plane normal to the façade their position in the parallel plane is taken in consideration.
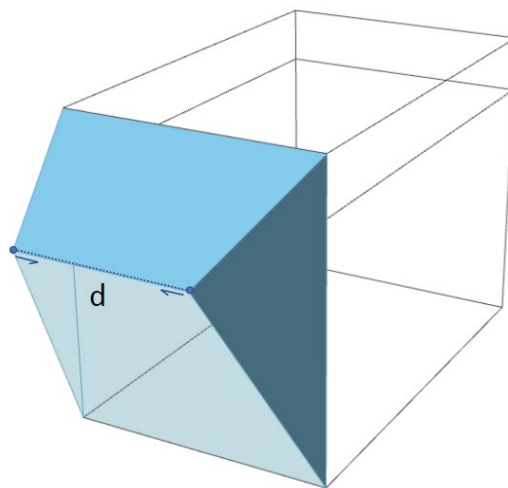
Figure 24 3D façade _ Type 1 subfamily d geometry.

51

3.1.8.   3D façade _ Type 2

The last stage of analysis considers again a façade geometry that evolves in 3D, but in this case following a different rule. The control points are the 4 vertices of the facade module that can move towards the centre of the module and back with respect to the facade plane.
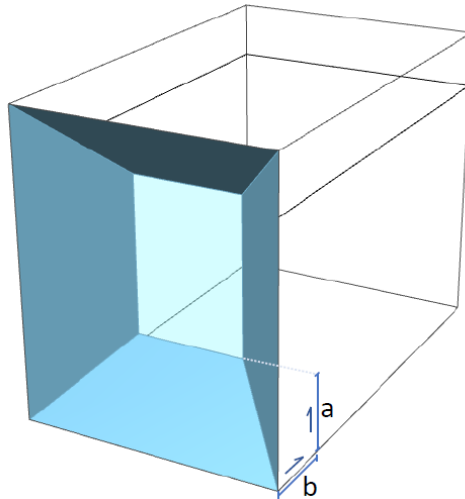
Figure 25 3D façade _ Type 2 geometry.

Again, this definition tries to reduce the solar radiation reflected by the glazed façade on the urban environment in front of the designed building but introduces the topic of the increased reflection of the opaque material directly on the square. It differs from the other geometries for the shape of the window but ensures the same daylight comfort standard.

3.2. Materials

For the purpose of the workflow, the materials need two different definitions: one for the Thermal simulation and one for the Radiation simulation.

To calculate the external surface temperature, it is necessary to know the materials that compose the building envelope and all the urban surfaces and their characteristics, in particular:

- the thickness,
- the conductivity,
- the density,
- the specific heat capacity,
- the absorbance.

This last parameter is the only one that links the thermal and the optical definition of the envelope material. Indeed, it depends on the reflectance and transmittance, both characteristics defined in the Radiance primitives for each material.

In the normal application, the definition of the materials in Radiance the reflectance value only concerns the visible portion of the radiation, but for the application in this work, the reflectance value includes the total incident solar radiation, as the goal is to evaluate its effect on the thermal sensation on the subjects. The solar reflectance of a surface is variable in time and place, as function of atmospheric conditions and solar position change, assuming constant albedo (solar reflectance) values, it is assumed spectral and angular independent[11].

The definition of the optical properties of the materials is the same for DIVA and Honeybee since they both are based on a Radiance library and at the same time allows the user to use custom Radiance definitions. For the indoor daylight analysis, the materials are defined in the previous paragraphs and are fixed by the LEED standard, while for the outdoor simulations will be defined following the prescriptions here reported.

One often-cited quality of Radiance is that it is physically based and capable of simulating complex geometries with flexible reflection and transmittance material properties using a mixed stochastic, deterministic backward raytracing algorithm. The ability to model specular components constitutes an advantage over radiosity-based simulation approaches which treat all surfaces as Lambertian diffusers. Radiance's scientific reputation is further founded on a series of independent validation studies [41].

3.2.1.   Thermal calculation Material definition

The materials that compose the building envelope and all the urban surfaces are considered as uniform for all their thickness, therefore the characteristics are considering a typical stratigraphy. The only varying parameter is the absorbance of the opaque elements of the façade, as the finishing material is changing according to the Radiance definition.

The materials used for the simulations of the T_{sup} are:

- Asphalt for the streets,

- Soil for flowerbeds,

- Standard glass for the transparent parts of the façade under consideration,

- A stratigraphy with standard thermal characteristics for the opaque parts of the façade and the context and with absorbance that depends on the characteristics of the finish.

The properties of the materials used are summarized in the tables shown here.

Asphalt	
Thickness [m]	0.5
Conductivity [W/mK]	0.75
Density [kg/m^3]	2360
Specific Heat Capacity [J/kgK]	960
Absorbance [-]	0.9

Table 4 Thermal properties of the asphalt [42].

Soil	
Thickness [m]	0.5
Conductivity [W/mK]	0.32-4
Density [kg/m^3]	2050
Specific Heat Capacity [J/kgK]	800-1480
Absorbance [-]	0.5

Table 5 Thermal properties of the ground [42].

Generic Façade	
Thickness [m]	0.3
Conductivity [W/mK]	0.84
Density [kg/m^3]	1700
Specific Heat Capacity [J/kgK]	840
Absorbance [-]	0.65

Table 6 Thermal properties of the generic façade [20] *(and honeybee library material definition).*

Opaque Façade	
Thickness [m]	0.15
Conductivity [W/mK]	0.08
Density [kg/m^3]	400
Specific Heat Capacity [J/kgK]	840
Absorbance [-]	1 − Rsol

Table 7 Thermal properties of the opaque façade [42] *(and honeybee library material definition).*

Glass	
Thickness [m]	0.04
Conductivity [W/mK]	0.09
Density [kg/m^3]	3000
Specific Heat Capacity [J/kgK]	840
Transmittance [-]	0.65

Table 8 Thermal properties of the glass [42] *(and honeybee library material definition).*

3.2.2.   Radiance Material Definition

To run the daylight simulation, the optical properties of the materials are considered. Their definition has been done using the radiance default script, which uses different parameters according to the type of material considered.

The material definition has been done following the Radiance guidelines for materials [43], which distinguish the definition according to the type of material, in this specific case we will consider Normal materials and Glass.

The first group considers opaque and translucent materials, they are characterized by a diffuse and specular component, a colour, and a roughness factor. A purely specular material would have a roughness factor of Ø. A totally diffuse material is treated as a Lambertian surface. For the object of this work, only opaque materials will be considered.

The Glass material is part of the dielectric materials, which are transparent materials that refract and reflects light, such as water or crystal. The material thus has an index of refraction and a specific spectral absorbance.

Opaque materials

The opaque materials include plastic and metal, the format for the script of their primitive is the same, but the definition of their optical properties is different.

```
modifier  plastic/metal  identifier
Ø
Ø
5  R  G  B
 spec rough
```

The definitions provided by the Radiance user manual are:

"Plastic is a material with uncoloured highlights. It is defined by a red, green, and blue reflectance value, a specularity value and by a roughness value. A positive roughness value will display highlights (uncoloured by the materials modifier) but not show any reflections from other objects."

"The metal material is similar to plastic except that its highlights are modified by the material colour."

Hence, the plastic material is considered as a diffuse material, a roughness value of 0 corresponds to a perfectly smooth surface, and a value of 1 would be a very rough surface. Specularity fractions greater than 0.1 and roughness values greater than 0.2 are not very realistic.

Instead, the reflectivity of the metal material depends on the RGB values that can vary from 0 to 1 (0-100%). Acceptable values for specularity and roughness are relatively between 0.5 1 and 0 and 0.5.

Glass

As previously specified the glass is a specific type of dielectric material.

The dielectric primitive is defined by the RGB transmission in each wavelength and by its index of refraction. An optional parameter, the Hartmann constant, (which is usually zero) describes how the index of refraction changes as a function of wavelength.

```
Modifier  dielectric  identifier
Ø
Ø
5  R  G  B
   n HC
```

The glass material definition provided by the Radiance user manual is:

"The glass type primitive is a specially modified dielectric. The material has been optimised to only produce one reflected ray and one transmitted ray through a single thin surface. In this way internal reflections are avoided. The glass type has a standard refractive index of 1.52 and all that is needed to be defined is the transmission at normal incidence."

And its primitive is:

```
modifier  glass  identifier
Ø
Ø
3  R1  G1  B1
```

Primitives Definition for the Simulation

For the definition of the materials applied to the opaque parts of the façade the Radiance Material components for metal and plastic materials by Honeybee are used.

This component allows to generate a proper primitive giving as input the RGB Reflectance, Specularity, and Roughness of the material.
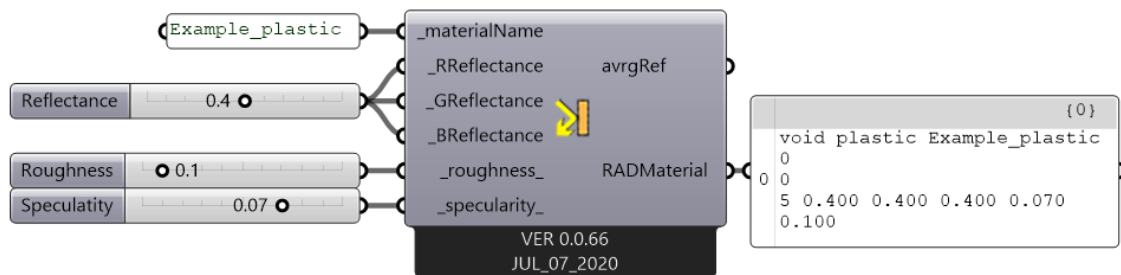
Figure 26 Honeybee Radiance Metal Material component.
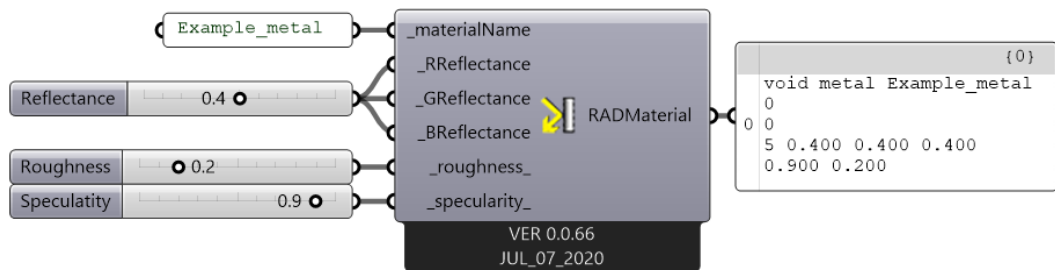
Figure 27 Radiance Opaque Material component.

Thanks to these components the definition of the material is parametric and allows to analyse them coupled with the different façade configurations generating a matrix of cases to analyse. In the next chapter, a pre-analysis will be performed to reduce the number of possible cases, considering the limits for each parameter set by the nature of the materials and the effect on a sample area in front of an ideal panel in terms of received radiation.

In the outdoor analysis also the context will assume a certain importance on the comfort of the area object of study, to avoid the variability of the influence of the envelope of the surrounding buildings their material will be fixed for all the analysis, both for the thermal and radiance definition. In particular, the optical properties of the opaque façades will be the ones of a generic façade, chosen from the DIVA library.

```
# material name: OutsideFacade_35
# material type: opaque
# comment: This is a purely diffuse reflector with a
standard reflectivity of 35%.
# author: Christoph Reinhart
void plastic OutsideFacade_35
0
0
5 0.35 0.35 0.35
  0 0
```

It is a plastic material, therefore it behaves as a Lambertian surface, a purely diffuse reflector material.

For the glazed façade the material has already been set during the module boundaries definition, it is considered fixed for all the cases and it has been chosen from the DIVA library. The choice was guided by the location and orientation of the module and should be changed according to the case of application of the simulation workflow.

As reminder here reported the chosen glass primitive:

```
# Glazing_DoublePane_LowE_Argon:
#Tau_vis = 0.65; SHGC= 0.27;
#U-Value= 1.32W/m2K
# visual transmittance: 65%
# visual transmissivity: 71%

void glass Glazing_DoublePane_LowE_Argon_65
0
0
3 0.71 0.71 0.71
```

3.3. Outdoor Simulation Methodology

This section is a brief presentation of the steps that must be followed in order to perform the outdoor simulation, it will be deepened in detail at the beginning of the Case Study chapter.

Once the study area is chosen and analysed in detail, a 3D model can be built. This model can be constructed all in Grasshopper or the fixed parts can be modelled in Rhino and then internalized and integrated with the parametric definition of the façade modules. It is important to remember that the focus of the analysis is the urban microclimate, therefore the model should include only the elements that can directly influence the conditions of the studied area.

The second stage is to define the analysis period. If the goal is to perform the simulation for the significant days and hours, a weather analysis is fundamental to understand how the conditions of the selected locations vary during the year. It is also important to analyse the context of the Case Study in order to understand the profiles of the users of the area and their needs during the different hours of the day and in the different seasons. According with this second step of the analysis, the subject and the consequent human model are defined.

The analysis is based on the EPW file of the available location nearest to the Case Study. Together with the analysis period is the base for the radiation analysis and from this file the climatic parameters, necessary to perform the other steps of the simulation, are

extracted, always according to the analysis period. The necessary parameters for the UTCI definition are the Air Temperature, the Relative Humidity, the Wind Velocity, while for the lw MRT estimation are the Air Temperature and the horizontal infrared radiation. The other ambient parameter needed for the lw MRT computation is the Indoor Air Temperature, which is a parameter fixed by the designer. In this work, the proposed reference is the Annex B of ISO 17772-2:2017 "*Recommended criteria for the thermal environment*"[44].

At this point is necessary to fix the Test Points. Despite a grid that covers all the area is always an option, this solution would require a long simulation time and provide a high number of information that may not be all necessary to represent the comfort on the area. The proposed definition for the Test Points is based on a polar reference system and takes into account only the significative points to analyse the influence of the façade. The reasons behind this choice are well explained in the presentation of the Comfort Analysis.

Lastly, the Radiance parameters setting, that defines the quality of the simulation, should be considered. The choice must be done according to the Sensitivity Analysis made on a test geometry in the next subchapter, considering the type of simulation that is performed.

3.4. Sensitivity Analysis of Radiance Parameters

As explained in the introduction one of the greatest strengths of choosing Grasshopper as base software for the simulations is that it gave the chance to perform all the required analysis in the same environment, both for indoor and outdoor comfort.

In particular, both the Honeybee (used for the radiation analysis that is the basis of the simulations for the calculation of the MRT and consequently the assessment of outdoor comfort) and DIVA (that directly provides the components for the lighting analysis and the comfort index evaluation) tools are based on the same calculation engine, Radiance.

Radiance achieves accurate results in a reasonable time by implementing a hybrid approach of deterministic ray tracing and the Monte Carlo method. The process applied is known as backward raytracing, in which the simulation engine takes a measurement point and traces the light beam back to the light source. There are three main sources for the calculations: the diffuse indirect component, the mirror indirect component, and the direct component.

Using Radiance through other programs, like in this case, allows the user to set a limited number of inputs and set up most of the simulation automatically. Among the required inputs to perform the simulation, what defines the quality of the results are the Radiance parameters.

Radiance allows users to set simulation parameters based on the geometry and position or size of the elements in the reference space. A wrong choice of these parameters can considerably affect the results. Therefore, before starting the simulation process, a literature review of the rendering options and a sensitive analysis have been performed.

The rendering options can be broken into four categories [45]:

- View Options
- Ambient Simulation Parameters
- Direct Simulation Parameters
- Other options

Ambient simulation parameters have been proven to affect the rendering time and the accuracy of results in a significant way [46]. This section includes five parameters (Table 9) that, according to the literature, have been identified as critical both for the precision of the results and for the simulation time and that will be the main subject of this subchapter.

RADIANCE PARAMETERS		DESCRIPTION
ab	AMBIENT BOUNCES	The number of diffuse bounces in the indirect calculation.
ad	AMBIENT DIVISION	The number of sample rays sent out into the hemisphere.
ar	AMBIENT RESOLUTION	Adjust the limit beyond which the accuracy of the indirect calculation will relax.
as	AMBIENT SUPER SAMPLES	The number of extra samples used for areas of high variability in the hemisphere.
aa	AMBIENT ACCURACY	The maximum error permitted in the indirect calculation.

Table 9 Ambient simulation parameters.

3.4.1. Parameter Setting

Due to the nature of the workflow and the consequent script, that includes two different scale of analysis, the required set of parameters should be consistent for both outdoor and indoor simulations.

Following is reported the Standard Set of Ambient simulation parameters used in the thesis work together with the level of accuracy of each parameter according with the general recommendation of the Radiance website:

RADIANCE PARAMETER	VALUE	LEVEL OF ACCURACY
-ab	5	> Accur
-ad	1000	> Accur
-ar	300	> Accur
-as	20	< Fast
-aa	0.1	> Accur

Table 10 Standard Set of Ambient parameters.

In the evaluation scale of the parameters provided the "fast" value gives a reasonably fast rendering, while the "accur" value gives a reasonably accurate rendering.

According with the literature, this set guarantees a good compromise between computational time and result accuracy [47][48] and is comparable with the set provided by DIVA for a Medium level of quality.

3.4.2.   Sensitive Analysis Through A Base Case

Starting from the set exposed a sensitivity analysis will be performed considering four of the Ambient simulation parameters: ambient bounces, ambient division, ambient resolution, ambient super samples, ambient accuracy.

The analysis is carried starting from the Base Cases for the indoor daylight analysis.

The room considered the is the IEA BESTEST test case taken from ANSI/ASHRAE Standard 140 [49], a rectangular single zone (8m wide x 6m long x 2.7m high) with an external wall on the side with the windows and adiabatic partitions on the three left sides.
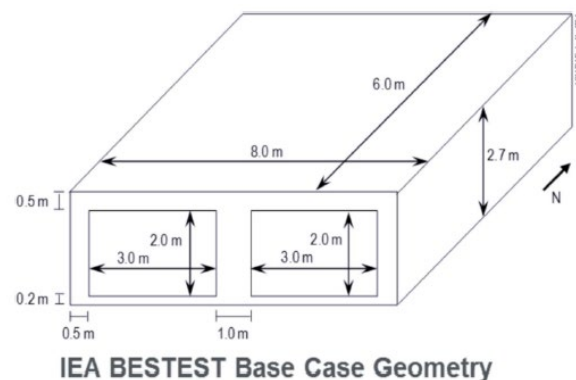
Figure 28 Indoor Base case geometry.

The analysis performed follows the methodology exposed in the Façade Configurations section, here are briefly summarized the settings.

According to the LEED prescriptions the room for the analysis has been designed as follow:

- *Period of Analysis:* The designs are evaluated from 9:00 to 18.00 during the working days with a lunch break from 13.00 to 14.00.

- *Analysis Points:* the analysis grid is 50 cm x 50 cm with a distance from the boundaries of 50 cm, at a height of 80 cm above the floor.

- *The default surfaces reflectance:* 80% for ceilings, 20% for floors, and 50% for walls.

- *Windows light transmittance*: 65%.

The base case is located in Milan, as the Case Study, with the windows facing south.

For the evaluation on the outdoor, this volume will be multiplied as shown in Figure 29 in order to create a significative building. To emphasize the impact of the façade on the

radiation hitting the adjacent area and to be more coherent with the Case Study of this thesis, it has been considered as an all-glazed continuous system.
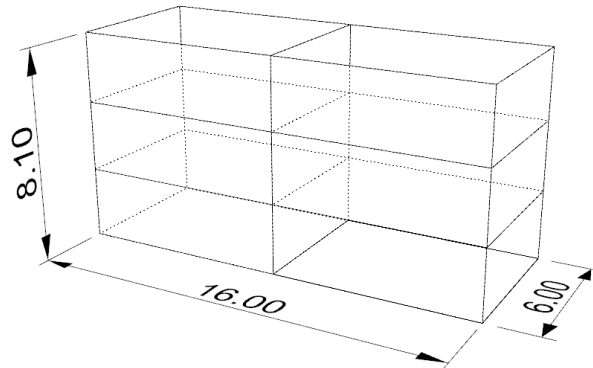
Figure 29 Outdoor Base Case geometry.

The 16x16 m study grid is divided into 1x1 m squares and is placed at 1.1 m from the ground to consider the offset of the human body, and at 1m from the façade.

Before proceeding with the actual analysis, it is important to remember that Radiance uses a Hybrid Deterministic/Stochastic Ray Tracing method, which means that performing twice the same simulation the results may be different. This method is explained by Gregory J. Ward in "The RADIANCE Lighting Simulation and Rendering System". Essentially, Radiance uses ray tracing in a recursive evaluation of Kajiya's rendering integral equation at each surface point. "Although it is possible to approximate a solution to this equation using uniform stochastic sampling (i.e. Monte Carlo), the convergence under most conditions is so slow that such a solution is impractical. [...] The key to fast convergence is in deciding what to sample by removing those parts of the integral we can compute deterministically and gauging the importance of the rest so as to maximize the payback from our ray calculations."

In the following tables the results and the error, relating to the Standard Set of the simulations performed varying the parameters, are reported. Being already values that provides an accurate rendering for each parameter a more precise and a less precise value will be considered. The only exception is -as whose value in the Standard Set is recommended for a fast rendering, for this parameter the value recommended for an accurate level of precision and a higher value are considered.

Rad Par	sDA	ASE	Average solar radiation (kWh/m²year)	Max solar radiation (kWh/m²year)
Standard Set	100	31.4	1033.79	1070.39

Table 11 Results for the Standard Set.

Rad Par	sDA	ASE	Average solar radiation (kWh/m²year)	Max solar radiation (kWh/m²year)
-ab 3	99.3	31.4	1033.60	1062.62
	0.700%	-	0.018%	0.726%
-ab 7	100	31.4	1033.98	1064.85
	-	-	0.018%	0.518%

Table 12 Results for the -ab variation.

Rad Par	sDA	ASE	Average solar radiation (kWh/m²year)	Max solar radiation (kWh/m²year)
-ar 128	100	31.4	1033.97	1062.36
	-	-	0.017%	0.750%
-ar 512	100	31.4	1034.02	1067.96
	-	-	0.023%	0.227%

Table 13 Results for the -ar variation.

Rad Par	sDA	ASE	Average solar radiation (kWh/m²year)	Max solar radiation (kWh/m²year)
-aa 0.15	100	31.4	1034.04	1065.56
	-	-	0.024%	0.451%
-aa 0.08	100	31.4	1034.74	1063.71
	-	-	0.091%	0.624%

Table 14 Results for the -aa variation.

Rad Par	sDA	ASE	Average solar radiation (kWh/m²year)	Max solar radiation (kWh/m²year)
-as 256	100	31.4	1034.21	1064.03
	-	-	0.041%	0.594%
-as 512	100	31.4	1035.16	1057.67
	-	-	0.132%	1.188%

Table 15 Results for the -as variation.

Rad Par	sDA	ASE	Average solar radiation (kWh/m²year)	Max solar radiation (kWh/m²year)
-ad 512	100	31.4	1034.60	1073.76
	-	-	0.078%	0.315%
-ad 2048	100	31.4	1034.50	1060.32
	-	-	0.069%	0.941%

Table 16 Results for the -ad variation.

The first focus for the analysis of the results is on the Indoor. The only parameter that affects the indexes is -ab that, as predictable, reducing the number of bounces reduces also the illuminance available and consequently the sDA percentage. What is significant is that between the standard -ab and the increased value there is no difference, meaning that the first one is already enough to provide reliable output.

The other parameters do not affect the indexes' values, but this doesn't mean that there are no changes at all in the illuminance values. Following are reported the illuminance distributions on the grid for the base case and then for the other cases.

65

-ar 128

-ar 512

-aa 0.15

-aa 0.08

-as 256

-as 512

-ad 512

-ad 2048
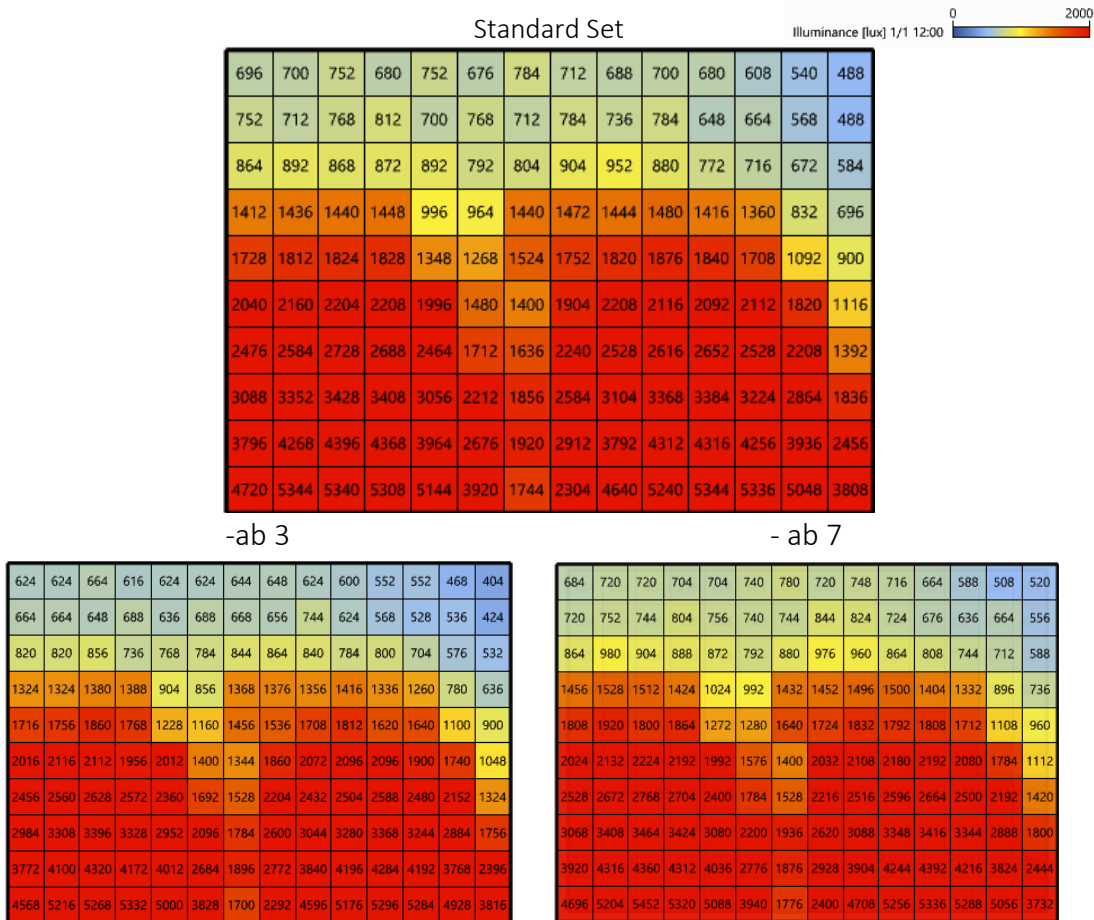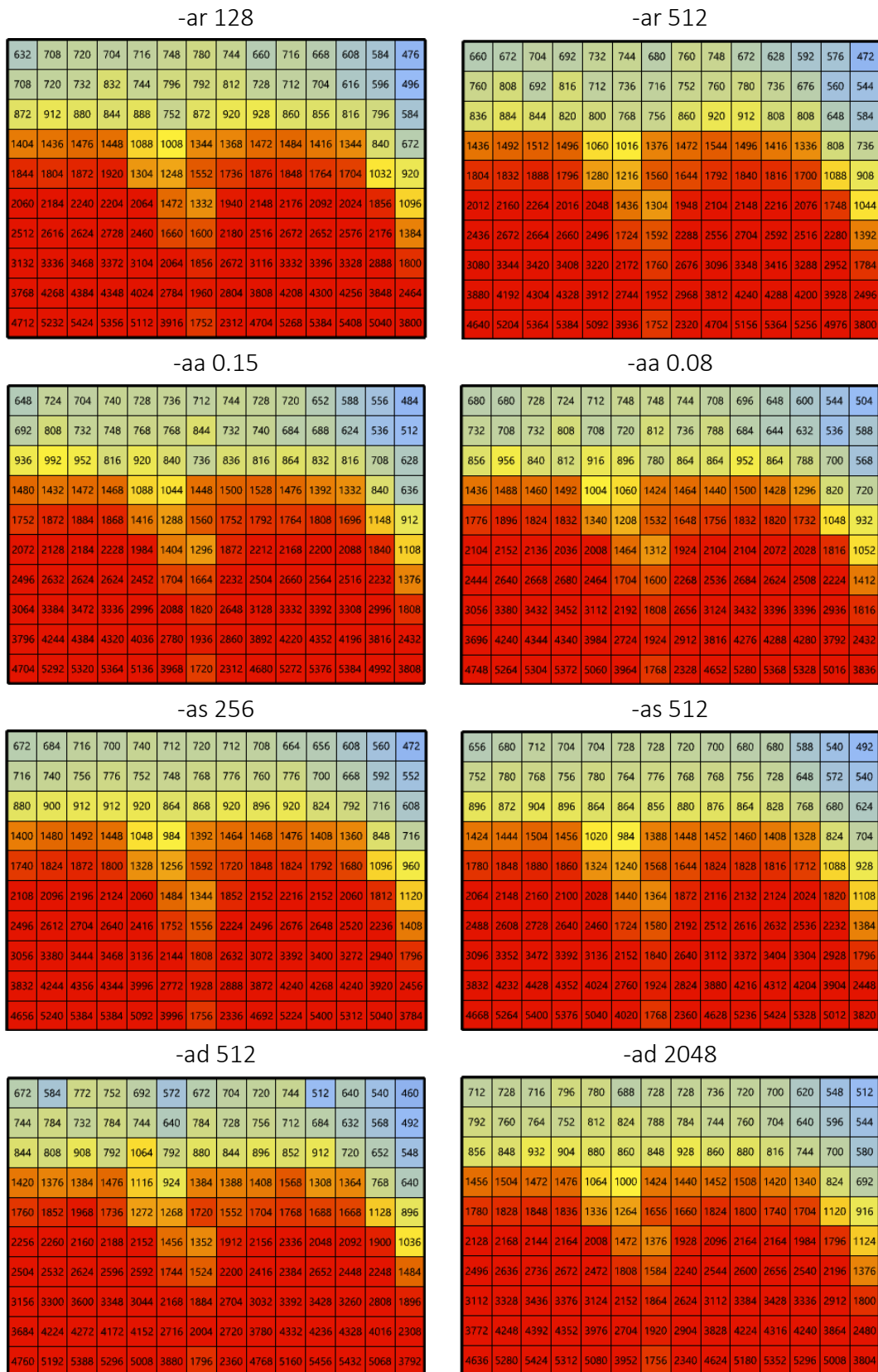
Figure 30 Illuminance distribution on the indoor grid for all the cases.

However, as the variations do not influence the indexes, increment the precision is not significant in this analysis.

The second focus is on the Outdoor, for this environment the metrics considered are the annual kWh/m^2 and in particular the average and the maximum values on the grid.

As previously mentioned, the nature of Radiance implies an intrinsic error for each time that a simulation is performed (with the same settings). In the following table the results of four simulations performed with the Standard Set of parameters and the variations, relative to the first one, are reported.

	Average solar radiation (kWh/m^{2}year)	Max solar radiation (kWh/m^{2}year)
Simulation 1	1033.79	1070.39
Simulation 2	1033.438	1070.37
	0.034%	0.002%
Simulation 3	1033.411	1064.31
	0.037%	0.568%
Simulation 4	1033.545	1066.05
	0.024%	0.405%

Table 17 Results for the repeated simulation with the Standard Set.

This error must be considered in evaluating the variation of the parameters. There is also an implication in the distribution on the grid, even though we should remember that the scale used to emphasize it.
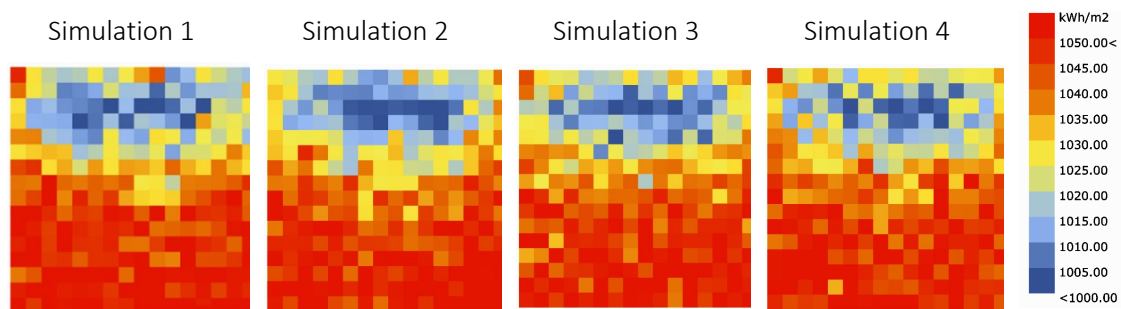
Figure 31 Annual irradiance distribution on the outdoor grid for all the repeated simulations.

Keeping this in mind the variations registered in the previous analysis, changing the Radiance parameters, are not significant.

To show the effect on the outdoor comfort evaluation, and to report a metric on which everyone can have a higher sensitivity, here are reported the short wave contributions in

the MRT computation arising from the previous analysis (the reflectance of the ground is not considered). Therefore, each parameter is varied maintaining the other fixed.

Rad Par	AV	MAX
Standard	37.922	39.264
-ab 3	37.915	38.979
-ab 7	37.929	39.061
-ar 128	37.928	38.970
-ar 512	37.930	39.175
-aa 0.15	37.931	39.087
-aa 0.08	37.956	39.019
-as 256	37.937	39.031
-as 512	37.972	38.798
-ad 512	37.951	39.388
-ad 2048	37.948	38.895

Table 18 sw MRT values corresponding to the parameters variation.

The variation in percentage with respect to the Standard case is the same reported for the annual irradiance values. Analysing the MRT values the conclusion is that the difference registered is not significant, therefore the Standard Set of parameters can be considered optimal for this outdoor analysis.

For completeness are reported the annual kWh/m2 distributions on the grid resulting from the study.
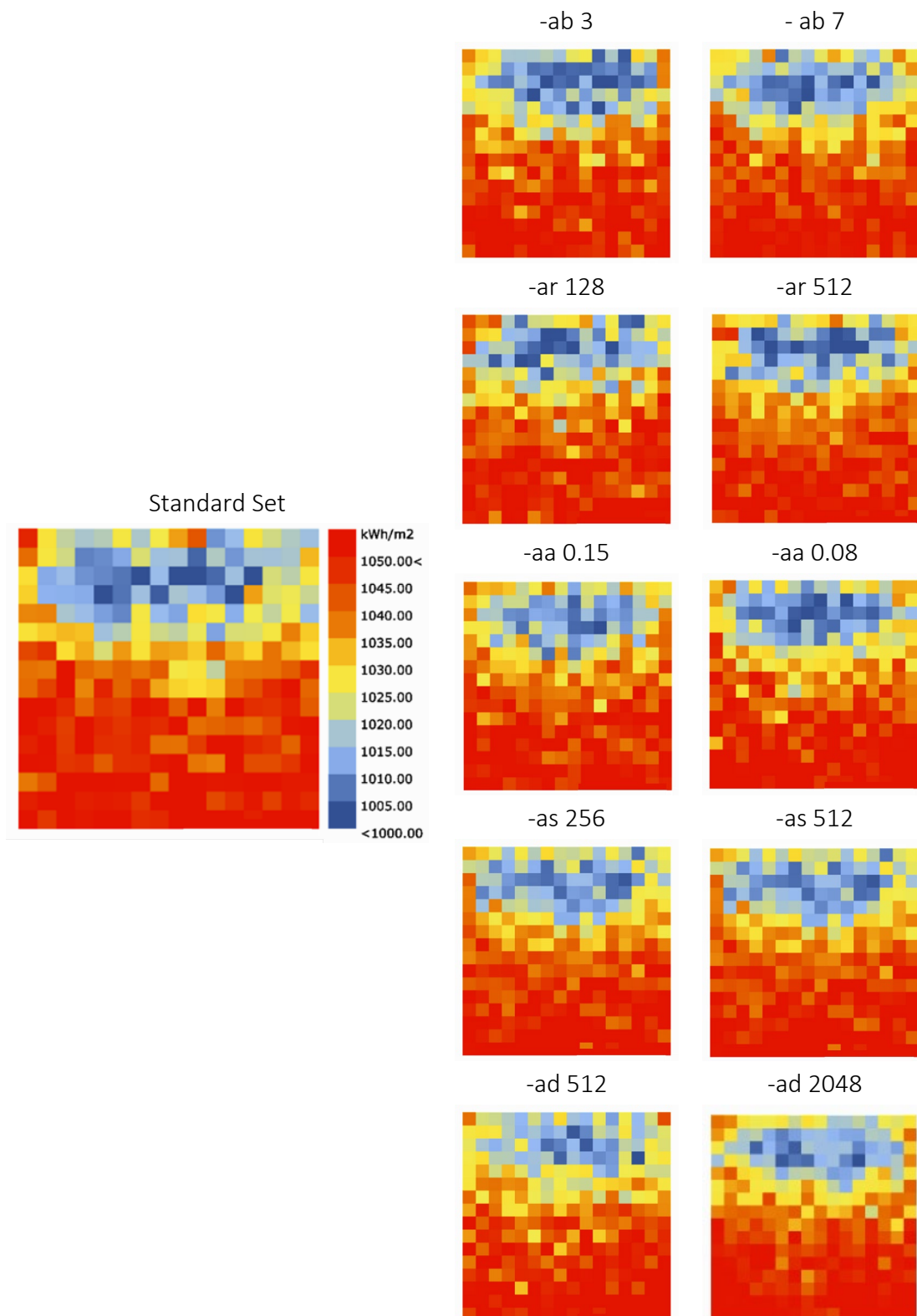
Figure 32 Annual irradiance distribution on the outdoor grid for all the parameters variations.

This last paragraph is focused on the outdoor simulation. Until now the parameters have been considered one at the time but, generally, they are related to each other, thus four different sets are tested. For example, the ar-aa combination defines the resolution of the scene. It is important to remember that the resolution of the scene is function of these parameters and of the scene scale. The sets that will be applied to the Case Study in this research work will be verified also in this sense.

Among the previously evaluated Radiance Parameters three of them have been modified simultaneously in order to create the new sets of parameters, two less accurate, but faster, and the others with higher precision.

RADIANCE PARAMETER	SET 1	SET 2	SET 3	SET 4
-ab	3	3	5	7
-ar	13	128	512	512
-aa	0.1	0.1	0.08	0.08

Table 19 Set 1 and Set 2 of Ambient parameters.

The aim of this section is to evaluate the timing of these Sets for the variation in the computed values:

Rad Par	Average solar radiation (kWh/m^{2}year)	Max solar radiation (kWh/m^{2}year)	Timing
Standard	1034.561	1067.57	2 m 28 s
Set 1	1033.429	1073.4	0 m 25 s
	0.109%	0.546%	
Set 2	1033.525	1070.52	0 m 26 s
	0.100%	0.276%	
Set 3	1034.41	1054.37	7 m 10 s
	0.015%	1.236%	
Set 4	1034.457	1054.79	7 m 55 s
	0.010%	1.197%	

Table 20 Results for the parameters Set1 and Set 2.

All the cases present a very low distance from the results of the Standard one. The distance increases for the Maximum for the sets with higher accuracy but is such a small difference that its influence on the comfort evaluation is negligible.

Following are reported the sw MRT contribution calculated with the different sets to show the limited impact of the different sets.
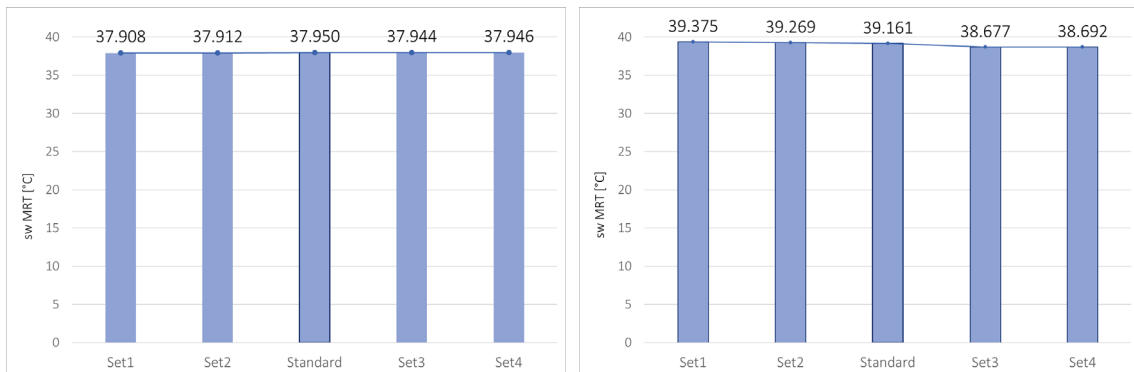
Graph 1 MRT$_{sw}$ contribution calculated with different Radiance Parameters sets.

The real influence is visible on the distribution of the radiation the grid, increasing the accuracy of the parameters the distribution is less dispersed.
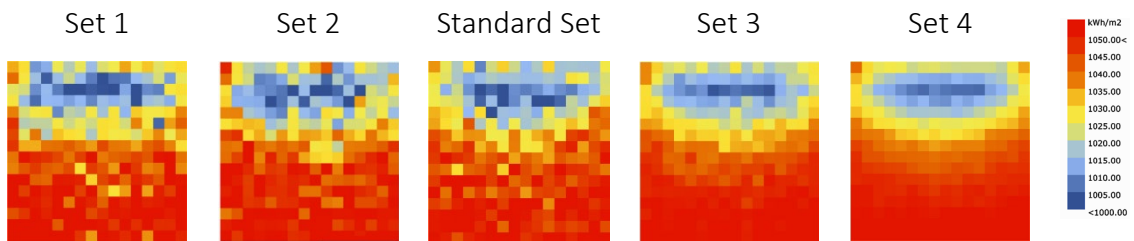
Figure 33 Annual irradiance distribution on the outdoor grid for Set 1, Standard Set, and Set2.

In this base case, whit the Standard Set, the simulation last 2 minutes and 28 seconds, but in the real Case Study, the bigger scale and the presence of obstacles due to the urban context the duration of the computation can increase significantly, hence even though the times here reported may seem fast for all the sets they should be evaluated only in proportion to the first one.

Sets 1 and 2 decreases the timing to $1/5 - 1/6$ of the standard one, while sets 3 and 4 triple the computational timing.

The conclusion is that for a broad-spectrum study in which the configurations to analyse are a high number the Standard Set can be substituted with the Set 2. On the other hand, Set 3, which needs a lot of time and whose results do not deviate significantly, should be used for those cases that need a high render resolution.

4

PRE-ANALYSIS

STUDY OF THE FAÇADE CONFIGURATIONS AND MATERIALS APPLICATION FOR THE DEFINITION OF THE SIMULATION MATRIX

4.   PRE-ANALYSIS

Before proceeding to apply the described workflow to the Case Study to evaluate the effect of the façades on the thermal comfort of the surroundings it is necessary to fix the cases that are going to be applied.

To define the matrix of the simulations that will be performed, the number of possible geometric configurations and of materials that can be used for the opaque portions must be reduced. To be able to do that a pre-analysis is performed following the methodologies exposed in the previous chapter.

As regards the indoor visual comfort the LEED standard is used to evaluate the geometric configurations, but, as no shading system is considered for the reasons already explained, the ASE limit imposed by the standard is increased up to 30%.

For each family, a different procedure for the identification of the best cases is applied according to the rule that defines them, despite the analysis for the indoor comfort follows the already mentioned methodology for all of them.

In the second section, the materials are considered. An annual radiation analysis is performed to understand the influence of an ideal panel exposed as the façade module. Among all the possibilities for the two families of materials considered, Plastic and Metal, the selection is done to represent all the possible architectural choices.

4.1. Façade configuration analysis

4.1.1.   Plane façade _ Opaque-transparency ratio

This configuration is based on ribbon windows, starting from considering only the spandrel made with an opaque material and with the lower opaque portion that will increase until the height of about 1m to guarantee a clear vision on the outside.

Starting from the configuration in which the module is considered all glazed, the percentage of transparency is 100% (T.0), taken as a reference case, all the percentages of transparency have been analysed with a step of 10%.
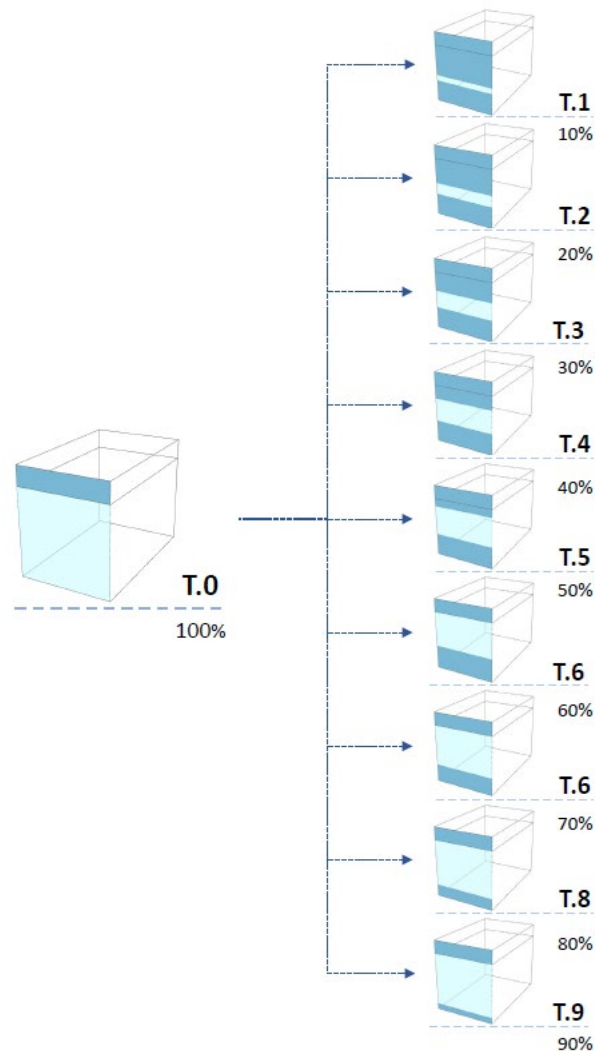
Figure 34 Opaque-transparency ratio configurations.

The maximum height of the parapet is the parameter that defines the cases that can be considered for this family as it influences the position of the window and consequently the daylight performances.

Three cases are defined with a height of relatively 1,0 m, 0,9 m, and 0,8 m.

CASE A   CASE B   CASE C

1,0 m   0,9 m   0,8 m
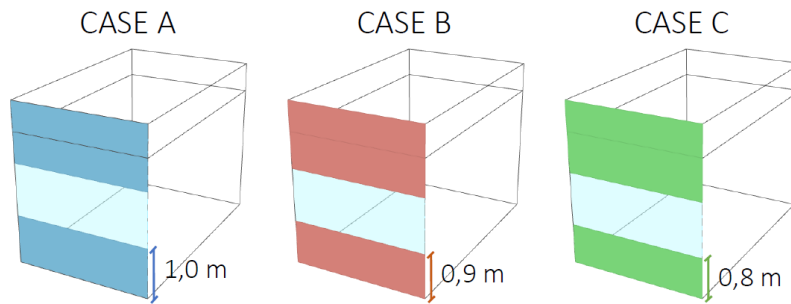
Figure 35 Opaque-transparency ratio sub-cases.

This difference only influences the geometry when the maximum dimension is reached, therefore for the cases with a percentage of transparency from 60% to 90% the results are the same for all three cases.
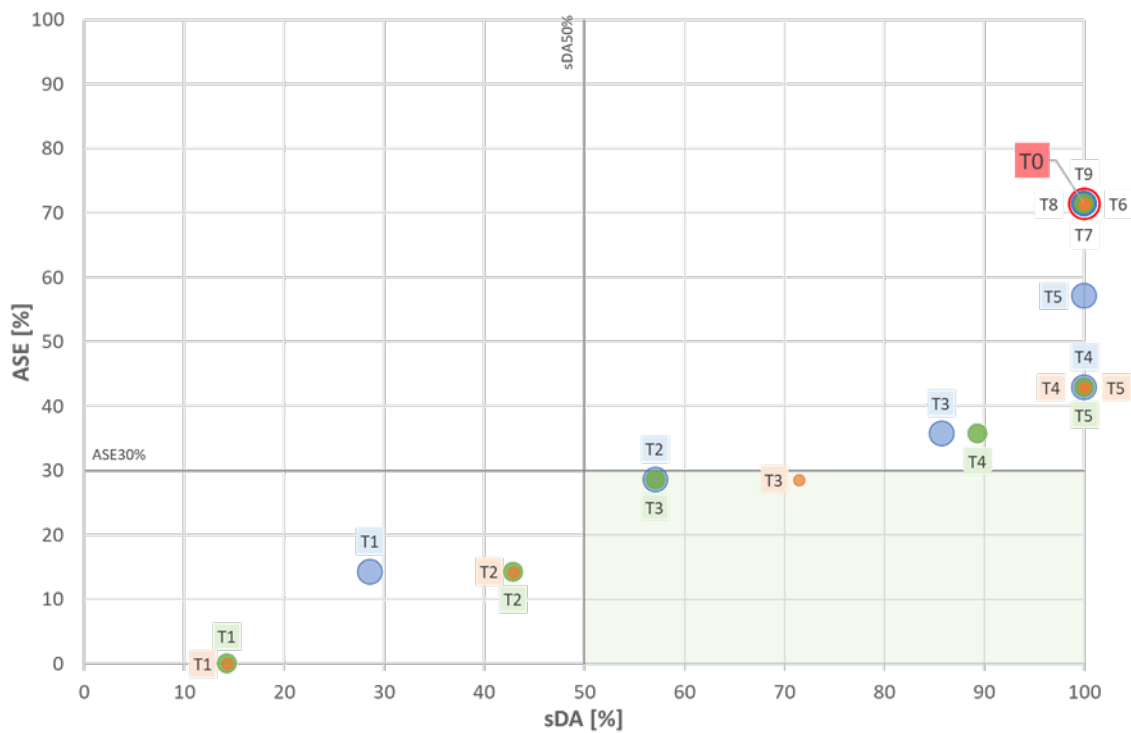
Graph 2 Opaque-transparency ratio sDA-ASE results.

From the results reports in the graph, it is easy to understand that only three configurations respect the limits imposed: T.2 Case A, T.3 Case B, and T.3 Case C.

4.1.2.   3D façade _ Type 1

In this second case, as mentioned in the definition of the rules, the starting point for the definition of these geometries was the thesis work of Pietro Pavesi, for this reason, I decided to follow his procedure of analysis of the geometry. All the analysis has been redone due to the different dimensions of the module considered and for some differences in the methodology procedure.

Subfamily α

The first subfamily is characterized by a fixed-length (L) of the upper panel; therefore, the control points can move along an arc of circumference with radius equal to L.

To understand which is the best length to use as fixed-parameter three cases are considered:
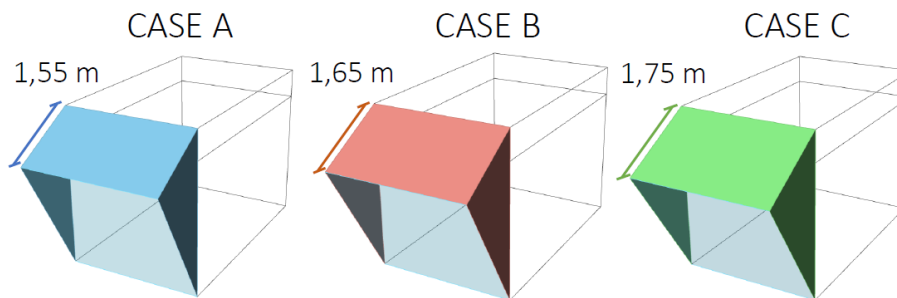
Figure 36 Subfamily α sub-cases.

The cases are analysed for an angle between the façade plane and the upper panel varying from 0° to 90° with a step of 5°.

		L					L		
		1.55 m	1.65 m	1.75 m			1.55 m	1.65 m	1.75 m
α	0°	A1	B1	C1	α	50°	A11	B11	C11
	5°	A2	B2	C2		55°	A12	B12	C12
	10°	A3	B3	C3		60°	A13	B13	C13
	15°	A4	B4	C4		65°	A14	B14	C14
	20°	A5	B5	C5		70°	A15	B15	C15
	25°	A6	B6	C6		75°	A16	B16	C16
	30°	A7	B7	C7		80°	A17	B17	C17
	35°	A8	B8	C8		85°	A18	B18	C18
	40°	A9	B9	C9		90°	A19	B19	C19
	45°	A10	B10	C10					

Table 21 Subfamily α sub-cases coding.

A first selection is done excluding the cases that have an ASE value over 50%.

In the following graph, the results are summarized, a first consideration is that by increasing the angle both indices increase simultaneously.

Considering the three cases it is possible to observe that with the length A the results present in general higher values with tree cases that exceed the ASE limit. While with the length C the results are lower and the cases that exceed the ASE limit are two, but four cases become not acceptable because the sDA values are lower than 50%. The length B guarantees a good compromise with just two unacceptable cases that may be characterized by glare presence.
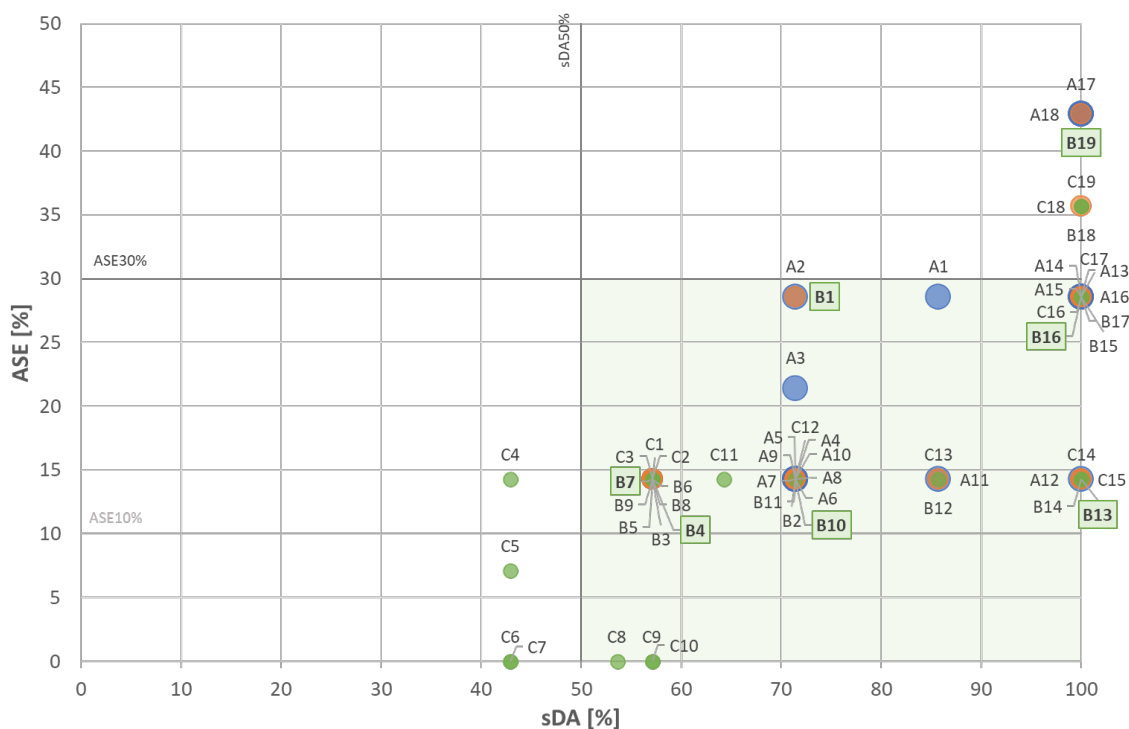
Graph 3 Subfamily α sDA-ASE results.

Therefore, among the three options, case B has been selected for a deeper analysis.

The number of configurations is reduced considering a step of 15°, highlighted in green in Graph 3. The resulting configurations are reported in the following figure, together with the new simplified coding:
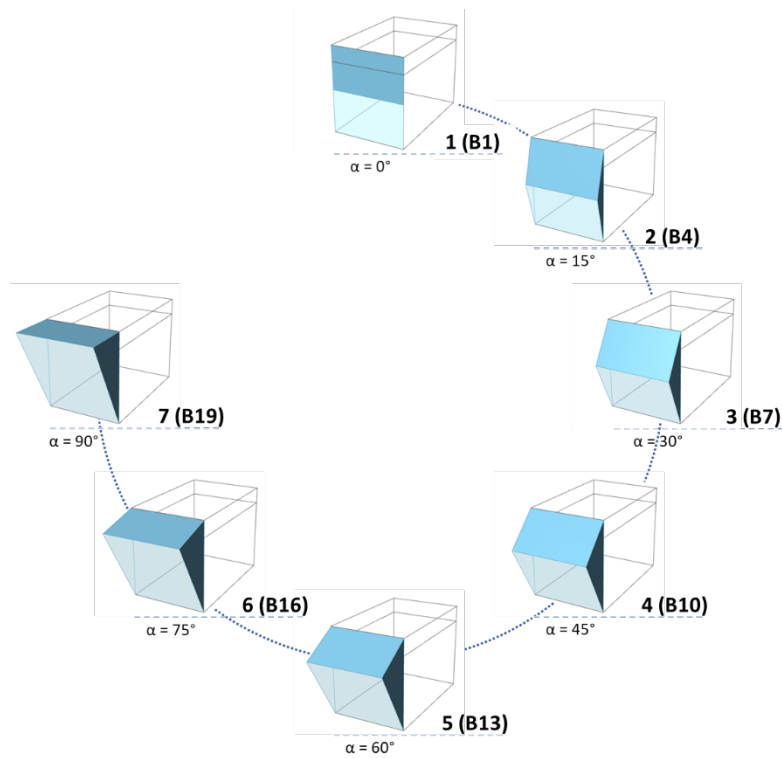
Figure 37 Subfamily α champions.

Also for this subfamily, not all the selected geometries are acceptable, in particular, as shown in Graph 4 in case 7 the ASE exceeds the limit, this means that with this configuration there is a risk of glare.
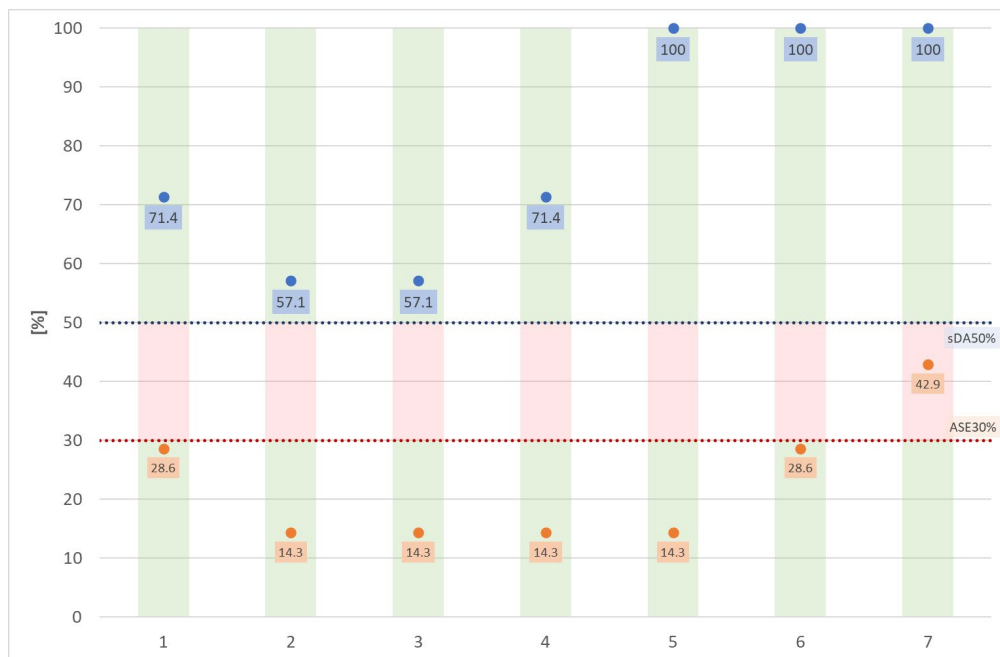
Graph 4 Constant upper-panel length champions sDA-ASE results.

Subfamily L

In this subfamily, the fixed parameter is the angle α between the plane of the façade and the upper panel. The control points are free to move on the lines starting from the vertices of the cell and inclined of α with respect to the vertical. To understand which is the best angle to use as fixed-parameter three cases have been considered:
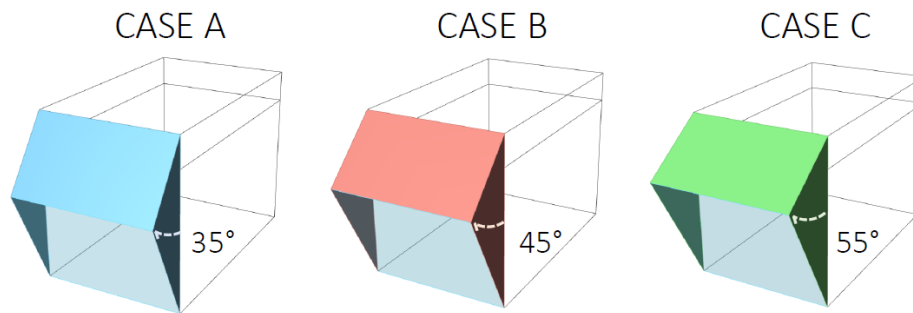
Figure 38 Subfamily L sub-cases.

The cases have been analysed for a length of the opaque panel starting from 0,1 m to 2,0 m with a step of 10 cm.

		α		
		35°	45°	55°
L	0.1 m	A1	B1	C1
	0.2 m	A2	B2	C2
	0.3 m	A3	B3	C3
	0.4 m	A4	B4	C4
	0.5 m	A5	B5	C5
	0.6 m	A6	B6	C6
	0.7 m	A7	B7	C7
	0.8 m	A8	B8	C8
	0.9 m	A9	B9	C9
	1.0 m	A10	B10	C10
	1.1 m	A11	B11	C11
	1.2 m	A12	B12	C12
	1.3 m	A13	B13	C13
	1.4 m	A14	B14	C14
	1.5 m	A15	B15	C15
	1.6 m	A16	B16	C16
	1.7 m	A17	B17	C17
	1.8 m	A18	B18	C18
	1.9 m	A19	B19	C19
	2.0 m	A20	B20	C20

Table 22 Subfamily L sub-cases coding.

Here are reported the results of the simulations only for the cases that have an ASE value lower than 50% for a first selection.
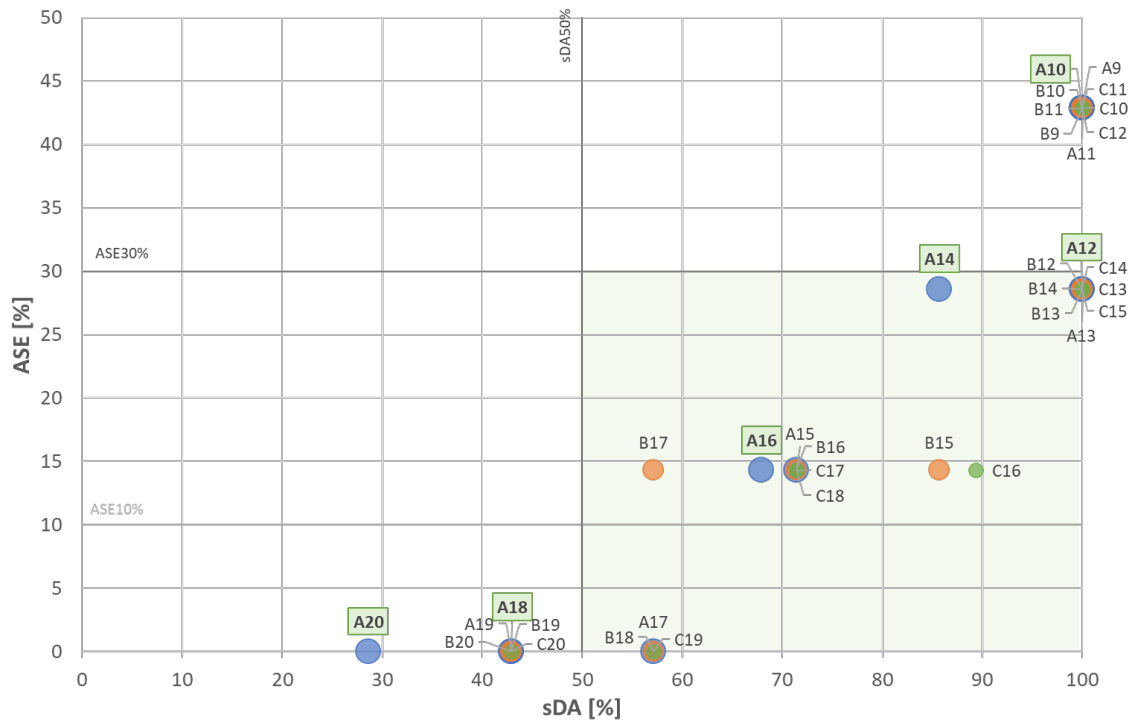
Graph 5 Subfamily L sDA-ASE results.

From the first selection results that for an overhang shorter than 0,9 m the risk of glare is high, as the value of ASE exceeds 50%.

Contrary to what was observed for the subfamily α, increasing the length both indices decrease simultaneously.

Therefore, among the three options, case B has been selected for a deeper analysis.

The number of configurations is reduced considering a step of 0.2 m, highlighted in green in Graph 5. The resulting configurations are reported in the following figure, together with the new simplified coding:
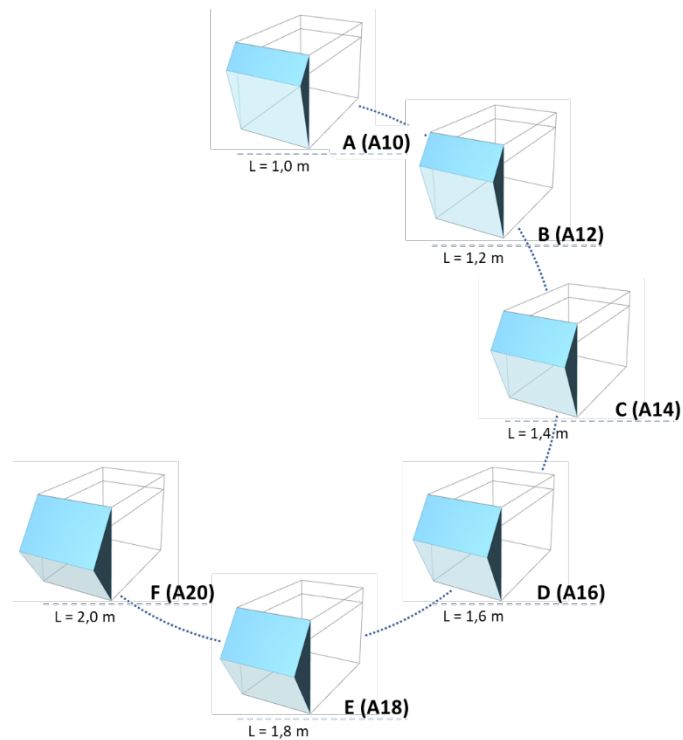
Figure 39 Subfamily L champions.

Among the selected geometries not all of them are acceptable, in particular as shown in Graph 6 in case A there is a potential visual discomfort in the module, while for cases E and F the daylight illuminance is not sufficient. This reduces the available configurations to 3 geometries: B, C, and D.
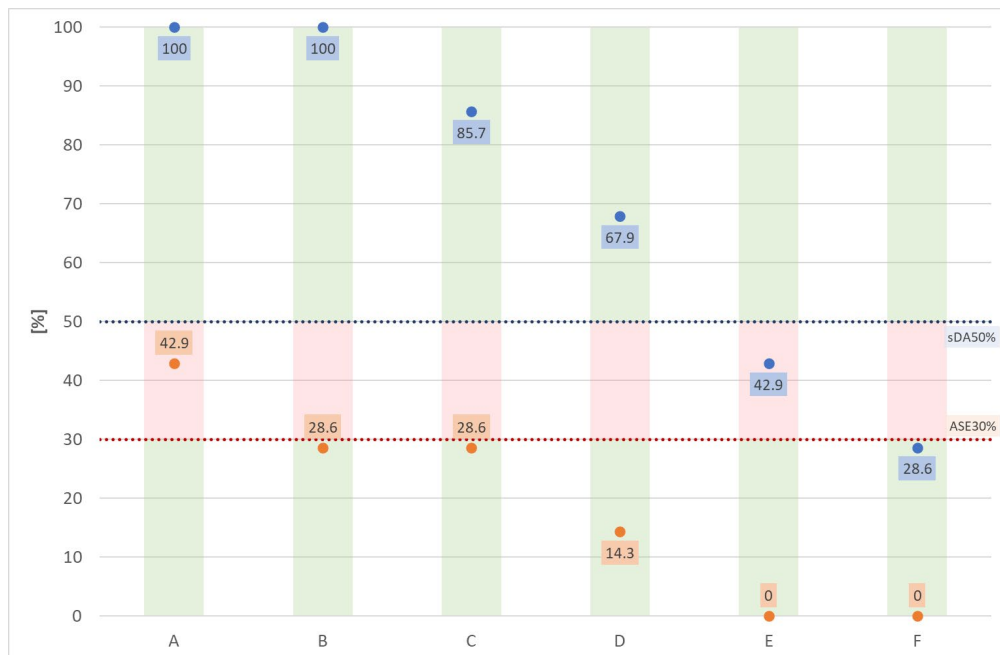
Graph 6 Subfamily L champions sDA-ASE results.

Subfamily d

In this third subfamily, the starting point is one of the cases already defined with the first two rules. So, while the position of the points in the plane normal to the façade is fixed, their position in the parallel plane is here considered.

Two cases will be considered from the previous analysis, the choice has been for two acceptable cases but with high values of ASE to see if this variation could provide better results. The cases are configuration B from subfamily L and configuration 6 from subfamily α.
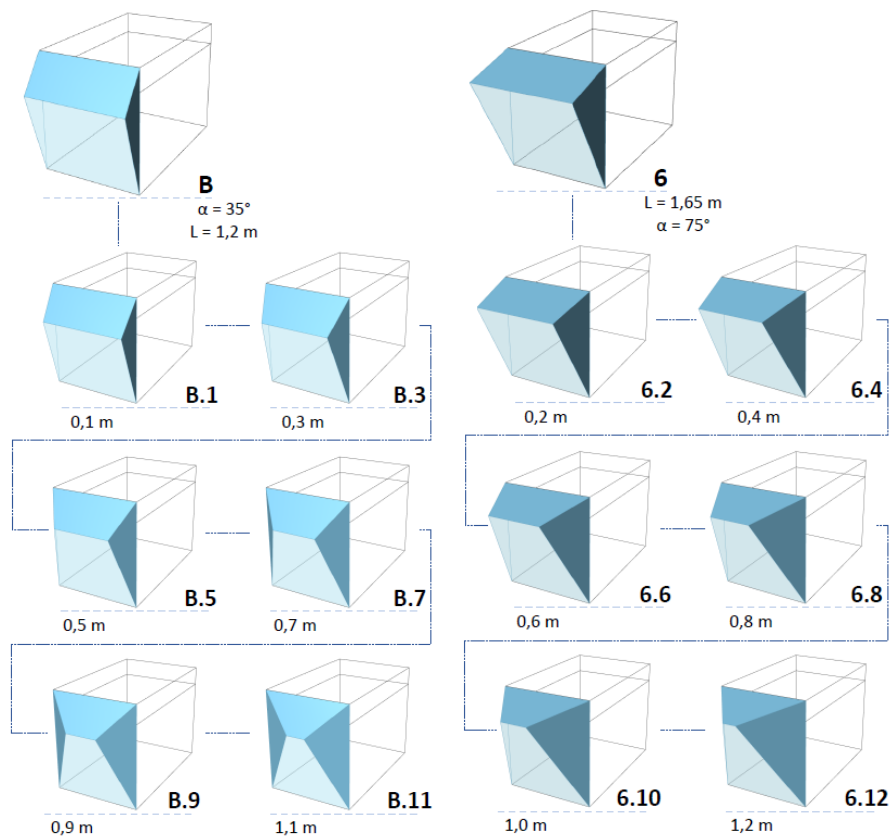
Figure 40 Subfamily d champions.

For case B the points will be moved on the plane parallel to the façade from 0,1 to 1,1 m each with a step of 0,2 m, while for case 6 the points will be moved on the plane parallel to the façade from 0,2 to 1,2 m each maintaining a step of 0,2 m.

In the following graph, the benefits of this variation are clear and in almost all the cases the comfort is improved, with also 2 cases that would not require any shading system integration according to the LEED requirements.
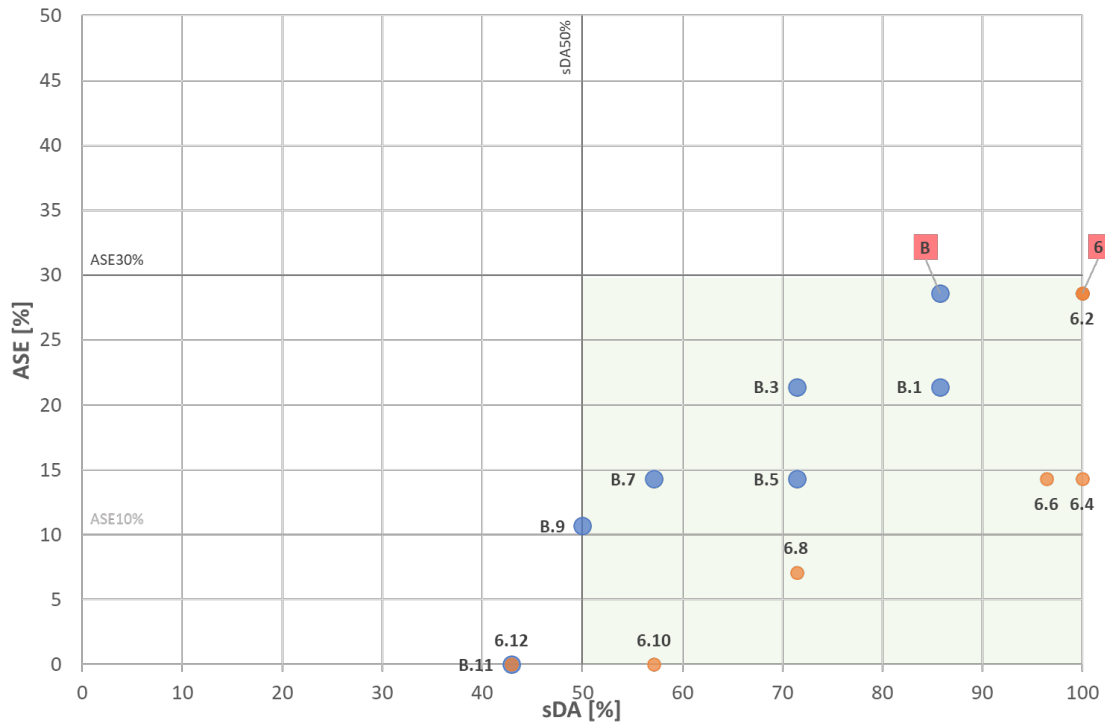
Graph 7 Subfamily d champions sDA-ASE results.

4.1.3.   3D façade _ Type 2

For this last category since two dimensions are varying, the simulations scheme is a matrix. To reduce the number of cases the movement normal to the façade plane is considered only varying from 0,4 m to 1,0 m with steps of 0,2 m.
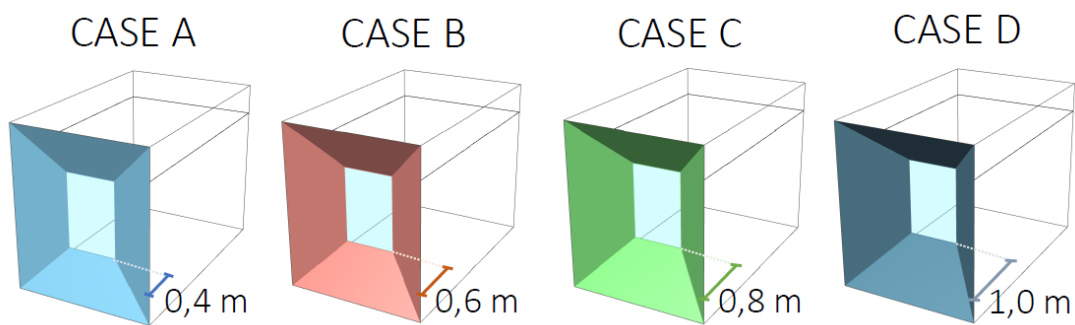
Figure 41 Type 2 family sub-cases.

The cases have been analysed for an offset of the control points starting from 0,1 m to 1,2 m with a step of 0,1 m.

	b			
	0.4 m	0.6 m	0.8 m	1.0 m
0.1 m	Ar1	Br.1	Cr1	Dr1
0.2 m	Ar2	Br2	Cr2	Dr2
0.3 m	Ar3	Br3	Cr3	Dr3
0.4 m	Ar4	Br4	Cr4	Dr4
0.5 m	Ar5	Br5	Cr5	Dr5
0.6 m	Ar6	Br6	Cr6	Dr6
0.7 m	Ar7	Br7	Cr7	Dr7
0.8 m	Ar8	Br8	Cr8	Dr8
0.9 m	Ar9	Br9	Cr9	Dr9
1.0 m	Ar10	Br10	Cr10	Dr10
1.1 m	Ar11	Br11	Cr11	Dr11
1.2 m	Ar12	Br12	Cr12	Dr12

Table 23 Type 2 sub-cases coding.

Here are reported the results of the simulations only for the cases that have an ASE value lower than 50% for a first selection.
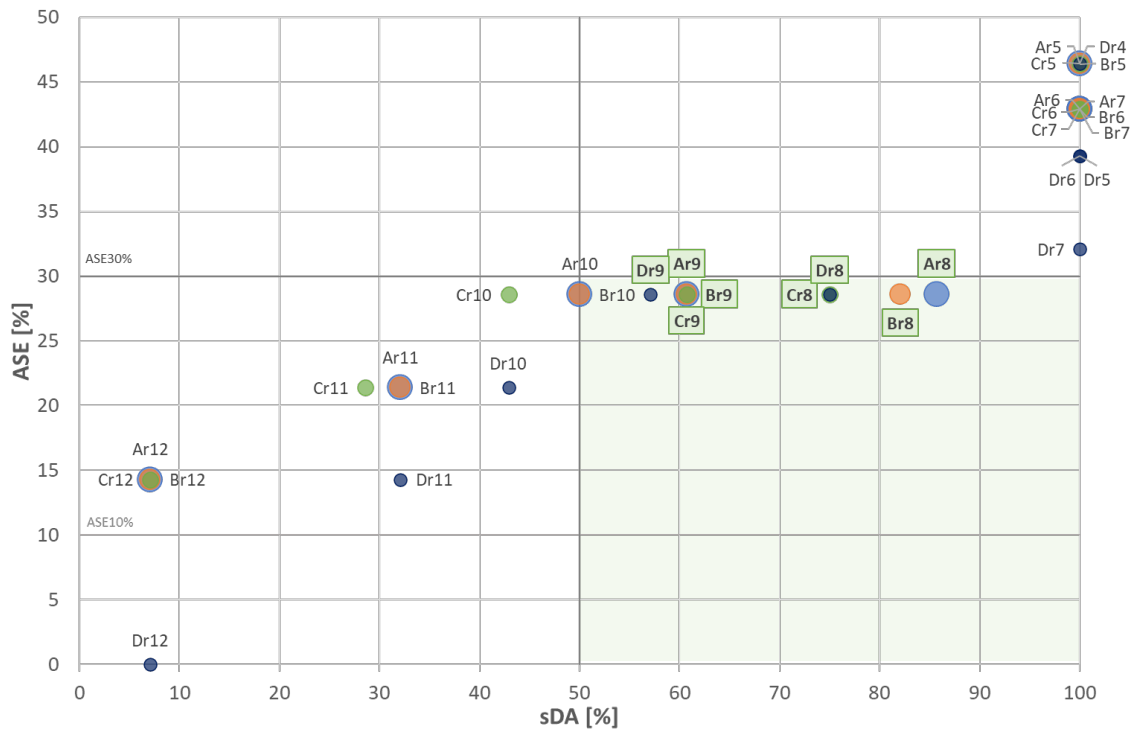
Graph 8 Type 2 family sDA-ASE results.

For this geometry definition all the acceptable cases, highlighted in green in the previous graph, have been selected and are here reported in the following figure, together with the new simplified coding:
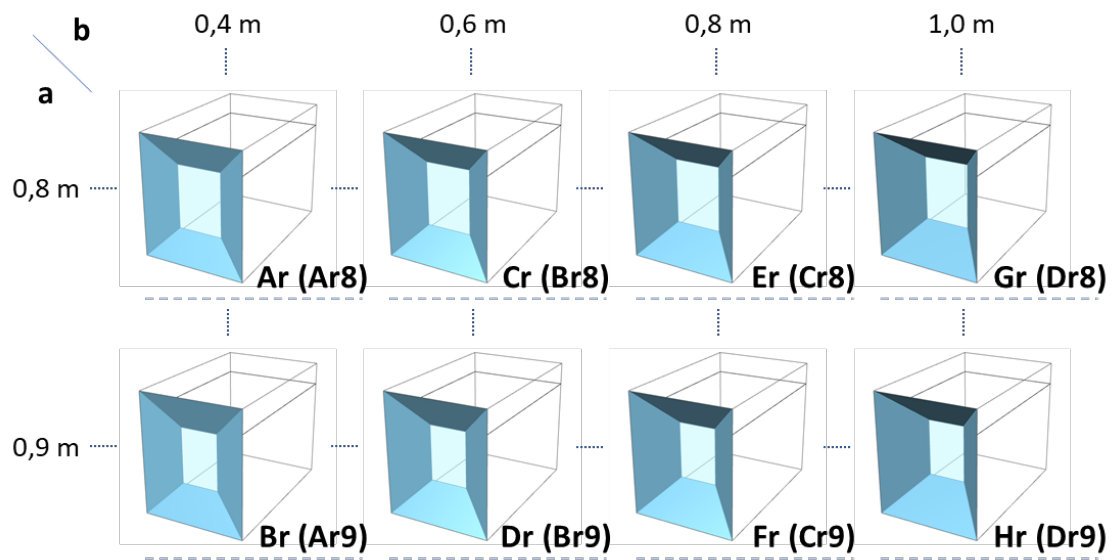
Figure 42 Type 2 family champions.

4.2. Materials choice

In the definition of the matrix of simulations the only material that is considered is the one of the opaque components of the façade module.

Speaking of the materials it is necessary to remind the distinction made for the thermal and optical characteristics. The definition of the thermal properties of the opaque part of the façade can be considered as fixed, only the absorbance, which depends on the finishing layer of the package, depends on the Solar reflection index of the chosen material.

As described before the definition of the Radiance primitive for the materials is parametric and the combinations of the three considered parameters (Reflectance, Roughness, and Specularity) can generate a very high number of materials to analyse.

To reduce the number of cases and consider only significant variation the materials have been tested in an ideal situation, applied on a panel of 3x5 m facing south, and evaluated with an annual radiation map simulation.
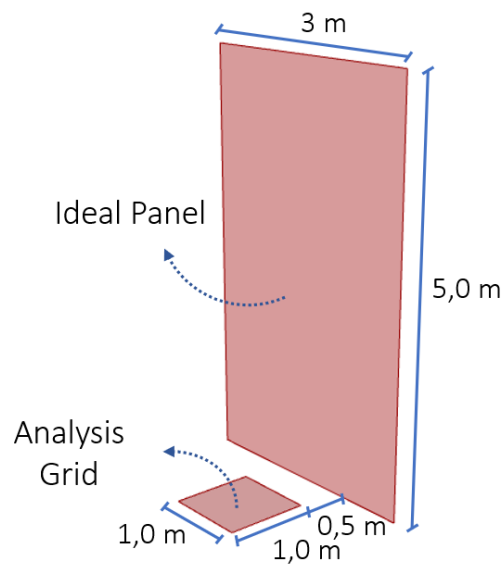
Figure 43 Material evaluation setup.

The simulation has been performed using the Diva component Radiation Map, that with geometrical and environmental inputs returns the solar radiant exposure (kWh/m^2) of the selected grid.
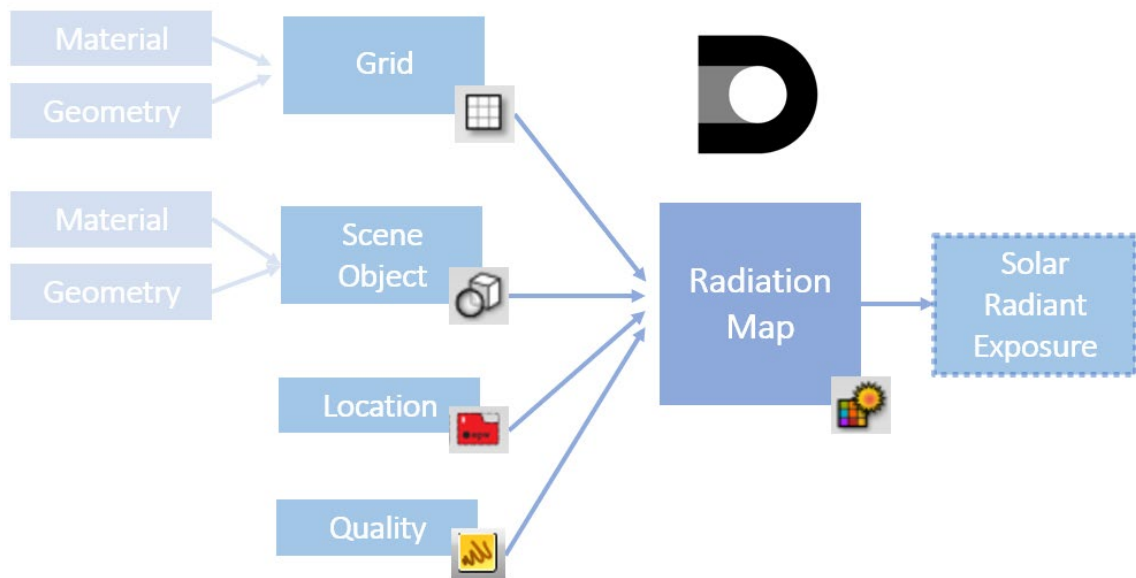
Figure 44 Schematic representation of the Radiation map simulation process.

The parameters set depend on the boundaries imposed by the Radiance definition according with their nature. The limit values, taken from the Radiance Users Manual [43], are here reported:

Plastic	MIN	MAX
Colour	0	1
	black	white
Specularity	0	0.07
	matte	satin
Roughness	0	0.02
	polished	low gloss

Table 24 Limit values for Plastic materials.

Metal	MIN	MAX
Colour	0	1
	0% reflectance	100% reflectance
Specularity	0.5	1
	dirty	clean
Roughness	0	0.2
	polished	roughened

Table 25 Limit values for Metal materials.

To do a first selection among all the possibilities and analyse only appreciable variation in the parameters for all the three parameters the minimum, the maximum, and a mean value are evaluated.

The nomenclature of the tested options is here described:
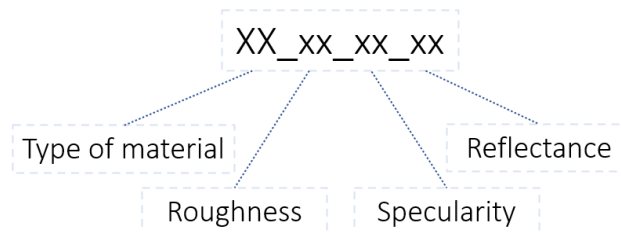
Figure 45 Material nomenclature scheme.

In the following graphs, the results of the simulation are reported.

It is clear that by increasing the solar reflectivity the incident radiation on the selected area raises. The same effect is obtained increasing the specularity of the material, while there is an inverse proportionality with the roughness coefficient.
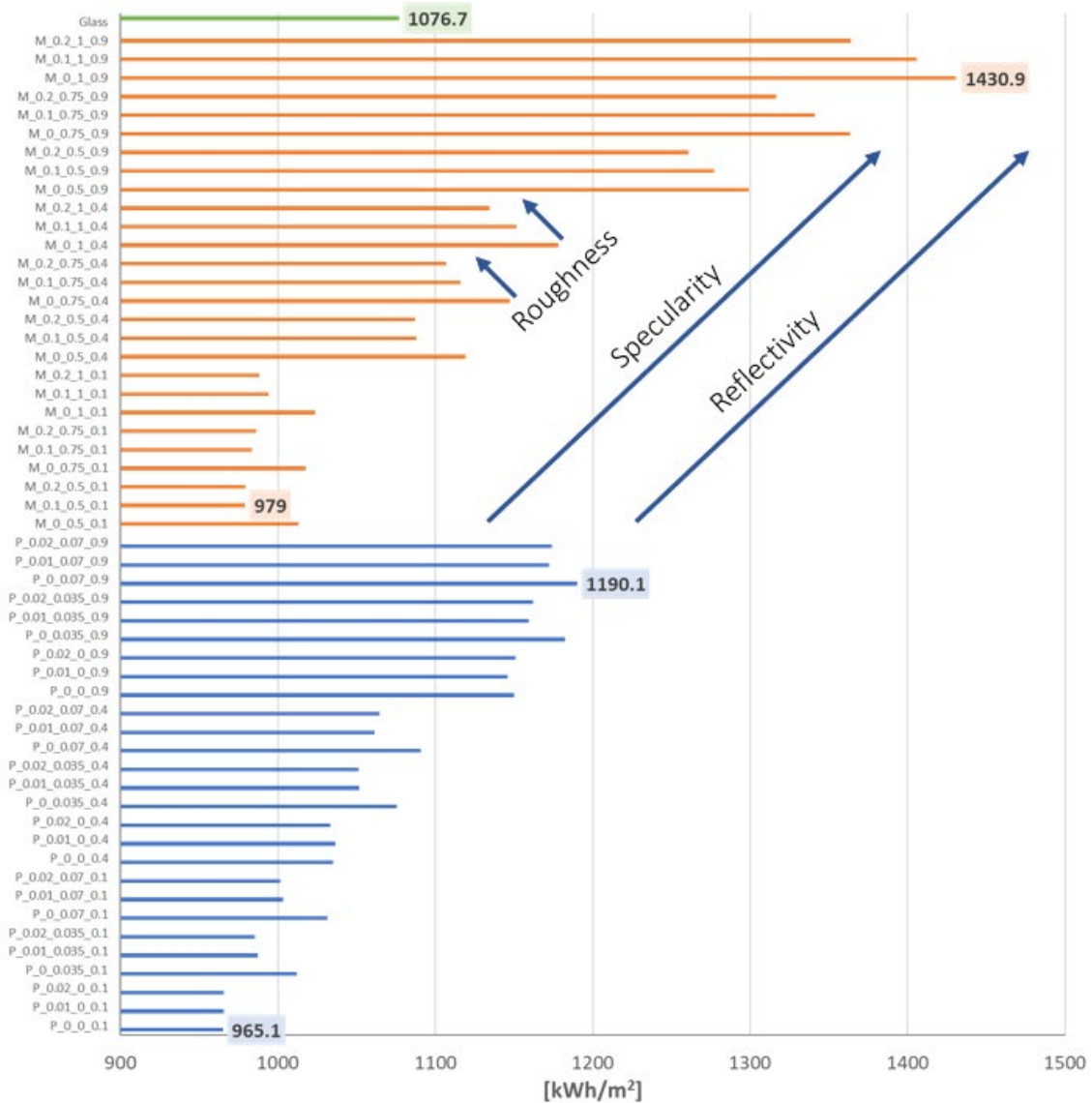
Graph 9 Materials results comparison: Glass (green), Metal (orange), Plastic (blue).

Due to their nature, there is an evident difference in their behaviour. In particular, because the reflectivity of the metal material depends on the colour, while the plastic ones are diffusive materials. In the previous graph is also reported the kWh/m^2 obtained with the glass applied to the transparent portions of the system to hypothesize a complete glazed façade, in this case, the value is close to the mean values obtained with metal and plastic.

Following the focus on the two families to appreciate the numerical values obtained.
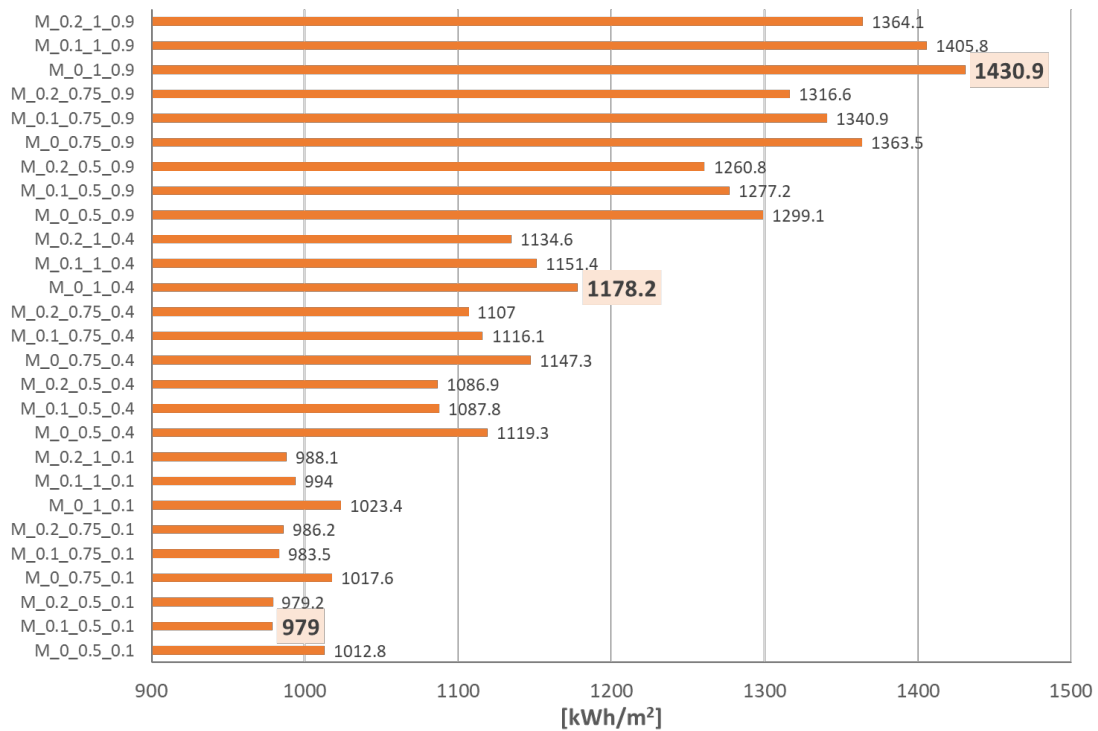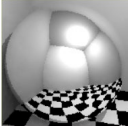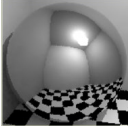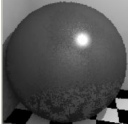
Graph 10 Metal solar radiant exposure.
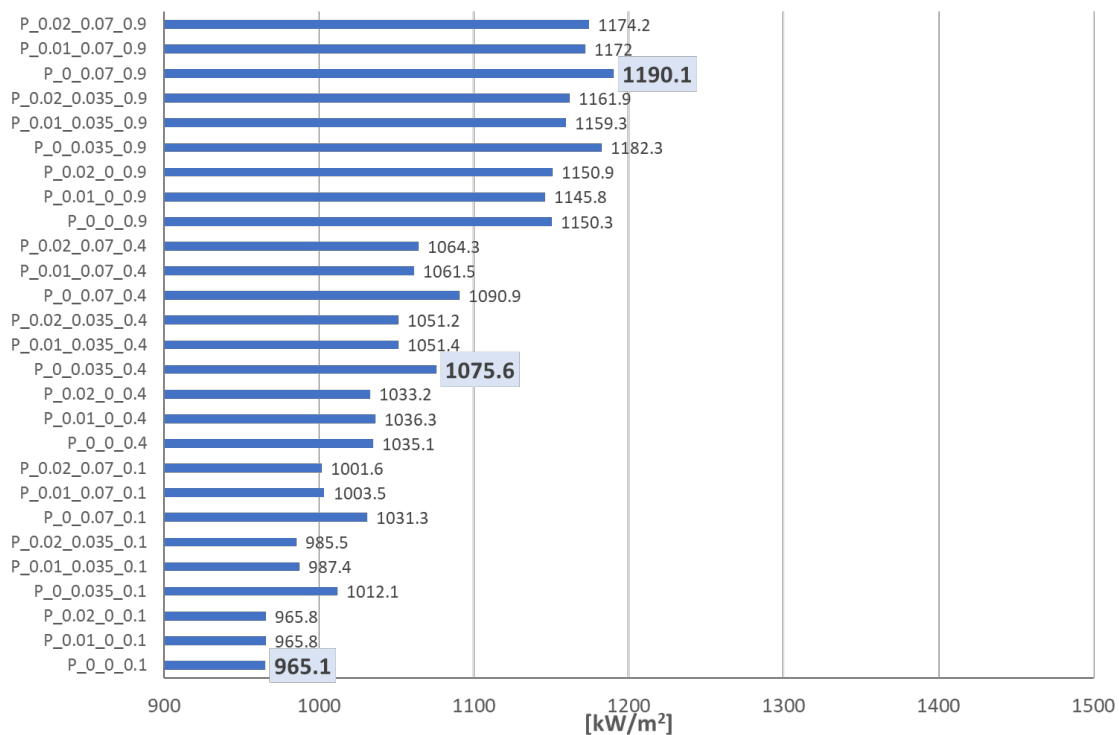
Graph 11 Plastic solar radiant exposure.

As previously mentioned, the pre-analysis aims to reduce the number of possible cases to create a simulation matrix comprehensive only of the notable configurations. For this reason, the chosen materials are three for each family the one which returns the higher value of solar radiant exposure, the lowest, and the mean value.

Therefore, the materials that will be applied to the case study will be:

-   M_0_1_0.9

-   M_0_1_0.4

-   M_0.1_0.5_0.1

-   P_0_0.07_0.9

-   P_0_0.035_0.4

-   P_0_0_0.1

Together with the materials identifiers also a rendered preview is reported. It has been generated through the Colour Picker web page.

The ones presented here are basic rendering options that represent the three main characteristics that influence the behaviour of the materials when exposed to solar radiation, but these characteristics can be achieved also with a different combination of the secondary parameters (hue, saturation, RGB combination).

For this reason, the definition of the selected materials can represent the behaviour of real materials, following are reported some examples in which the definitions are similar to real ones.
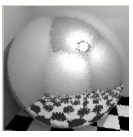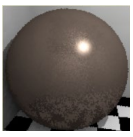
M_0_1_0.9		M_0.1_0.5_0.1	
Stainless Steel		Oxidized Copper	

	`#Reflectance: rho=0.8`
	`void metal identifier`
	`0`
	`0`
	`5    0.8 0.8 0.8`
	`     0.9 0.035`
			`#Reflectance: rho=0.11`
			`void metal identifier`
			`0`
			`0`
			`5    0.136 0.102 0.083`
			`     0.4 0.2`

P_0_0.035_0.4		P_0_0_0.1	
Light Concrete		Textured Light Terra Cotta Brick	

	`#Reflectance: rho=0.418`
	`void plastic identifier`
	`0`
	`0`
	`5    0.47 0.403 0.337`
	`     0.003 0`
			`#Reflectance: rho=0.13`
			`void plastic identifier`
			`0`
			`0`
			`5    0.195 0.11 0.071`
			`     0 0`

Table 26 Ideal and real material correspondence.

4.3. Simulation matrix

From the exposed simulations many configurations resulted acceptable for the application, but, as for the materials, the effect of the small variations in the geometries on the outdoor environment will not be as incident as for the indoor.

The number of cases to apply to the study case must be reduced to perform only significant analysis.

Among the three acceptable configurations of Opaque-transparency ratio, only the T.3 Case B will be considered for two main reasons: the first reason is that both T.2 Case A and T.3 Case C guarantee a lower daylight illuminance level, the second one is to let to the users the best view possible of the outdoor environment.

For the 3D façade Type1, the chosen cases are the ones with the best sDA-ASE combination. From the Subfamily L the case D, from the Subfamily α the case 6, and from the Subfamily d the cases B.5 and 6.8.

In the last family 3D façade Type2 the choice of the cases has been guided by the effect of the geometry on the outdoor. The cases Ar and Hr are the two with the most different inclination of the opaque portion, with a consequent different behaviour towards the reflection of the incident radiation.

Following is reported the matrix resulting from the combination of the cases with the previously selected materials.
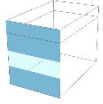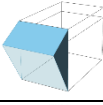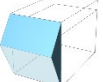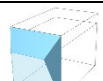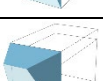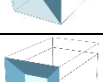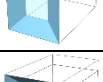
		M_0_1_0.9	M_0_1_0.4	M_0.1_0.5_0.1	P_0_0.07_0.9	P_0_0.035_0.4	P_0_0_0.1
	T.3	T.3_M.1	T.3_M.2	T.3_M.3	T.3_P.1	T.3_P.2	T.3_P.3
	5	5_M.1	5_M.2	5_M.3	5_P.1	5_P.2	5_P.3
	D	D_M.1	D_M.2	D_M.3	D_P.1	D_P.2	D_P.3
	B.5	B.5_M.1	B.5_M.2	B.5_M.3	B.5_P.1	B.5_P.2	B.5_P.3
	6.8	6.8_M.1	6.8_M.2	6.8_M.3	6.8_P.1	6.8_P.2	6.8_P.3
	Ar	Ar_M.1	Ar_M.2	Ar_M.3	Ar_P.1	Ar_P.2	Ar_P.3
	Hr	Hr_M.1	Hr_M.2	Hr_M.3	Hr_P.1	Hr_P.2	Hr_P.3

Table 27 Simulation Matrix.

5

CASE STUDY

OUTDOOR COMFORT ANALYSIS OF AN EXISTING AREA AND RESULTS REPORT

5.   CASE STUDY

Once the path has been defined completely, both in terms of script and configuration options, it has been decided to apply it considering a real building, the proper conclusion of the workflow is the application of the procedure to a building.

The chosen building is P39, ex UTC, located in the Porta Nuova district in Milano. This choice is due to the geometry of the building and the context: the area located right next to the south elevation of the building is an open green area where, due to its location and orientation, the comfort is highly influenced by the configuration of the façade previously mentioned.

This chapter will show the results of the application of the outcome of the pre-analysis, optimized to guarantee the Indoor Daylight Comfort, describing the reasonings which guided the process of analysis and the choices, underlining which solutions are good, and describing their influence on the users' comfort.

5.1. Identification of the study area

The object of study of this work is an area located in the center of the Porta Nuova – Gioia district, in a strategic position between the Central station, to the east, and Scalo Farini, to the west, and represents the access point to Porta Nuova coming from the north towards the city center. It is part of the regeneration process of the area on a neighbourhood scale started by COIMA with Gioia 22 in 2015 and that will be completed in the next few years.

In particular, the area is between the buildings of Via Pirelli 39 and Via Pirelli 35.
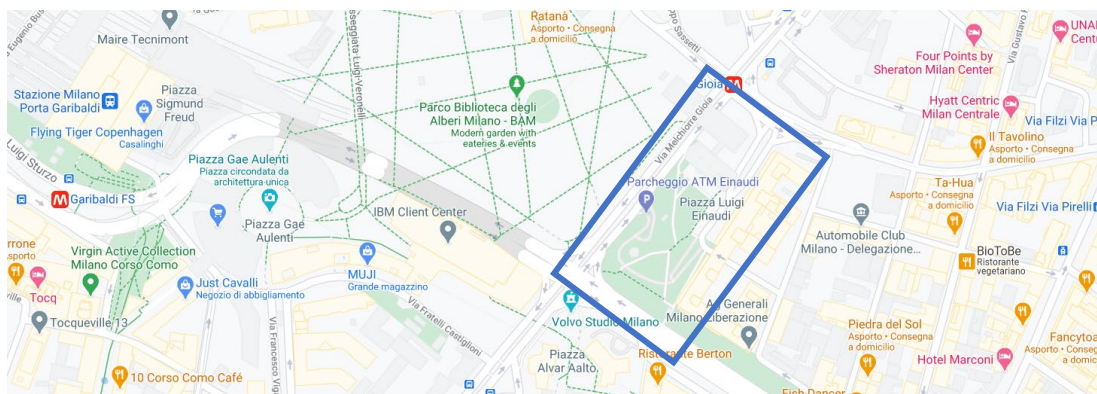
Figure 46 Identification of the study area (from Google Maps).

The building in via Pirelli 39, ex Uffici Tecnici Comunali (UTC), consists of a skyscraper of 90 meters by 26 floors and a low body built as a bridge with an arch on via Melchiorre Gioia, while Via Pirelli 35, ex Telecom building, consists of a long body with 9 floors above ground and 2 underground.

The first stage of the study will be focused on the effect of different layouts of the southwest façade of the tower on the green area adjacent to the two buildings.

Today the P39 building, dismissed by the Municipality of Milan in March 2015, represents an urban fracture that interrupts the different parts of the surrounding neighbourhoods: lacking in sustainability certifications, not compliant with anti-seismic regulations, inefficient for modern use and with structural problems, pollution, and environmental-urban-building degradation.

The winning project is the one presented by Diller Scofidio + Renfro / Stefano Boeri Architetti, who interpreted the guidelines shared by COIMA and the Municipality of Milano proposing a model of mixed-use of public-residential-tertiary spaces through the recovery of the existing tower, the bridge-building over Melchiorre Gioia and the construction of a new tower.
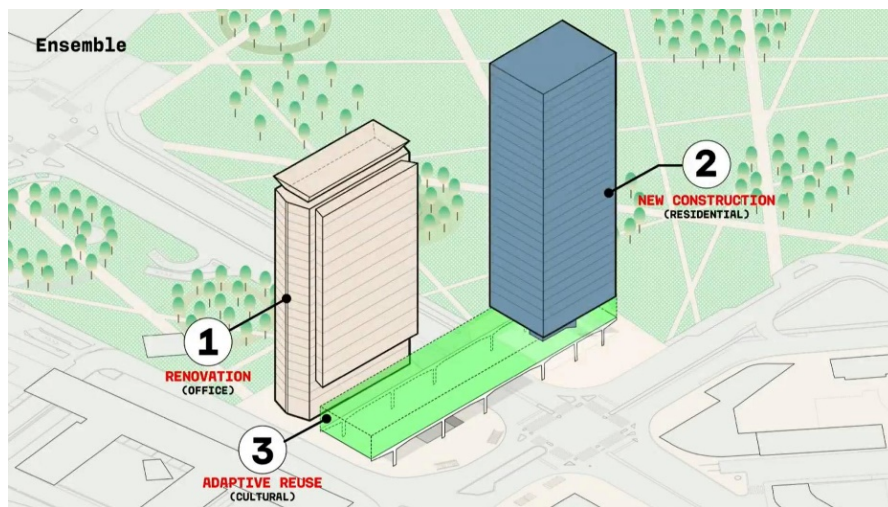
Figure 47 P39 Renovation plan (from blog.urbanlife.org).

The renovation of the existing tower, object of this work, provides an expansion on the north elevation, while the south façade will maintain the layout of the original building.

The tower is characterized by curtain-wall facades in glass and aluminum, the south façade shading system was created with a huge self-supporting reinforced concrete grid formed by seven pillars, high as the tower, joined by protruding string courses.
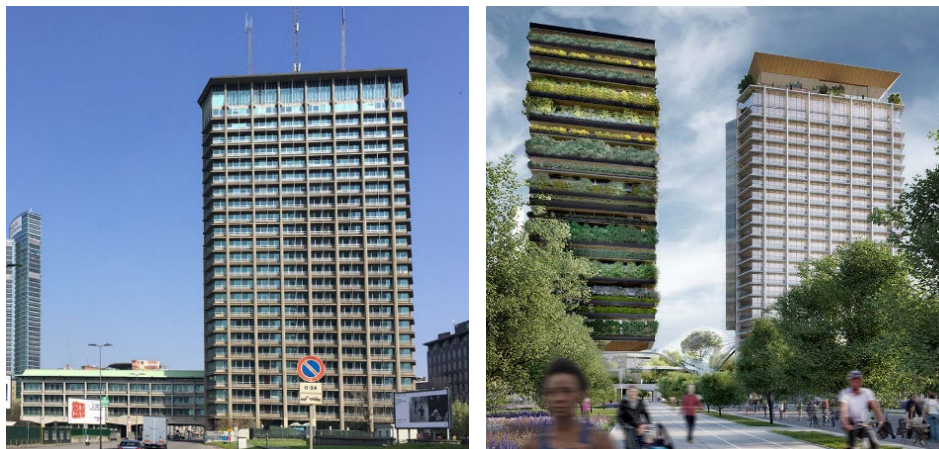
Figure 48 Photograph of the current layout on the left (from blog.urbanlife.org) vs render of the renovation project on the right (from Stefano Boeri architetti website).

In this work the starting point for the analysis will be a plane completely glazed curtain wall, the geometry will be evolved as a unitized system with modules characterized by 2D and 3D geometries, without any exterior or interior additional shading systems.

5.1.1.   3D Model

The 3D model of the area has been built in Rhino starting from the DWG drawings provided in the topographic database by the municipality of Milano on the "Milano Geoportale" (https://geoportale.comune.milano.it/sit/download-utili/).

Since the target of the work is focused on the urban microclimate and in the surroundings there are no other buildings that can significantly influence the comfort of the area, only the two buildings before mentioned have been modelled. To reduce the time needed for the simulations, the context has been slightly simplified (e.g. any particularities of the geometry have been schematized as rectangular boxes and the streets have been linearized).

Since the work aims to understand and quantify the influence of the composition of the façade, in terms of geometry and materials, on the comfort level, the vegetation present in the area has not been modelled.
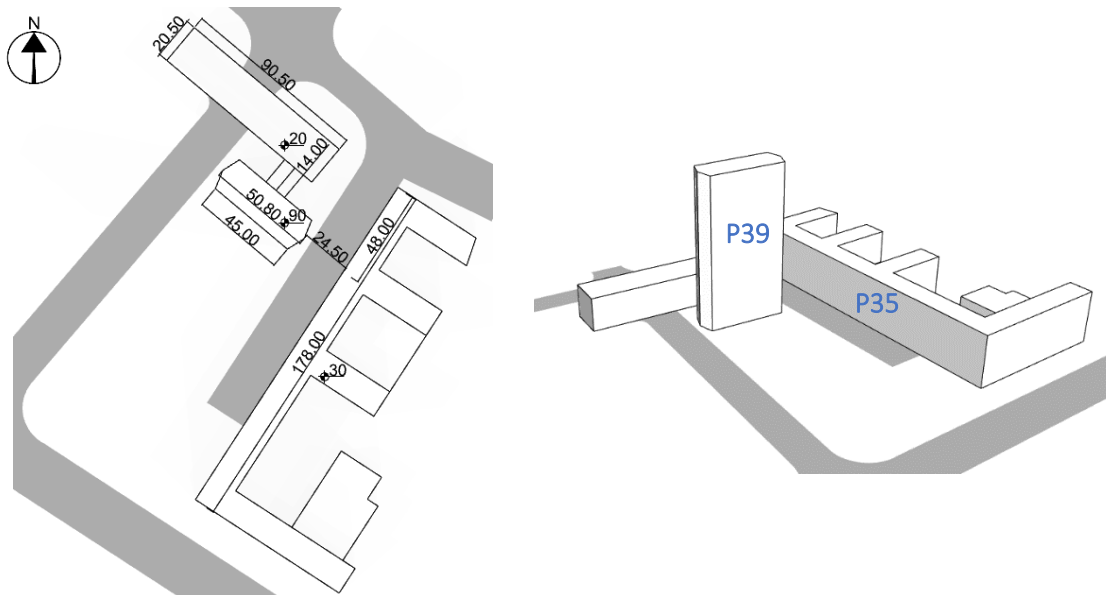
Figure 49 Masterplan of the study area.

5.1.2.   Weather analysis

To evaluate in a proper way the influence of a façade on the surrounding microclimate and, consequently, on the comfort of the users of the urban spaces is necessary to have previous knowledge of the macroclimate of the site considered.

According to the location of the area subject of the study the most appropriate weather file to use is the one located at the Linate airport (available on the EnergyPlus website): *"ITA_Milano-Linate.160800_IGDG.epw"*.

Lying on 133m above sea level Milano's climate is warm and temperate. It is classified as Cfa by the Köppen-Geiger system, which means a Temperate humid subtropical climate.

The average temperature is 13.0 °C. The rainfall is significant, with precipitation even during the driest month, about 1162 mm of precipitation falls annually.

The following graph shows the trend of temperature and humidity during the year:
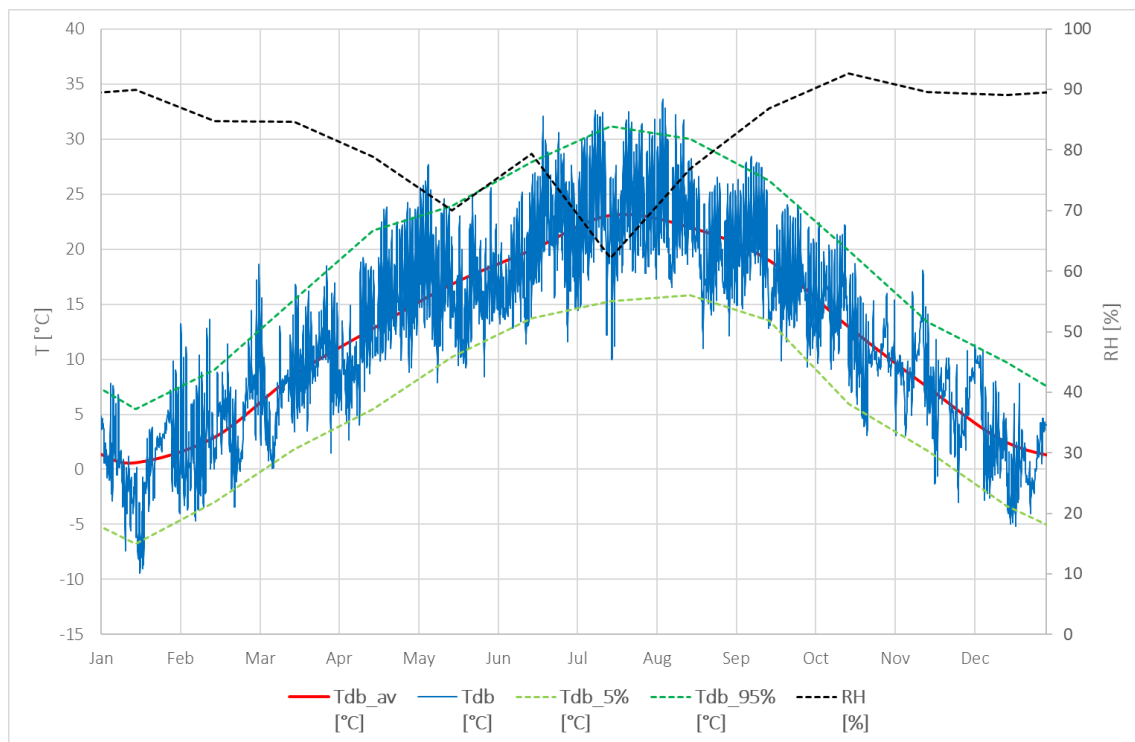
Graph 12 Average annual temperature and RH level.

The maximum dry bulb temperature that is observed is 33.6°C on the 6th of August, while the minimum is -9.4°C on the 17th of January.

It is possible to identify a hot season of about 3 months between June and August with a maximum daily temperature over 25°C and a cold season between December and February with a maximum daily temperature lower than 10°C.

The different conditions that characterize the seasons are visible in Graph 13.
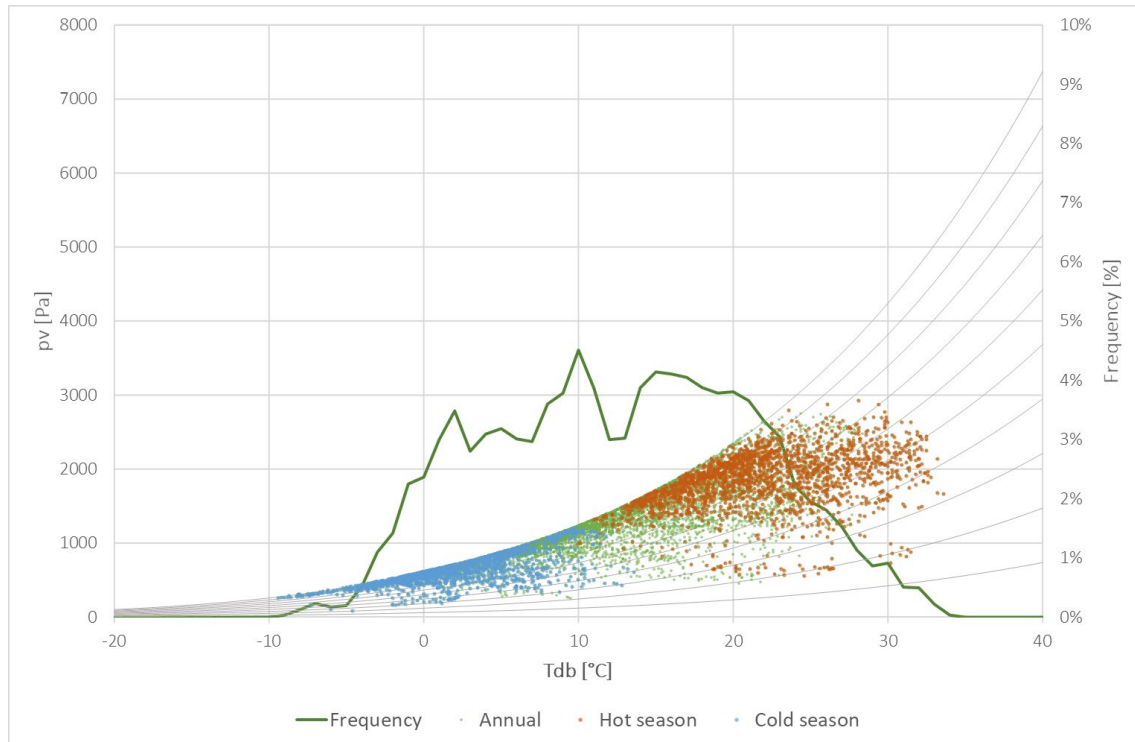
Graph 13 Psychrometric chart representing the conditions of each hour.

Milano experiences significant seasonal variation in the perceived humidity and during the hot season the comfort level is muggy and oppressive.

From this analysis the significant days that will be the object of the study can be chosen, in particular, the comfort of the hot and the cold season will be analysed. The extreme days are well known and previously reported, but to be able to consider more significant conditions the simulations will be performed for the Summer and Winter Solstice.

The mean temperature during the hot season is 21.65°C and the daily mean temperature for the 21st of June is 24.38°C, likewise, the cold season mean temperature is 1.96°C and the daily mean temperature for the 21st of December is 1.15°C.

Going more into deep the site analysis, to understand how the orientation will impact the thermal comfort, the following graphs have been plotted.

The Sun path indicates how the sun rays are going to hit the site during the analysed period. The sun is represented in the months of the hot and cold seasons at 9:00, 12:00, and 16:00 to represent the sun position at significant hours of morning and afternoon.
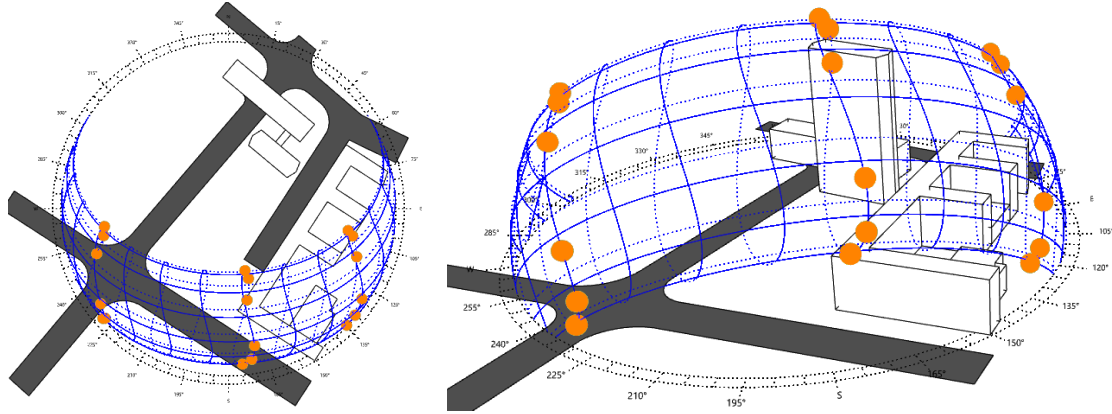
Figure 50 Sun path diagram referred to the analysis period.

As anticipated the significant days chosen for the analysis are the summer and winter solstices, for these days at first simulations at 12:00 will be performed. The simulation executed for the same hour in different periods of the year allows understanding the influence of the height of the sun on the comfort of the square. In particular, it will affect how the radiation hits the context and will be reflected on the study area. Moreover, in the hot season, during which the outdoor area is most exploited, this is a critical time for the comfort of users. While in the cold season this may be one of the times when the improvement in perceived temperature can make the area comfortable despite the air temperature being outside the comfort range.

The other two hours that resulted significant are 9:00 for the morning and 16:00 and for the afternoon. These two hours have been chosen considering the nature of the district, in the morning around 9:00 the offices are opening so the target users are the people headed to work, while in the afternoon the presence of the green area and the proximity to the Biblioteca degli Alberi park can attract students and children.

5.2. Comfort Analysis

The first step for the analysis is to set the points that will represent the positions of the users in the space. To do that a polar reference system has been defined with the pole at the center of the façade object of the study, the distance between the circumference is 7 meters and the angles are 18° each. This kind of reference system is useful for this analysis because it can be superimposed with the sun path to understand the direct influence of the sun position on the comfort results.
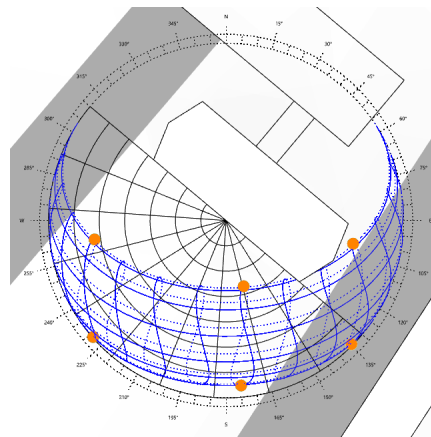
Figure 51 Reference system and sun-path overlap.

Among the 78 points that have been defined only 7 will be considered. These have been chosen by observing how the solar radiation is reflected by the façade (considering a plane completely glazed façade) during the day in the summer and winter solstice. The points represent the location reached by the maximum and minimum radiation.
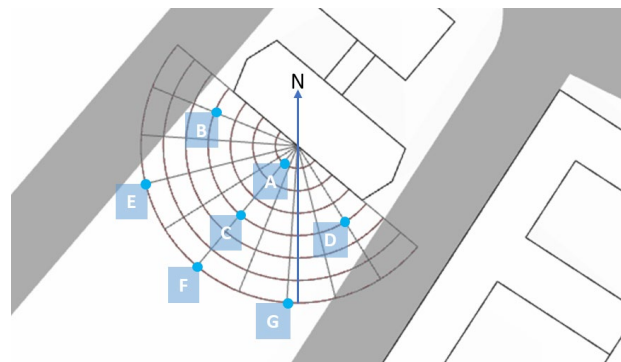
Figure 52 Selected point for the analysis.

The second stage in the preparation for the analysis is to choose the subject that will be considered to properly set the human model in the script. In this first round of simulations, a male user has been considered and placed in the previously selected point facing the P39 building.
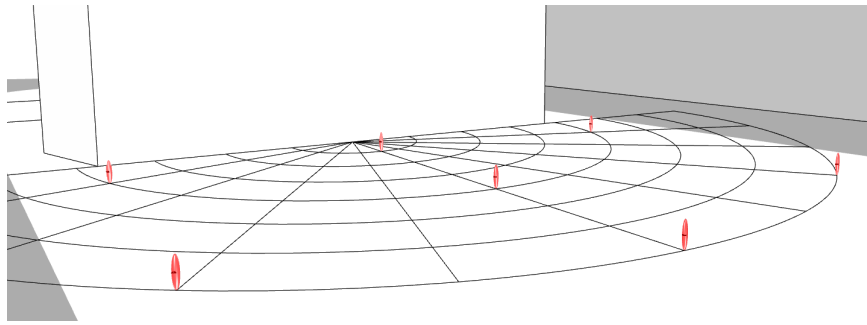
Figure 53 Human models subject of the simulation placed in the space.

The next setting to define is the indoor temperature of the building that must be assigned to calculate the surface temperature. To find the design temperature the reference standard is the Annex B of ISO 17772-2:2017 "Recommended criteria for the thermal environment"[44].

The standards define 4 categories of indoor environmental quality related to the level of expectations the occupants might have for comfort. A normal level would be "Medium" so we will choose the reference comfort range related to that.

Category	Level of Expectation
IEQ_I	High
IEQ_{II}	Medium
IEQ_{III}	Moderate
IEQ_{IV}	Low

Table 28 Categories of indoor environmental quality.

It gives examples of recommended design values of the indoor operative temperature for different types of buildings. In this specific case, the Case Study is an office building and the category for the level of indoor comfort considered will be IEQ_{II}, a Medium level of comfort expected.

Type of building/space	Category	Operative Temperature [°C]	
Single Office	I	21,0	25,5
(cellular office)	II	20,0	26,0
Sedentary - 1,2 met	III	19,0	27,0
Landscape Office	I	21,0	25,5
(open-plan office)	II	20,0	26,0
Sedentary - 1,2 met	III	19,0	27,0

Table 29 Recommended design values of the indoor temperature for the design of buildings and HVAC systems (Table B2 on the standard).

So, the indoor temperature will be set at 20,0°C for the cold season and 26,0°C for the hot season.

Once all the settings are defined and the simulation is performed, the evaluation of the comfort condition in the selected point will be done according to the UTCI scale previously described.
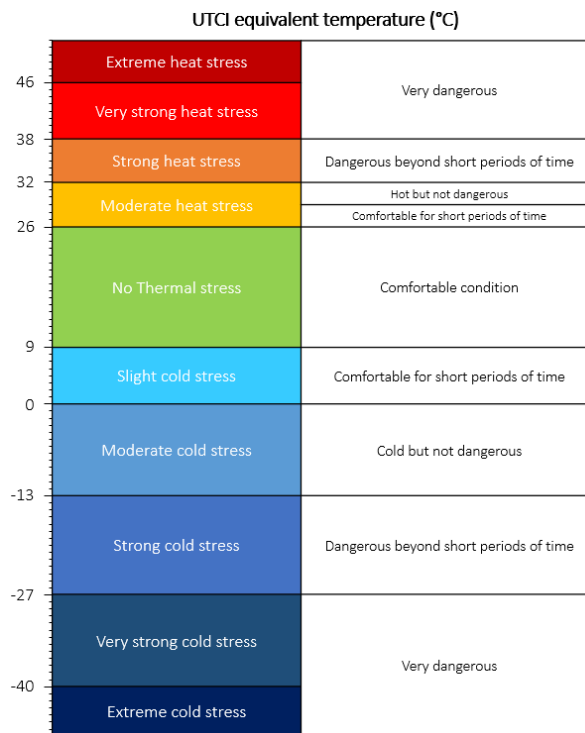
Figure 54 UTCI assessment scale of heat stress categories and sensation scale comparison.

Lastly, the Radiance parameters setting should be considered. According to the Sensitivity Analysis made on a test geometry for this first set of simulations, which includes a high number of cases, but requires fast computational times the Set 1 is used.

SET 1	
-ab	3
-ad	1000
-ar	128
-as	20
-aa	0.1

Table 30 Radiance Parameters Set 1.

5.2.1.   Base Case

The first simulation has been performed considering an all-glazed plane façade, this will be taken as a reference case to evaluate all the configurations defined in the simulation matrix. The analysed hours are 9:00, 12:00, and 16:00 as identified previously as significant hours. The first analysed date is the 21st of June, here is reported the sun position, and following the radiation, Surface Temperatures, and UTCI results.
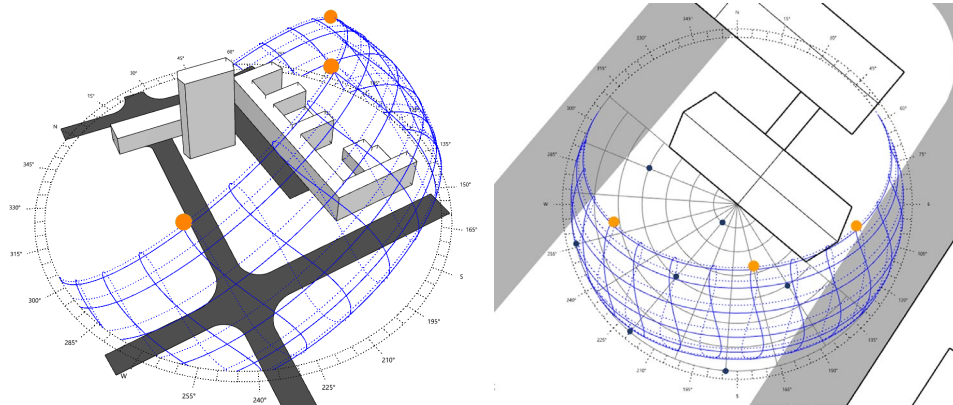
Figure 55 21st of June sun position at 9:00, 12:00, 16:00.
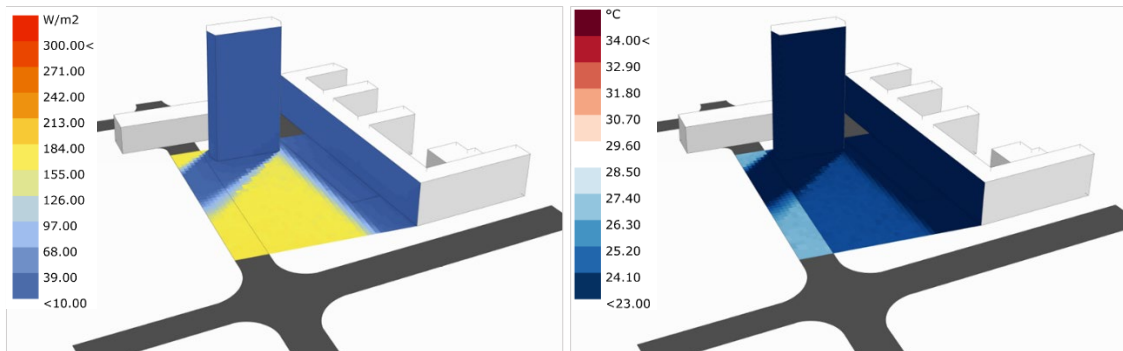
Figure 56 Total incident radiation and Surface Temperatures - 9:00 21/06.

09:00	UTCI	sw MRT	lw MRT
A	21.968	2.935	18.285
B	22.216	3.522	18.538
C	27.697	22.896	18.368
D	25.625	15.851	17.992
E	23.864	8.806	18.893
F	28.211	24.657	18.485
G	26.350	18.199	18.212
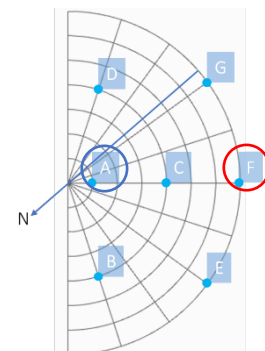
Table 31 UTCI, sw MRT, and lw MRT results - 9:00 21/06.
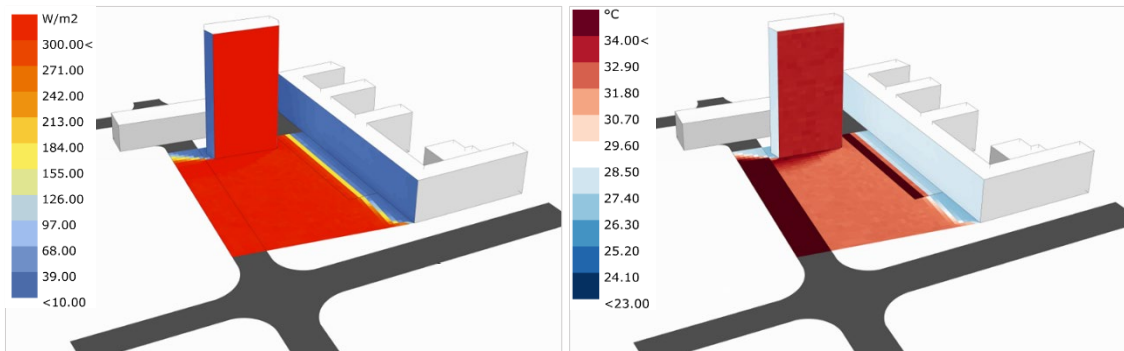
Figure 57 Total incident radiation and Surface Temperatures - 12:00 21/06

12:00	UTCI	sw MRT	lw MRT
A	42.822	61.643	26.622
B	44.206	66.927	26.923
C	39.967	49.901	26.727
D	39.998	50.489	26.270
E	40.115	49.901	27.335
F	40.002	49.901	26.872
G	40.060	50.489	26.521
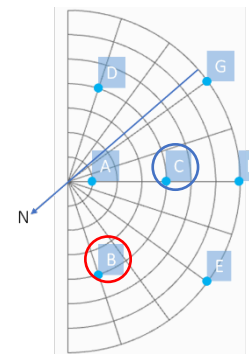
Table 32 UTCI, sw MRT, and lw MRT results - 9:00 21/06.
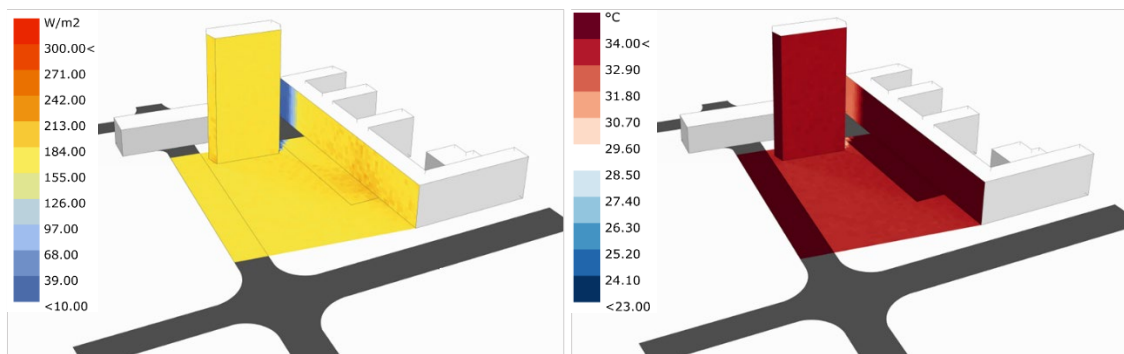
Figure 58 Total incident radiation and Surface Temperatures - 16:00 21/06

16:00	UTCI	sw MRT	lw MRT
A	38.887	29.941	28.438
B	38.392	27.593	28.735
C	38.765	29.354	28.519
D	38.806	29.941	28.101
E	38.483	27.593	29.112
F	38.368	27.593	28.633
G	38.859	29.941	28.321
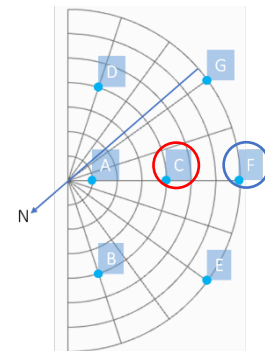
Table 33 UTCI, sw MRT, and lw MRT results - 9:00 21/06.

The second analysed date is the 21st of June, here is reported the sun position, and following the radiation, Surface Temperatures, and UTCI results.
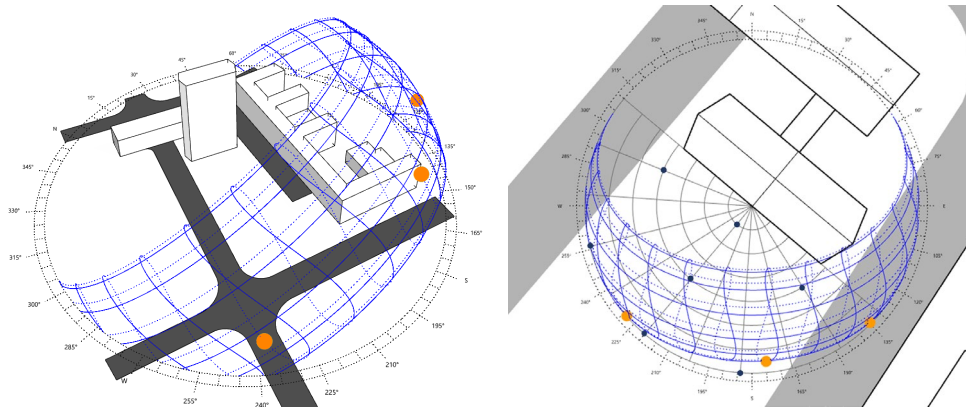
Figure 59 21st of December sun position at 9:00, 12:00, 16:00.
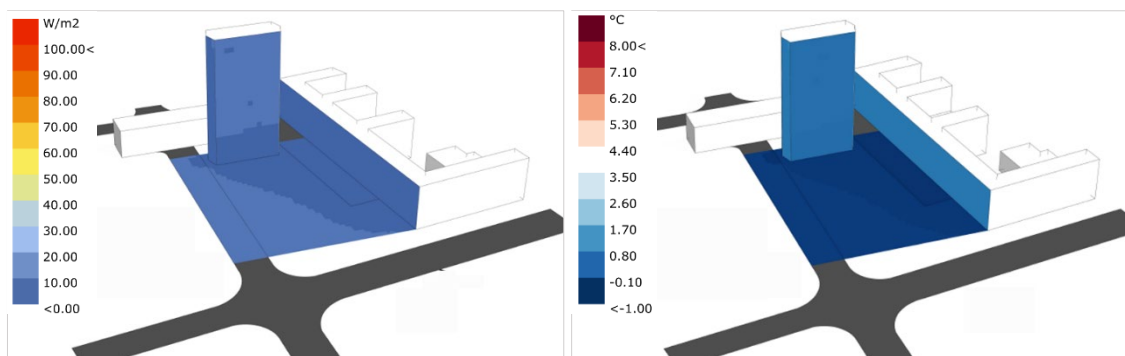
Figure 60 Total incident radiation and Surface Temperatures - 9:00 21/12.

09:00	UTCI	sw MRT	lw MRT
A	-6.482	0.881	-9.137
B	-6.336	0.881	-8.721
C	-6.420	0.881	-8.959
D	-6.658	0.881	-9.642
E	-5.780	1.761	-8.022
F	-6.332	0.881	-8.710
G	-6.492	0.881	-9.167
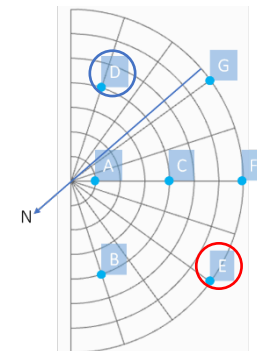
Table 34 UTCI, sw MRT, and lw MRT results - 9:00 21/12.

109
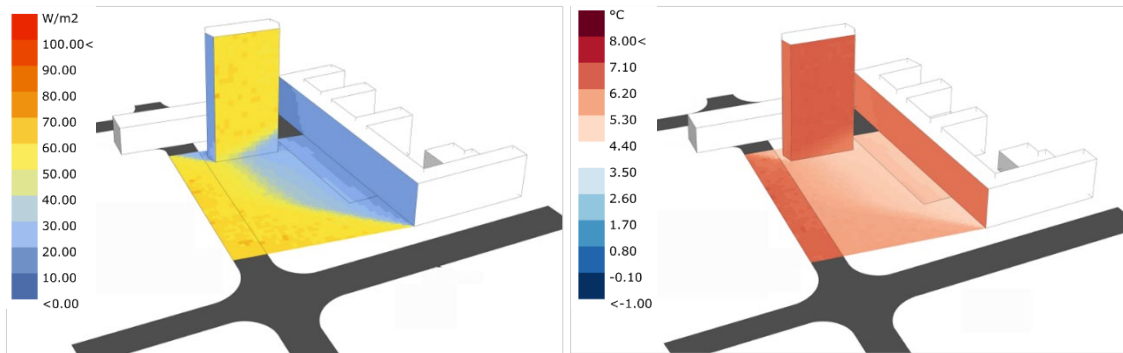
Figure 61 Total incident radiation and Surface Temperatures - 12:00 21/12.

12:00	UTCI	sw MRT	lw MRT
A	1.455	5.284	-1.593
B	2.653	8.219	-1.274
C	1.719	5.871	-1.461
D	0.884	4.110	-1.979
E	3.065	8.806	-0.749
F	2.004	6.458	-1.274
G	1.013	4.110	-1.626
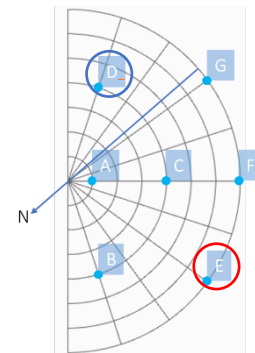
Table 35 UTCI, sw MRT, and lw MRT results - 12:00 21/12.
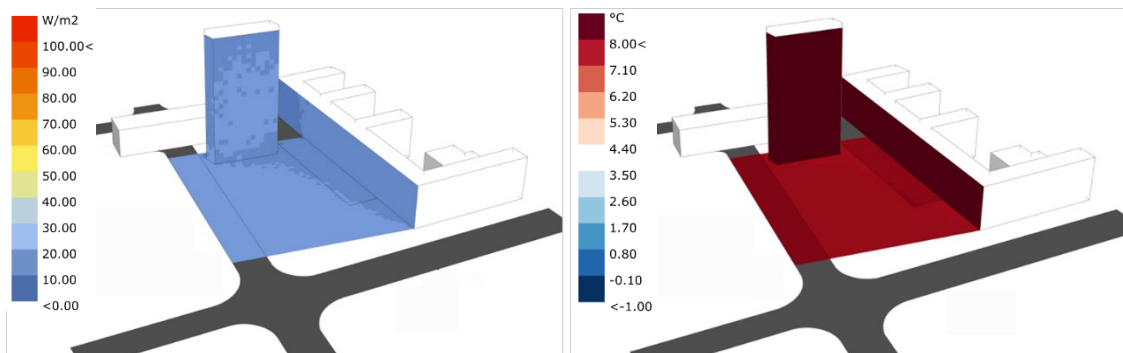
Figure 62 Total incident radiation and Surface Temperatures - 16:00 21/12.

16:00	UTCI	sw MRT	lw MRT
A	2.911	2.348	-1.850
B	3.280	2.935	-1.411
C	3.189	2.935	-1.665
D	2.720	2.348	-2.383
E	3.543	2.935	-0.678
F	3.282	2.935	-1.404
G	3.109	2.935	-1.886
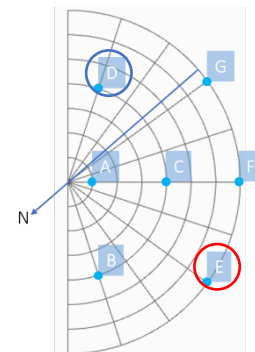
Table 36 UTCI, sw MRT, and lw MRT results - 16:00 21/12.

Discussion

The first observation that can be done is about the UTCI assessment.

Despite not in all the six cases all the Test Points are in the same heat stress category, the values are always pretty close, indeed only for the 21/06 at 09:00 the results are in two different categories. More specifically:

- 21/06 – 09:00, No Thermal stress/Moderate heat stress (Hot but not dangerous)

- 21/06 – 12:00, Very strong heat stress (Very dangerous)

- 21/06 – 16:00, Very strong heat stress (Very dangerous)

- 21/12 – 09:00, Moderate cold stress (Cold but not dangerous)

- 21/12 – 12:00, Sligh cold stress (Comfortable for short periods of time)

- 21/12 – 16:00, Sligh cold stress (Comfortable for short periods of time)

As predictable, during the hot season, the users will be in a comfort condition in the morning, while during the cold one in the central hours of the day.

As regards the peak temperatures, the maximum temperature among the tested points does not coincide with the sun position generally. We can state that in general the temperature distribution on the area is not influenced by the direct radiation, meaning not by the sun position directly, but on the contrary, it is clear the dependence from the interaction of the radiation with the P39 building and façade. This is visible in the images, but also comparing the values of sw MRT for the Test Points with the UTCI values.

Comparing the images representing the solar radiation incident on the contest and the surfaces' temperature we can notice the dependence of the second one, but at the same time, it is clear the influence of the materials that compose the envelopes and urban surfaces in the T_{sup} calculation.

From the graphic representation is also visible how during the cold season the fraction of diffused radiation is higher, and this is reflected also in the UTCI results as they are way more uniform compared with the hot season.

The distribution of the results on the Test Points is also influenced by the position of the sun compared with the orientation of the building and the context. If we consider the hot season, in the case 21/06 - 16:00 the azimuth of the sun is 261.8°, so the angle with respect to the normal to the façade is 41°, due to the urban configuration the reflected radiation does not hit the green area but the P35 façade and the close street, consequently, the temperature on the square is constant, this is also visible in the sw MRT values reported.

During the morning (21/06 - 09:00) the phenomenon that occurs is different, the sun is at an angle (with respect to normal) greater than 90° (119°) and therefore the building casts its shadow on the square, creating differences between the Test Points exposed to the sun and those protected by the shade.
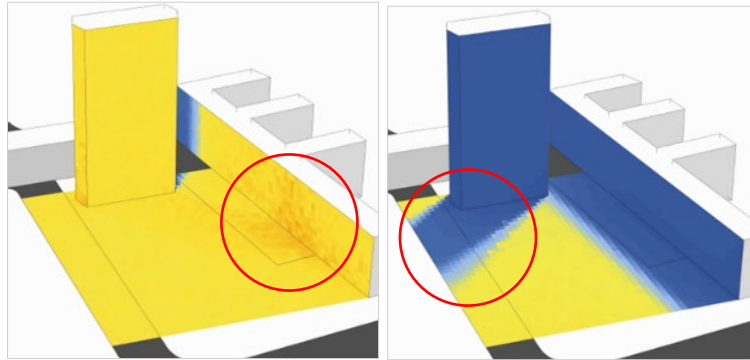
Figure 63 21/06 highlights.

Only at 12:00, when the azimuth is 165° and the angle with the normal 54°, we can observe the actual effect of the radiation reflected by the façade on the square.

During the cold season as previously mentioned the radiation is more diffused therefore the influence of the reflected radiation is less incident, despite this, the sun position is different than in the hot season and therefore also its effect on the context.

The 21/12 at 16 the angle with the normal is 9° meaning that the sun is almost in front of the façade and the radiation should be completely reflected on the square, indeed the results are uniform. At 09:00 the angle becomes 85° meaning that there is no shade projected on the square, but the angle of incidence is so high that the radiation is reflected out of the interest zone.

At 12:00 the position of the sun, at 45° but considerably lower than during the hot season, causes the shadow of the P35 building to be projected on part of the façade and the square influencing the results, while for the 21/06 the shade was shorter and did not influence the sw results.
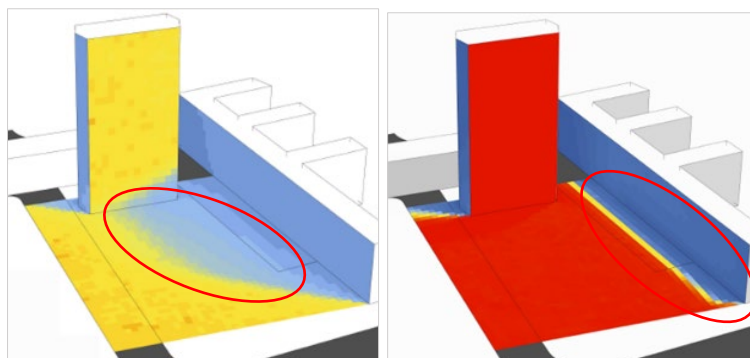
Figure 64 21/12 and 21/06 12:00 shade comparison.

5.2.2.   Selected Configurations

From the first round of analysis, it is possible to conclude that, despite the shade presence, the simulation performed at 12:00 is the most representative of the effect of the façade configuration on the comfort on the square, for this reason, the simulation matrix will be studied for this specific time of the day.

Before proceeding with the simulations, it is necessary to validate the simulation matrix as it was developed considering a generic module facing south while the exposition of the façade is southwest.

Daylight comfort validation

An example cellular office has been modelled adapting the dimensions used in the pre-analysis to the case study and placed at mid-height in the building.

In the following table the results are reported:

	sDA	ASE
T.3	57.1	28.6
5	78.6	14.3
D	57.1	14.3
B.5	58.7	32.1
6.8	50.0	17.9
Ar	71.1	39.3
Hr	57.3	32.1

Table 37 Indoor comfort results for the Case Study.

The B.5 and Ar configurations do not respect the required performances for the Indoor Daylight Comfort, in particular, the ASE limit of 30% is exceeded causing the risk of glare inside the office.

To overcome this risk the configurations have been changed in the matrix with more stringent ones.

The B.5 has been substituted with the B.7 case:

0,5 m		0,7 m	
58.7	32.1	71.4	25.0
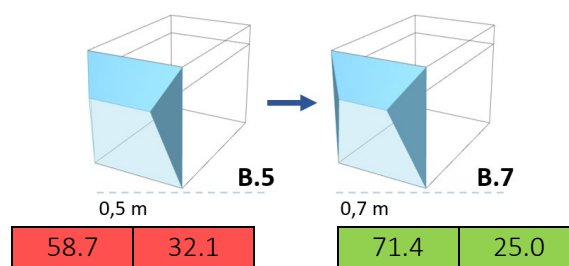
Figure 65 B.5 to B.7 change and verification.

113

Among the 8 cases identified for the 3D façade _ Type 2 as acceptable in the pre-analysis phase no one respect the limits imposed for the Indoor Daylight Comfort, for this reason only the Hr case will be considered as it exceeds the limit of ASE of 2%, which can be considered as a precision error by the program.

Results and discussion

As previously mentioned, the all-glazed configuration is the reference case, for this reason here are reported the UTCI results for the significant days at 12:00.

	21/06	21/12
A	42.822	1.455
B	44.206	2.653
C	39.967	1.719
D	39.998	0.884
E	40.115	3.065
F	40.002	2.004
G	40.060	1.013

Table 38 All glazed façade UTCI results – 12:00.

During the hot season, the UTCI equivalent temperature is in the Very strong heat stress range, while for the cold season in the Slight cold stress one. This means that the condition during summer is worse than the winter one as it is very dangerous for the users, while in the second case it is comfortable for short periods of time.

Following is reported the radiation distribution on the area subject of study for the considered cases, the scale has been adapted to properly show the distribution.
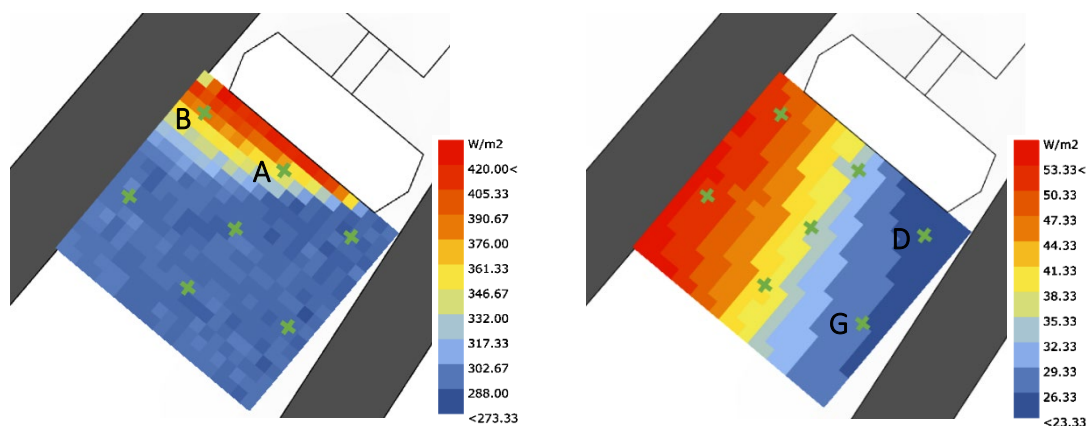
Figure 66 Radiation Maps for 21/06 and 21/12 at 12:00.

According to the radiation maps the interest points during the hot season are A and B, which receive more radiation, while on the contrary for the cold season the interest

points should be D and G. These are respectively the points with the highest and lowest UTCI result. However, points D and G are in this situation due to the shadow of the P35 building, as shown before, therefore they will not be consistently interested by the variation of the radiation reflected by the façade. For this reason, the interest points will be again the ones that receive more radiation.

It will be interesting to understand how the combination of sw MRT and lw MRT and consequently the comfort condition will evolve with the different configurations.

The first configuration that will be analysed is the Plane façade _ Opaque-transparency ratio with 30% of transparency.

The first table reports the results for the hot season. The results remain in the Very strong heat stress range for almost all the materials applied, also increasing the UTCI values in some cases. It is clear how maintaining the same geometry as the base case the main influence factor is the material applied to the opaque parts. The only material that returns better results is P.3 (P_0_0_0.1), it is a plastic material, therefore a diffusive material, with a dark colour, this means that the radiation is mostly absorbed by the façade and not reflected directly on the square. Due to its nature, this material develops a higher surface temperature causing the highest lw MRT in the Test Points (reaching 35°C vs a mean value of 26°C for the other materials), but the reduction in sw MRT is so significant that allows to all the points to reduce the heat stress losing between 2 and 6 °C passing to the Strong heat stress category. Point A is the only one that remains in the Very Strong heat stress category, it resents the influence of the ground floor which is all glazed, this is why it presents UTCI values considerably higher than the other points.

	M.1	M.2	M.3	P.1	P.2	P.3
A	45.209	43.254	39.930	42.690	42.141	41.511
B	45.216	44.374	40.069	43.673	43.116	36.269
C	39.710	39.429	39.550	40.115	39.700	36.272
D	39.354	39.354	39.211	40.040	39.491	36.303
E	39.934	39.786	39.211	40.059	39.918	36.237
F	39.643	39.633	39.743	40.042	39.764	36.379
G	39.617	39.607	39.307	39.879	39.601	36.361

Table 39 30% - 21/06 12:00 UTCI results.

For the cold season, the temperature variation is lower in absolute value, but that can be significant too. In general, the influence of the material is coherent with what has been described previously, obviously the positive effect is the opposite in this season. In the UTCI distribution, the materials with a higher reflectivity improve the comfort condition increasing the equivalent temperature of almost 1°C.

	M.1	M.2	M.3	P.1	P.2	P.3
A	1.785	1.372	1.371	1.993	1.579	1.165
B	3.335	2.709	2.499	2.918	2.709	2.499
C	2.095	1.886	1.677	2.303	1.886	1.677
D	0.824	0.823	0.822	1.030	0.823	0.822
E	3.640	3.220	3.009	3.431	3.011	3.009
F	2.233	2.024	2.022	2.441	2.231	2.022
G	1.275	1.273	1.065	1.481	1.273	1.065

Table 40 30% - 21/12 12:00 UTCI results.

The configurations considered next are those of the family 3D façade _ Type 1, in particular, Subfamily α case 5 and Subfamily L case D.

These two cases are analysed together as their results are comparable.

Both the solutions reduce the UTCI in the interest points A and B and increase, for less than 1°C, the other ones during the hot season. While in the cold season the equivalent temperature is slightly reduced for all the Test Points.

The interesting thing about these results is that their dependence on the material is minimal, what prevails is the geometry of the façade. The inclined opaque component reflects the radiation upward reducing the one hitting the square, this is why the temperature is reduced in both seasons.

The second point that can be noticed is that the angle of inclination of the opaque and glazed portions do not influence the results significantly, this depends on the relation between the height and the position of the sun and the geometry of the façade. The angle of the modules overcomes the limit for which the glass reflects the light. Moreover, the overhang that is created with this configuration generates a self-shade on the modules that reduce the radiation hitting the façade.

	M.1	M.2	M.3	P.1	P.2	P.3
A	39.253	39.116	38.979	39.115	38.978	39.116
B	39.422	39.147	39.285	39.284	39.422	39.147
C	39.543	39.406	39.406	39.543	39.406	39.406
D	39.210	39.210	39.211	39.485	39.348	39.211
E	39.619	39.618	39.481	39.481	39.618	39.481
F	39.426	39.426	39.564	39.701	39.701	39.564
G	39.524	39.386	39.386	39.386	39.524	39.249

Table 41 3D5 - 21/06 12:00 UTCI results.

116

	M.1	M.2	M.3	P.1	P.2	P.3
A	1.298	1.093	1.094	1.298	1.093	1.094
B	2.374	2.374	2.375	2.374	2.374	2.375
C	1.553	1.553	1.553	1.553	1.553	1.553
D	0.809	0.810	0.810	0.809	0.810	0.810
E	2.530	2.529	2.529	2.738	2.530	2.529
F	1.825	1.824	1.824	1.825	1.825	1.824
G	0.930	0.929	0.929	0.930	0.929	0.929

Table 42 3D5 - 21/12 12:00 UTCI results.

	M.1	M.2	M.3	P.1	P.2	P.3
A	38.978	39.116	38.980	38.978	38.842	39.117
B	39.560	39.148	39.285	39.285	39.285	39.285
C	39.406	39.406	39.269	39.544	39.269	39.406
D	39.073	39.486	39.211	39.210	39.348	39.211
E	39.482	39.619	39.619	39.482	39.482	39.619
F	39.702	39.289	39.564	39.565	39.565	39.289
G	39.387	39.387	39.524	39.387	39.387	39.387

Table 43 3DD - 21/06 12:00 UTCI results.

	M.1	M.2	M.3	P.1	P.2	P.3
A	1.296	1.296	1.297	1.296	1.297	1.297
B	2.581	2.581	2.581	2.581	2.581	2.581
C	1.551	1.551	1.551	1.552	1.552	1.551
D	0.808	0.808	0.809	0.808	0.808	0.809
E	2.737	2.737	2.529	2.738	2.737	2.737
F	1.824	1.824	1.824	1.825	1.825	1.824
G	0.929	0.929	0.929	1.135	0.929	0.929

Table 44 3DD - 21/12 12:00 UTCI results.

The third group of geometries considered are those of the family 3D façade _ Type 1, Subfamily d cases B.7 and 6.8.

All the considerations made for the previous cases are applicable here, but the geometry of these configurations reduces again the UTCI as the glazed portion is reduced and the opaque elements have an orientation that is not facing the tested area.

Despite all the tested Points have a significant UTCI reduction (4 to 9°C) they remain in the Strong Heat stress range.

This reduction is almost all due to the view factor of the façade, indeed despite the sw MRT is increased compared with the reference case, the lw MRT is considerably reduced and compensates the short wave effect.

	M.1	M.2	M.3	P.1	P.2	P.3
A	34.603	34.895	34.749	35.179	35.039	34.894
B	35.324	35.324	35.469	35.469	35.470	35.033
C	35.372	35.226	35.226	35.519	35.663	35.081
D	34.431	34.578	34.723	35.013	34.869	34.723
E	36.499	36.211	36.210	36.358	36.357	36.355
F	35.838	36.128	35.693	35.986	35.840	35.838
G	35.163	35.453	35.163	35.745	35.599	35.308

Table 45 3DxB7 - 21/06 12:00 UTCI results.

In the cold season, a positive effect can be observed, the UTCI increases of few degrees and remains in the Slight Cold stress, which is comfortable for short periods of time. As observed for case T.3 the materials with a higher reflectivity have a better effect, in particular, the material P.1 for B.7 and M.1 for 6.8 show a significant increase in the comfort condition. The main difference with the plane façade configuration is that also with the materials with a low reflectivity a positive effect is registered.

	M.1	M.2	M.3	P.1	P.2	P.3
A	1.697	1.482	1.482	2.620	2.621	2.404
B	2.876	2.876	2.875	3.767	3.766	3.765
C	1.999	1.781	1.781	2.892	2.674	2.673
D	0.893	0.893	0.892	1.872	1.872	1.872
E	3.179	3.177	3.176	3.964	3.963	3.743
F	2.136	2.135	2.134	2.981	2.979	2.979
G	1.345	1.344	1.129	2.246	2.245	2.028

Table 46 3DxB7 - 21/21 12:00 UTCI results.

	M.1	M.2	M.3	P.1	P.2	P.3
A	35.641	35.206	34.914	35.204	35.060	34.769
B	35.488	35.487	35.341	35.487	35.341	35.196
C	35.383	35.381	35.089	35.528	35.526	35.235
D	35.179	35.034	34.742	34.887	34.888	34.742
E	36.362	36.359	36.214	36.506	36.214	36.214
F	35.989	35.842	35.841	35.843	35.697	35.696
G	35.314	35.312	35.312	35.313	35.312	35.312

Table 47 3Dx68- 21/06 12:00 UTCI results.

	M.1	M.2	M.3	P.1	P.2	P.3
A	2.626	2.409	2.192	2.408	2.409	2.192
B	3.553	3.552	3.334	3.552	3.334	3.552
C	2.895	2.676	2.676	2.677	2.676	2.676
D	2.092	1.875	1.875	1.875	1.875	1.875
E	3.968	3.747	3.746	3.967	3.966	3.746
F	2.983	2.982	2.981	2.983	2.982	2.981
G	2.248	2.030	2.030	2.248	2.030	2.030

Table 48 3Dx68 - 21/12 12:00 UTCI results.

The last configuration is the 3D façade _ Type 2 case Hr.

This last façade geometry has a completely different behaviour compared with the ones analysed before.

In the first table is shown how the particular configuration reduces the temperature for all the tested points. As for the T.3 case, the nature of the geometry and the prevalence of opaque elements on the glazed ones lead to a higher influence of the material on the comfort results. The values show how the materials with a higher absorbance (meaning for the metals the materials with lower reflectivity and plastics the material with a darker colour) return a better result in reducing the UTCI and in particular for the plastic materials. With respect to the plane façade, the effect is reduced due to the self-shadow of the modules due to their geometry.

Excluded the points A and B whose UTCI values are significantly reduced (4 to 5°C), the other points experience a variation in the distribution, but the comfort condition is not improved.

119

	M.1	M.2	M.3	P.1	P.2	P.3
A	39.564	39.564	39.421	40.860	40.282	39.278
B	39.741	39.741	39.741	40.463	40.029	39.884
C	39.867	39.724	39.867	40.589	40.156	40.010
D	39.664	39.664	39.664	40.528	40.238	39.664
E	40.088	40.088	40.088	40.382	40.234	39.945
F	40.175	39.888	39.745	40.181	40.034	40.175
G	40.134	39.704	39.704	39.996	40.136	39.847

Table 49 3DrHR - 21/06 12:00 UTCI results.

The configuration in the cold season has a reduced effect, but still, the considerations made before for the materials are confirmed also in this case. The variability of UTCI among the Test Points is reduced, and also among the different materials.

	M.1	M.2	M.3	P.1	P.2	P.3
A	2.022	1.589	1.158	2.024	1.590	1.158
B	2.723	2.287	2.285	2.723	2.503	2.285
C	2.293	2.074	1.640	2.293	1.858	1.640
D	1.083	0.867	0.865	1.298	0.867	0.865
E	2.668	2.663	2.877	3.101	2.879	2.660
F	1.928	2.140	1.921	2.359	2.139	1.921
G	1.852	1.418	0.987	1.421	1.203	0.987

Table 50 3DrHr - 21/12 12:00 UTCI results

Looking at the results it is clear that the comfort condition during the hot season is more critical than in winter, therefore the next step of analysis will focus on those configurations that resulted as the best in reducing the UTCI on the 21st of June. The cases that will be deepened are those of the family 3D façade _ Type 1 Subfamily d as their application allowed to bring the selected locations closer to the comfort condition during the hot period maintaining an acceptable UTCI value or Improving it in the cold season.

5.2.3.   Best case (3D façade _ Type 1 Subfamily d)

Before proceeding only one of the two cases of Type 1 Subfamily d will be applied as there is no significant difference in the results obtained with their application. The chosen one is the B.7 case, because it guarantees a better daylight comfort condition, as it allows a higher daylight illuminance level maintaining the ASE under the required limit. Moreover, this configuration is more buildable due to the higher angles between the opaques and glazed parts of the module.
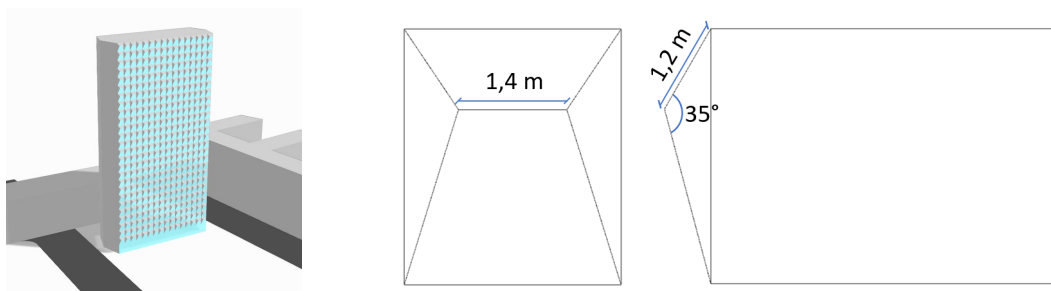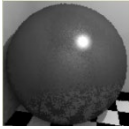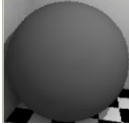
Figure 67 B.7 geometry and application.

The simulation will be performed applying the two materials that provided the best results from the matrix analysis for the hot season:

-     M_0.1_0.5_0.1

-     P_0_0_0.1

These are materials with the lowest reflectivity, the consequent high absorbance increases the surface temperature of the opaque elements of the façade, but due to its geometry this does not influence the outdoor comfort.

For this second stage of simulation the Standard Set of Radiance parameters is applied:

Standard Set	
-ab	5
-ad	1000
-ar	300
-as	20
-aa	0.1

Table 51 Standard Set of Radiance parameters.

Results and discussion

At first, the hot season is analysed as it showed the most critical conditions. The hourly values are computed from 08.00 to 18.00.
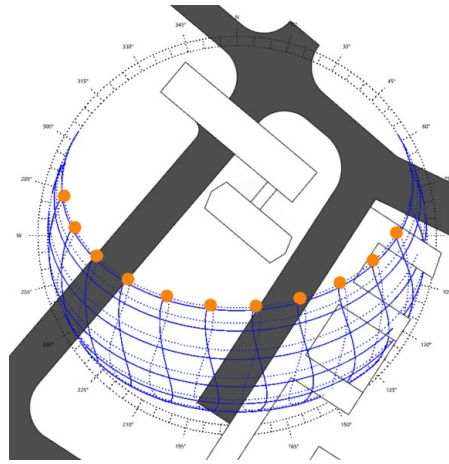
Figure 68 21/06 Hourly sun path.

The first graph represents the UTCI average on the Test Points for the Base case and for the B.7 configuration with the two materials previously mentioned applied.
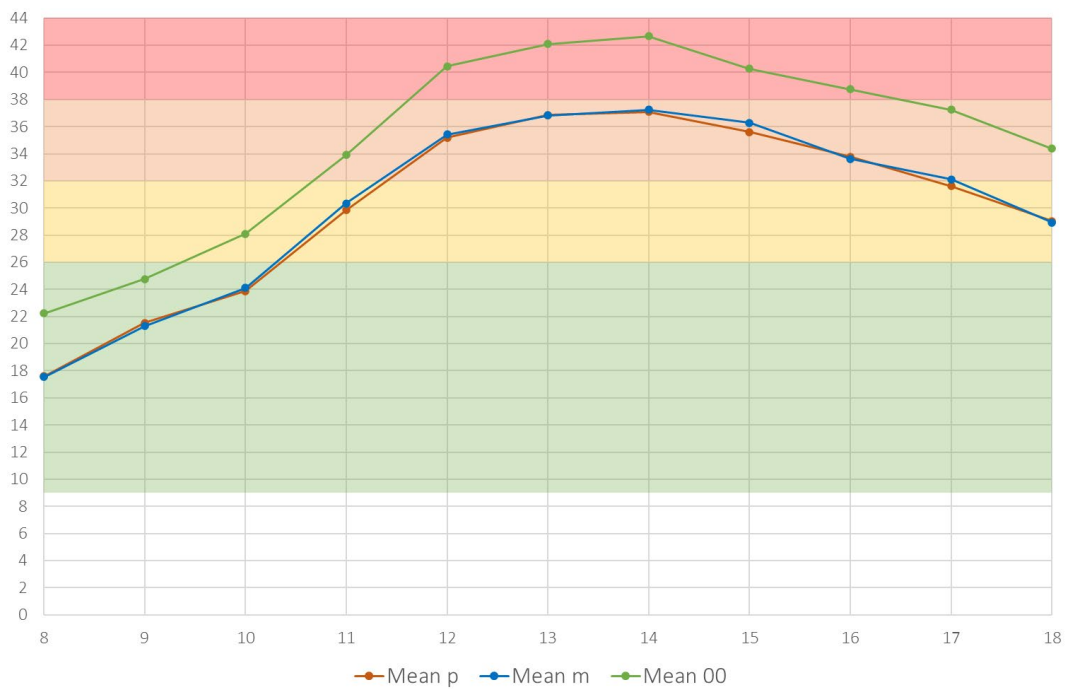
Graph 14 UTCI hourly mean values – 21/06.

122

The consideration made for the values obtained for 12:00 are extendable to the whole day: compared with the base case this façade solution reduces the UTCI value during all the hours of the day in the hot season. This reduction allows to maintain the average condition among the area in a comfort condition until 10:00, and in Moderate heat stress at 11:00 and after 17:00. The peak in the average is reached in the central hours of the day but never overcomes the Strong heat stress.

This kind of analysis however does not take into account the variability among the area of the comfort condition, which can be significant. The Test Points selected at the beginning of the Case Study chapter are meant to represent all the significant locations on the square both for the short wave and long wave contribution, as each point receives a different amount of radiation and has a different view factor of the façade and the other surfaces.

Following are reported two graphs that represent the distribution for each hour of the values registered on the seven Test Points with the two materials applied.
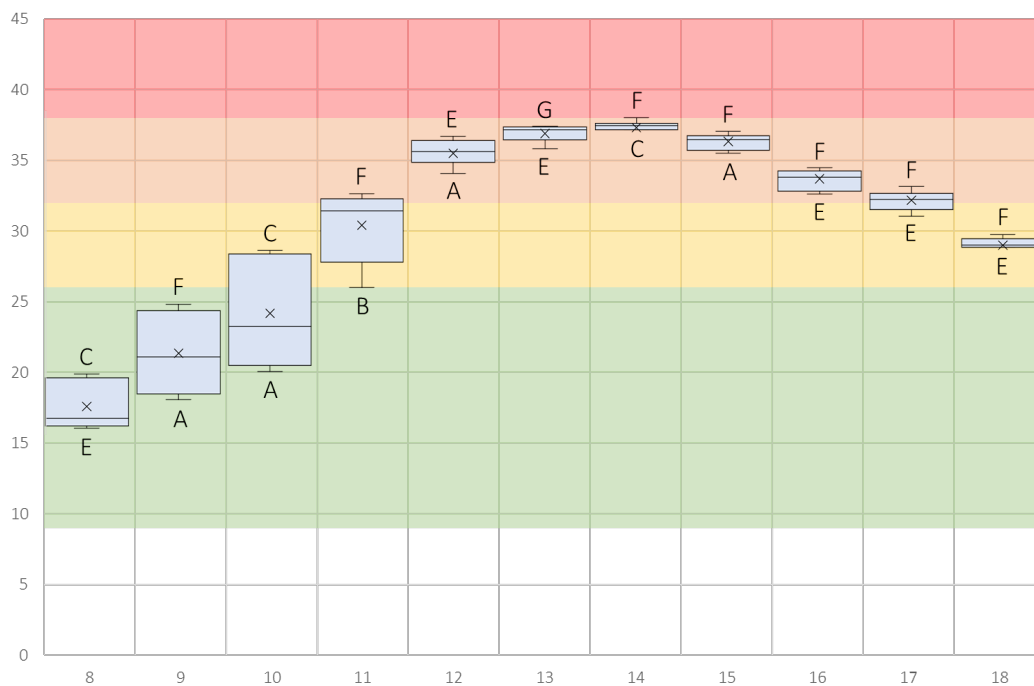
Graph 15 Distribution of the hourly values on the Tets Points – Metal – 21/06.
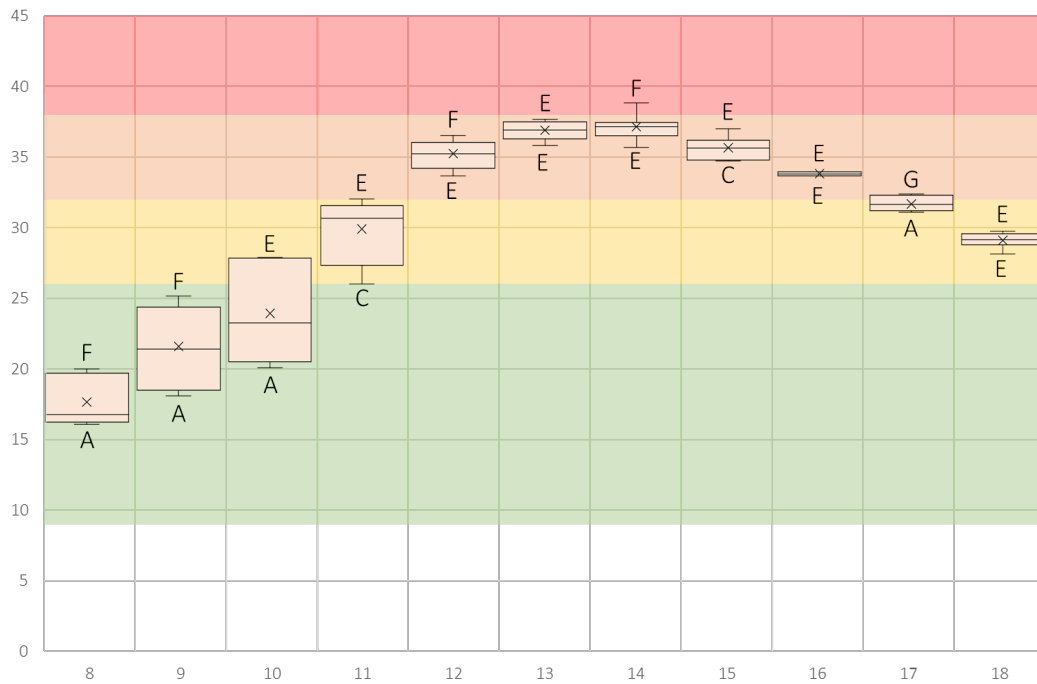
Graph 16 Distribution of the hourly values on the Tets Points – Plastic – 21/06.

The first thing to notice is that the mean value is not representative of the morning conditions of all the area, while in the afternoon the variability of the results is reduced and the UTCI average among the points can become a significative information. This is due to the distribution of the reflected radiation and of the shadows, the phenomenon depends on the location and orientation of the building, it is described in the Base Case discussion.

Then the focus can move to the difference between the materials. They both have the same reflectivity coefficient, but their behaviour is expected to be different as the plastic material is considered as a Lambertian surface while the metal material no. The geometry of the modules reduces considerably the effect of the applied opaque material, as there is no reflection of the radiation from these parts of the façade directly on the area, while it was visible in the T.3 configuration (this phenomenon will be deepened in the next pages, together with the glass behaviour in different geometries).

However, even if a direct influence of the material is not clear the distribution of the UTCI values among the Test Points is different. Considering as an example the 10:00 results, as at this time the variability is the highest registered during the whole day, here are reported the distributions on the square of the UTCI values.
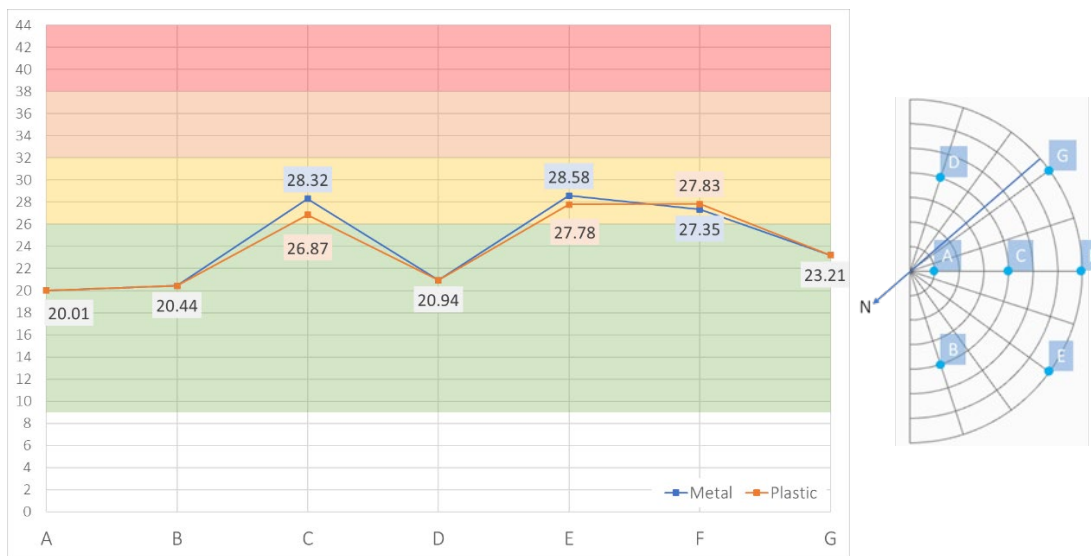
Graph 17 UTCI values for the Test Points – 10.00 – 21/06.
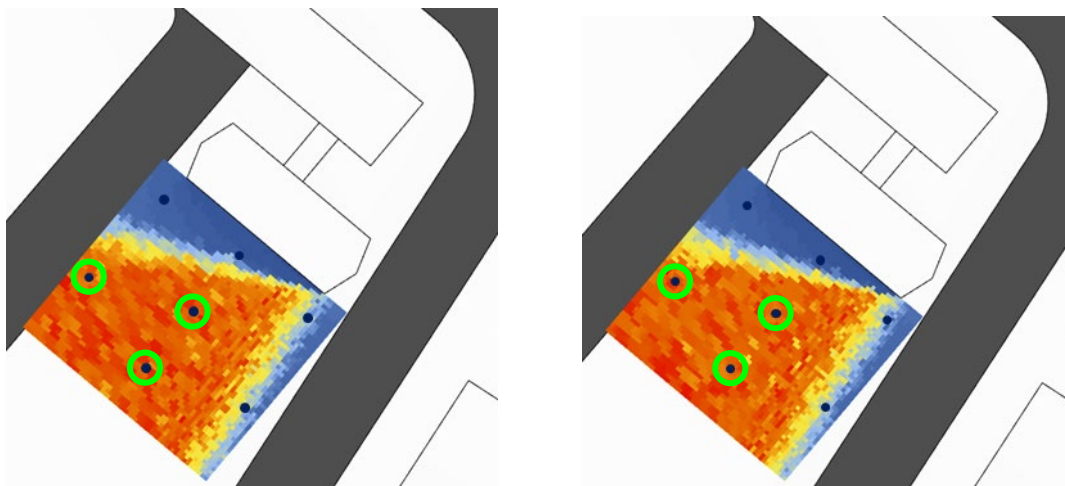
Figure 69 Radiation distribution on the square – 10.00 – 21/06.

As said in the first observation the high variability in the morning in this season is due to the presence of the shadow of the P39 building and the context on the square. In particular, points A, B, D, and G are in comfort conditions due to the shade that covers them. On the contrary, the 3 points out of the shaded area are in a Moderate heat stress condition, which is comfortable for short periods of time. In these points in the base case, the UTCI value registered was about 31°C, which is in the same stress range but in the sensation scale, move to a hot but not dangerous condition. This means that even though the average value is not representative of the whole condition the considerations made comparing the B.7 configuration with the Base Case are correct.

125

The three points hit by the direct and reflected radiation show different results for the two materials. This difference becomes more significant when the points are closer to the building, indeed in point C a difference of almost 1.5°C is registered. This implies that even though the direct effect is hidden by the geometry, the different nature of the opaque material influences the UTCI distribution on the studied area.

The effects of these configurations in the cold season are then considered. The hourly values are computed from 09:00 to 17:00, according to the sun path.
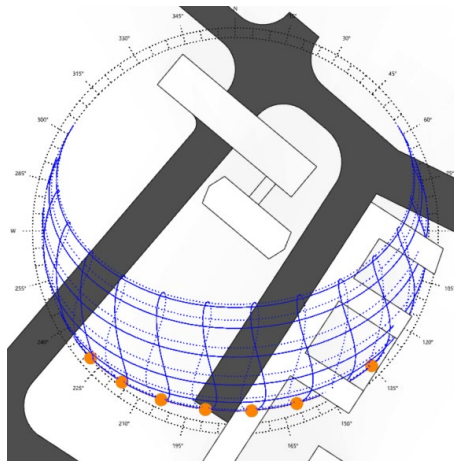
Figure 70 21/12 Hourly sun path.

As for the previous condition, the first graph represents the hourly UTCI average on the Test Points.

Graph 18 UTCI hourly mean values − 21/12.

126

The average condition is slightly better for the B.7 configuration in some hours but without significative changes in the comfort for the users. However as previously described is important to consider the distribution of the results.
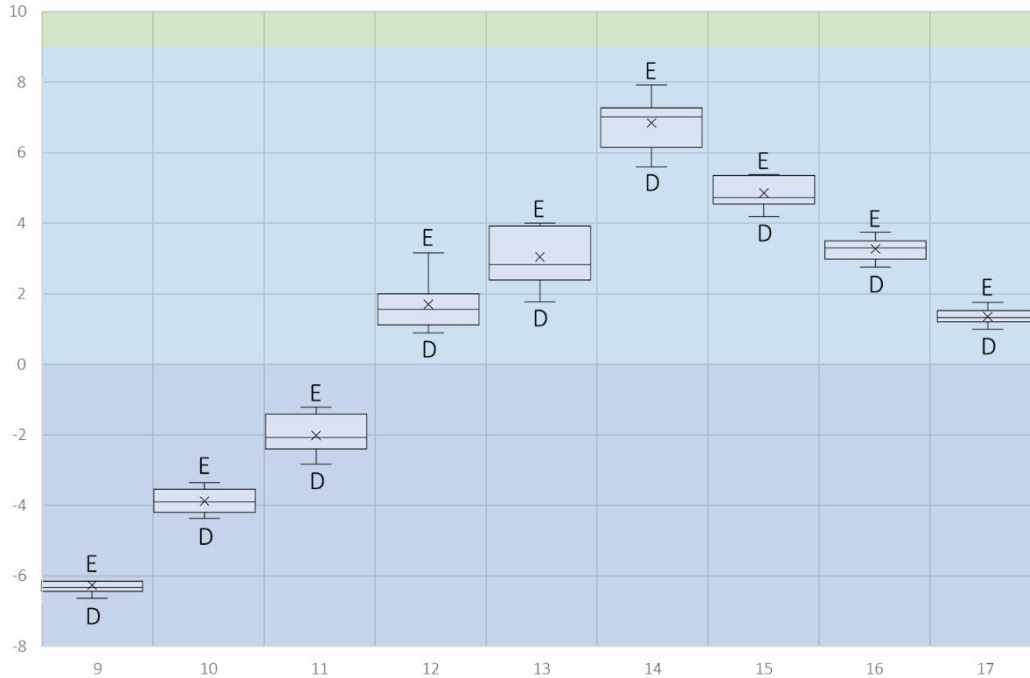
Graph 19 Distribution of the hourly values on the Tets Points – Metal – 21/12.
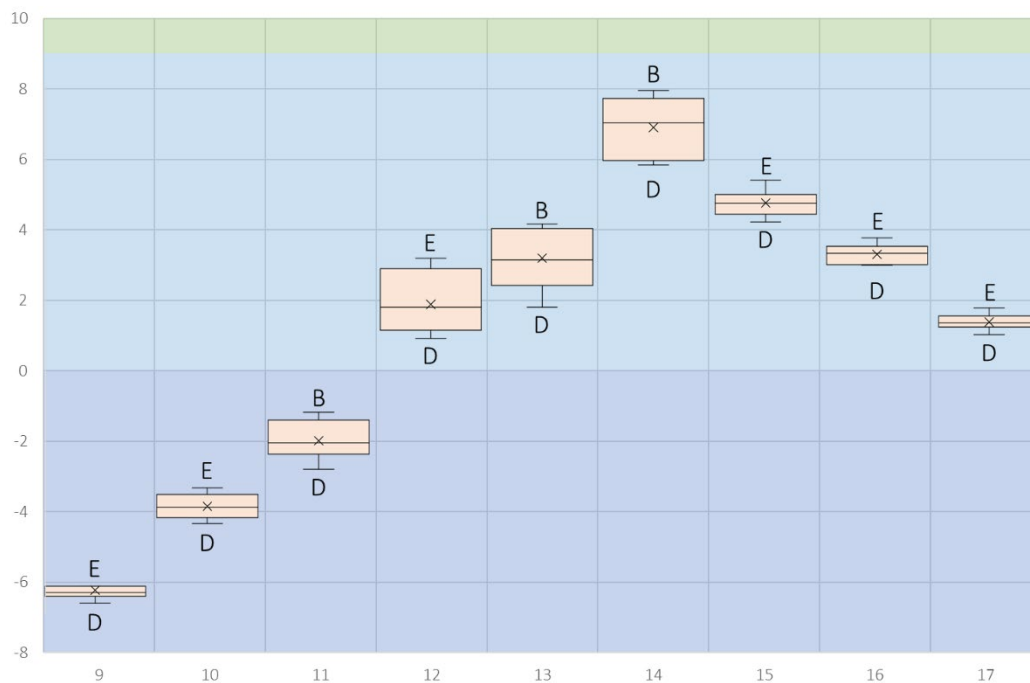
Graph 20 Distribution of the hourly values on the Tets Points – Plastic – 21/12.

As already highlighted in the Base Case discussion the higher fraction of diffused radiation during the cold season is reflected in a more uniform distribution of the UTCI results on the area. However, a significative difference between the points is registered during the central hours of the day. This is mainly due to the presence of the shadow of the P35 building that covers the eastern part of the square in these hours.
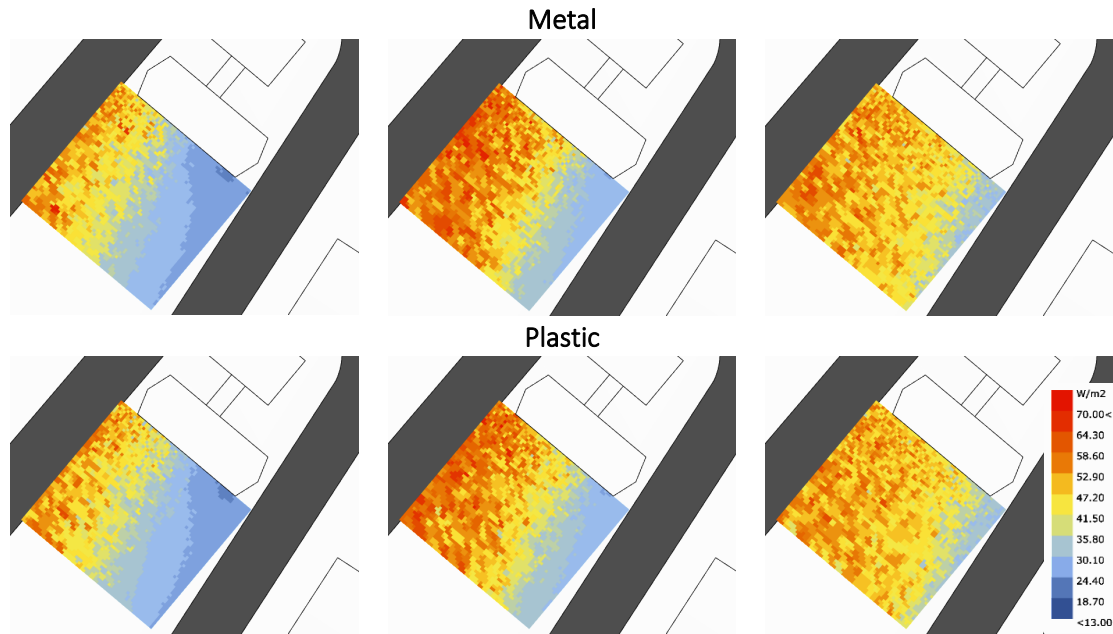
Figure 71 Radiation distribution on the square – 12:00, 13.00, 14.00 – 21/12.

The following table compares the results for 12:00, 13:00, and 14:00 with the Base Case:

	Base Case	B.7 Metal	B.7 Plastic		Base Case	B.7 Metal	B.7 Plastic		Base Case	B.7 Metal	B.7 Plastic
A	1.45	1.26	1.26	A	2.60	2.70	3.12	A	6.64	6.93	6.49
B	2.87	2.01	2.87	B	3.44	3.93	4.15	B	6.81	7.29	7.94
C	1.72	1.56	1.78	C	3.10	2.84	3.05	C	6.93	7.05	7.27
D	0.88	0.89	0.89	D	1.73	1.78	1.78	D	6.01	5.60	5.82
E	2.63	3.17	3.17	E	4.61	4.01	4.01	E	7.52	7.94	7.72
F	1.79	1.92	1.92	F	3.43	3.71	3.71	F	7.03	7.03	7.03
G	1.01	1.13	1.13	G	2.15	2.39	2.39	G	6.19	6.16	5.95

Table 52 UTCI values comparison for the Test Points – 12:00, 13:00, 14:00 – 21/12.

As observed comparing the averages in many cases the temperature is increased during the three hours. Highlighted with the darker green are the occasions in which the increment is more than 0.5°C, which may not change the heat stress category of the point, but during the cold season can be a good result. A different opaque material could

provide even better results, for example applying P.1 in the point E the UTCI is increased by more than 1°C as seen in the previous analysis.

All the considerations done until now are based on the body model of an average man, but this is not the only user that can benefit of this open area. For this reason, the same simulations have been performed for a 5yo children, whose body model considerably smaller than the ones of a man. This difference does not influence only the area exposed to the radiation, but also the view factors of the surrounding surfaces.

Figure 72 Average man and 5yo child models. Front and lateral view.

Following reported the hourly distribution of the results for the new subject, with the plastic material applied to the opaque elements. In this case, the variability among the Test Points is considerably reduced and the average UTCI value can be significant for the whole comfort condition because even though there are peaks the percentiles are close.
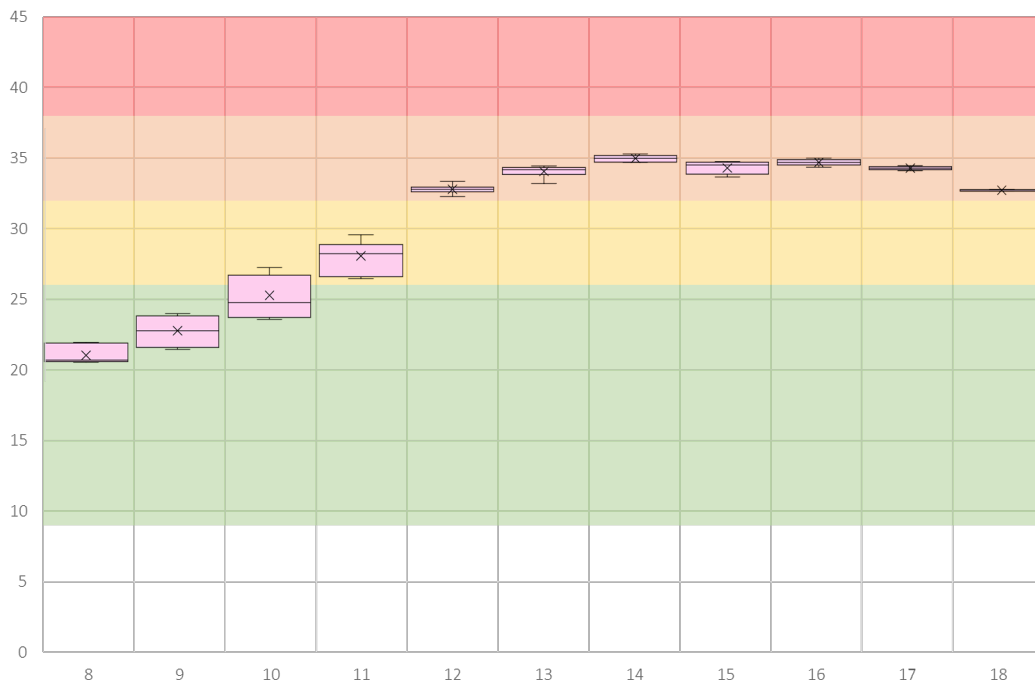
Graph 21 Distribution of the hourly values on the Tets Points – 5yo child – 21/06.
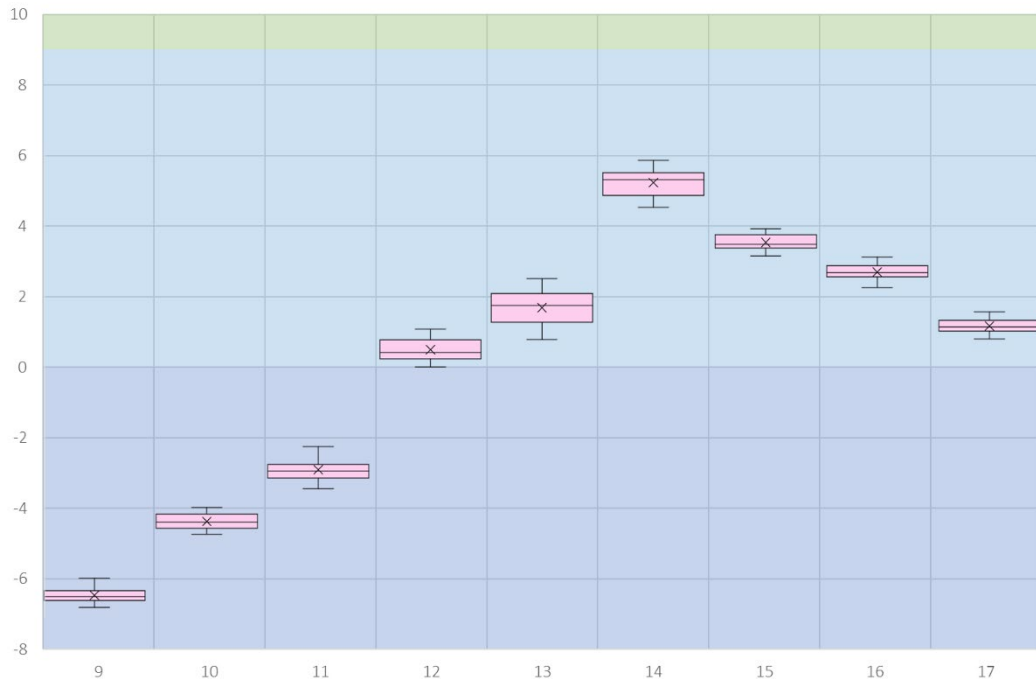
Graph 22 Distribution of the hourly values on the Tets Points – 5yo child – 21/12.

To compare the results with the ones obtained previously a simple parallel among the averages UTCI values would not be significant. For this reason, in the next graphs, the mean values of the 5yo child and the distribution of the average mane are reported.
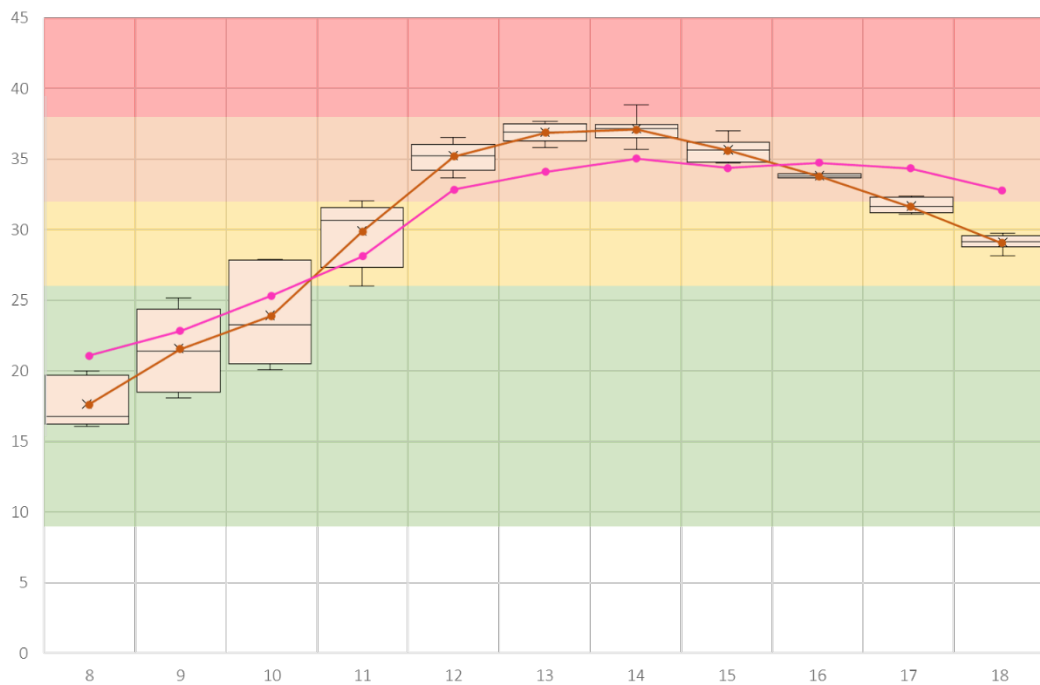
Graph 23 5yo child and Average man comparison – 21/06.
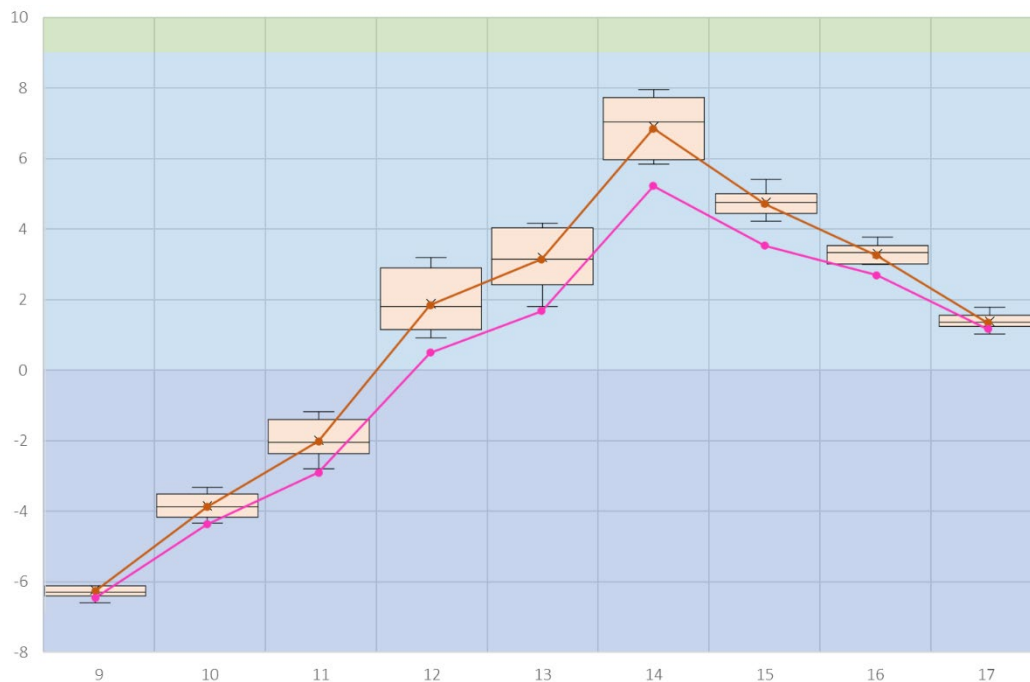
Graph 24 5yo child and Average man comparison – 21/12.

In the hot season representative day, the hourly trend is different than the previous one. The review can be divided into three parts:

1. 8.00 and after 16:00

    In this first set of hours, the average UTCI for the 5yo child is over the Man distribution. This means that it is a worst comfort condition for the new subject.

2. From 12:00 to 15:00

    In the central hours of the day on the contrary the values are lower, meaning that the comfort conditions are better for a 5yo child.

3. From 9:00 to 11:00

    During these three hours, the mean UTCI is higher than the average for a Man for the first two hours and then lower for the third, but the result is always included in the previous distribution. At this time we can state that the comfort is comparable with the one experienced by an adult.

The situation for the cold season is different. Excluded the results at 9:00 and at 17:00 where the comfort condition is comparable for the child and the adult, during the whole day the UTCI value is lower than the one registered previously. Hence, for a child, this design creates a worst comfort condition during the cold season.

5.2.4.   Borderline Cases

Due to the limits imposed by the will to respect the LEED requirements for internal visual comfort, some geometries were excluded from the study. For this reason, in this section, the geometry of the façade modules will be studied only concerning its effect on the surrounding urban environment, excluding the internal comfort.

In particular, the 3D extrusion of the façade module can lead to concertation of the radiation on the area in front of the building causing an increase of the discomfort in the hot season.

The settings currently considered create overhangs that overshadow the glazed parts during the central hours of the day and that create secondary reflections between the modules that limit the radiation incident on the square. This phenomenon is the reason why in some cases the effect of the applied opaque materials is not as noticeable as expect.

Following are reported the cases of the simulation matrix, to emphasize the impact of the geometry in these images the materials are considered with a specular behaviour.
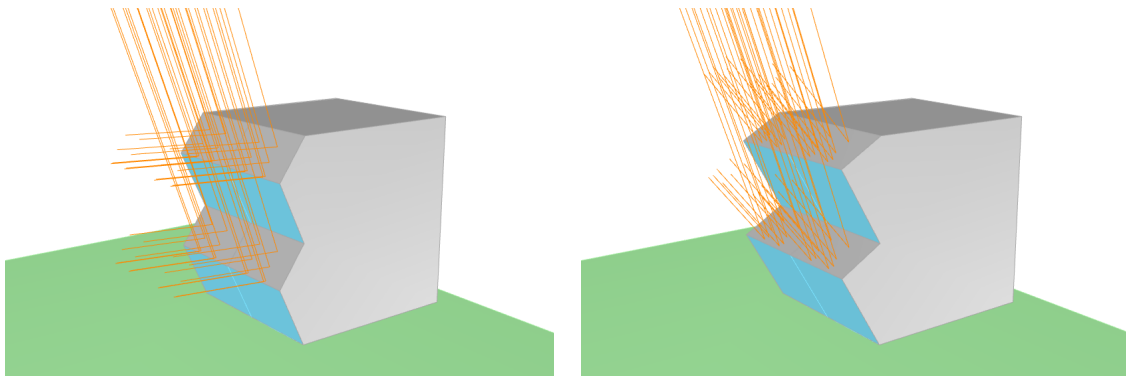
Figure 73 Radiation reflection – cases D and 5.
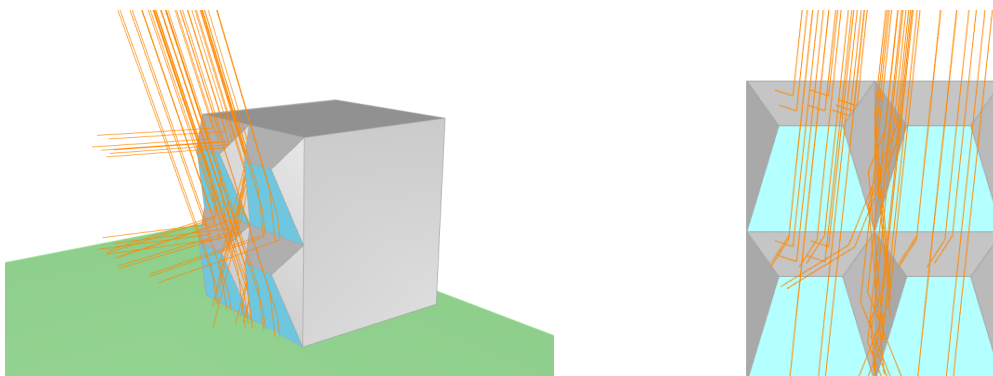
Figure 74 Radiation reflection – cases B7.
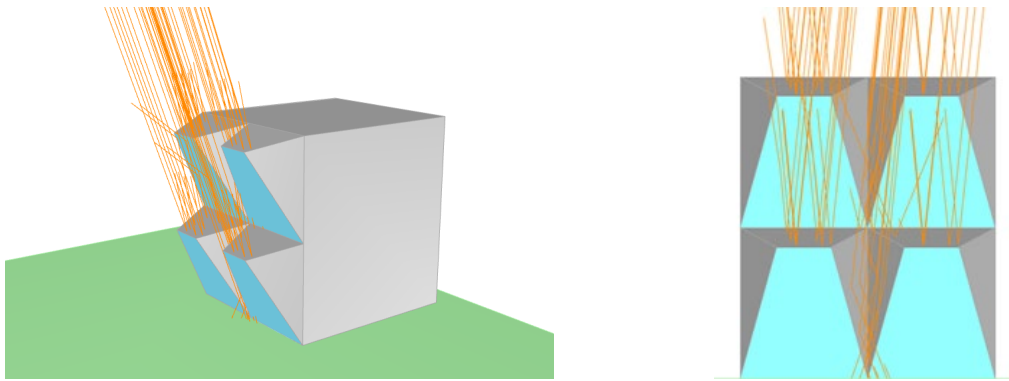
Figure 75 Radiation reflection – cases 68.
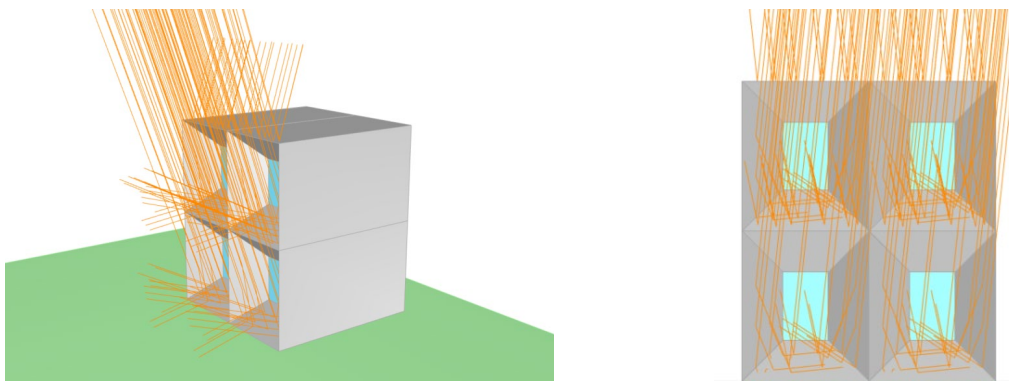
Figure 76 Radiation reflection – cases Hr.

These models are facing south, and the chosen time is 12:00 because is when the solar altitude is maximum.

To have a reflection on the square the angles of inclination of the glass must be reduced, while for the Hr case the transparent part must be advanced so that the opaque inclination is reduced.

Among the cases of the families only two of them are considered for this analysis:

- 3D type 1 subfamily L
- 3D type 2

This is to avoid performing simulations whose result overlaps and to consider with the first family the impact of the glazed surface, while with the second one the impact of the high reflective materials.

According to the orientation of the case study, the hour of the day that maximizes the reflection on the area is 14:00, despite it does not coincide with the hour of the day with the highest sun position.
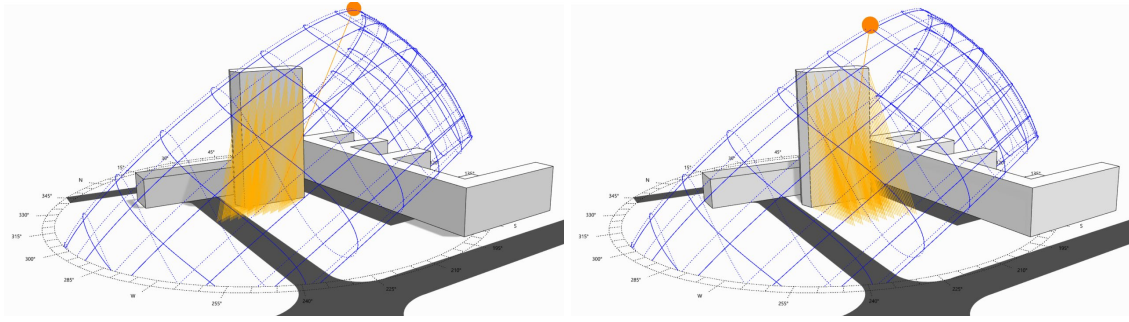
Figure 77 Radiation reflection from the plane façade – 12:00 and 14:00.

In this analysis, higher precision in the simulation is required as the focus is on the distribution of the radiation on the grid. For this reason, the adopted Radiance Parameters are the one of the Set 3:

SET 3	
-ab	5
-ar	512
-aa	0.08

Table 53 Radiance Parameters Set 3.

3D façade _ Type 1 subfamily L

The critical configurations are the ones here reported, the range goes from the minimum value that departs the configuration from the plane façade to the maximum value before there is an interaction with the opaque element. For each case the length of L and the angle between incident rays and the normal to the glazed surface:

L [m]	0.2	0.4	0.6
Angle [°]	63.24	65.55	68.11

Table 54 Critical cases of the subfamily L.

	0.2	0.4	0.6
A	47.374	47.754	48.328
B	46.850	47.226	47.415
C	47.027	46.278	44.985
D	45.081	45.081	45.081
E	45.645	45.093	44.910
F	45.024	44.841	44.841
G	44.969	44.786	44.786

Table 55 UTCI results for the critical cases of the subfamily L.
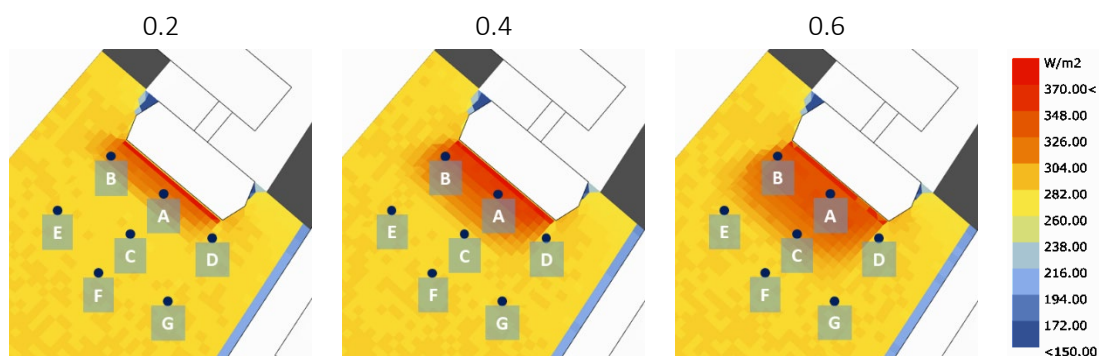
Figure 78 Radiation distribution on the square for the critical cases of the subfamily L.

The UTCI results register a difference between the points interested by the reflected radiation and those out of the zone hit directly of 3-4°C.

This difference is relevant and should be considered in the design process, it is also important to remember that the material applied is not a metal but a glass, which is not completely reflective. The more we get close to the critical angle of this transparent material (which is about 80° between the incident ray and the normal) the more it behaves as a specular material. With this geometry the closer that we can get to that angle is 68.11°, due to the limitations deriving from interaction with the other modules, indeed it is the configuration that shows the highest UTCI difference.

Another important point is that, even if also in the previous configurations the impact of the opaque elements was limited, now the secondary reflections are removed and therefore the influence of the material is removed.

3D façade _ Type 2

The study of this geometry is harder as the rays are reflected in different directions from each opaque surface, in particular, the upper panel reflects the radiation on the other surfaces since the very first inclinations.

To reduce secondary bounces on the glazed part in order to maximize the impact of the material for this specific time of the day, the only configuration chosen is the one with an extrusion of the window of 0.2m.
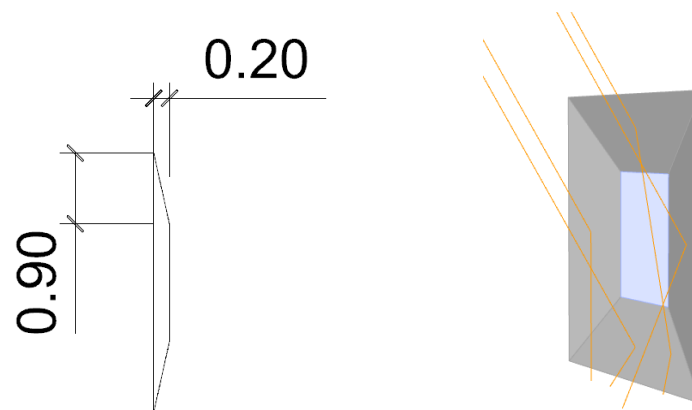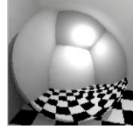
Figure 79 Geometry definition and Radiation reflection of the module for type 2.

Also the application to the case study highlights the complexity of the pattern created by the radiation reflected by the façade, in the following images only the rays coming from the opaque elements are reported.
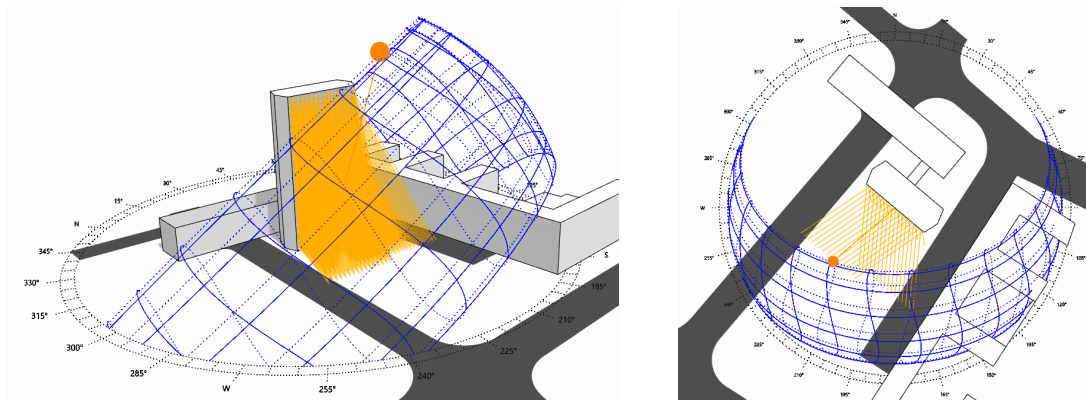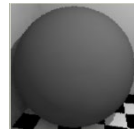
Figure 80 Radiation reflection from the type 2 configuration applied to the Case Study.

To highlight the effect of high reflective opaque material, two different simulations are performed, the first material applied is a metal material with a high reflective coefficient, the second one is a plastic material with a high absorptance.

```
void metal Metal_ro(0)_sp(1)_re(0.9)
0
0
5  0.9 0.9 0.9
   1.0 0.0
```

```
void plastic Plastic_ro(0)_sp(1)_re(0.9)
0
0
5  0.1 0.1 0.1
   0.0 0.0
```

These two cases were chosen to understand the behaviour of the two different types of materials in relation to a façade geometry in which opaque parts are prevalent and with a significant impact on the comfort of the adjacent area.

	P_0_0_0.1			M_0_1_0.9		
	sw	lw	UTCI	sw	lw	UTCI
A	48.646	28.089	42.095	76.191	28.174	49.134
B	48.646	28.273	42.140	63.297	28.357	45.815
C	48.646	28.215	42.126	66.228	28.319	46.557
D	48.059	27.852	41.895	54.506	27.931	43.497
E	48.646	28.665	42.236	55.953	28.791	43.856
F	48.059	28.364	42.019	60.954	28.491	45.252
G	48.059	28.133	41.963	53.334	28.252	43.286

Table 56 Results for the family 3D type 2.
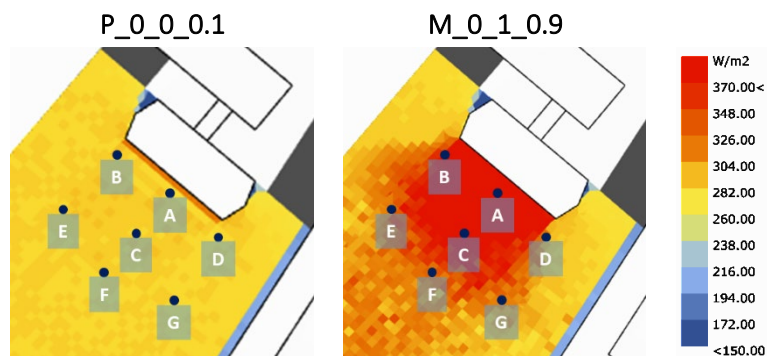
Figure 81 Radiation distribution on the square for the family 3D type 2.

The first material applied is a plastic one, this mean that the surface is treated as Lambertian. Lambertian reflectance is the property that defines an ideal "matte" or diffusely reflecting surface.
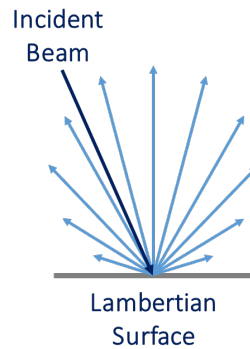
Figure 82 Lambertian surface behaviour.

As consequence the distribution of radiation on the square is even and so are the sw MRT and the UTCI values among the Test Points.

In the second case, a metal material is applied, it is the same as plastic except that the specular component is coloured by the material. The consequence is that the radiation is reflected on the study area following the pattern previously described. Points A and C are the ones invested by the highest amount of radiation and indeed they are characterized by a UTCI value even 6°C higher than the points out of the direct impact of the reflected radiation and 7°C higher than the corresponding point in the previous case.

The difference in the incident radiation distribution on the grid is reflected in the values of short wave MRT computed, for the plastic material the values are lower and almost equal, while for the metal material the results are higher and there is a considerable difference between the Test Points.

6

CONCLUSION
RESULTS DISCUSSION AND FUTURE
SCENARIOS

6.   Conclusions

The purpose of this thesis work was to understand the impact on the Outdoor Thermal Comfort of different façades configurations designed with the focus of achieving Indoor Daylight Comfort according to the LEED standards.

The focuses of the thesis have been therefore two: the design of a unitized façade and the development of a tool to evaluate it.

To do so, a new workflow based on a Grasshopper script was developed. While for the indoor simulations a well-known procedure was applied, for the outdoor impact evaluation the available tools presented different limitations. This led me to decide to study and understand the physical models behind the calculation of the Indexes used to assess the thermal comfort in the urban environment and then translate them into a programming language for the actual computation. The resulting script is a combination of available components for the environmental analysis and custom components for the actual outdoor comfort parameters computation.

The design process was at first performed for a generic south-oriented unitized façade and only on a second step applied and adapted to the Case Study. The project of the modules was characterized by two main points: geometry and material.

For the geometry one, three main rules have been defined, to be able to study the impact of different geometries, and tested, in order to find the best cases to apply. The materials for the opaque elements have been chosen to represent all the possible architectural choices.

The Case Study highlighted a fundamental difference between the plane façade and the 3D modules, in particular, due to the way they reflect the radiation.

Compared to the Base Case, an all-glazed plane façade, the "Plane façade _ Opaque-transparency ratio" configuration does not change the pattern of the radiation incident on the square with its geometry, but the influence of the material is evident. Indeed, the UTCI distribution observed on the Test Points does not change, while the values mutate according to the variation of material. As consequence, the design combinations for which a positive effect was found in the hot season do not coincide with the best ones for the cold season.

On the contrary, the 3D families reflect the radiation in a completely different way, away from the square when the sun is higher and when is lower directly on the study area. As consequence, these configurations return a positive effect in both seasons.

The impact of the opaque material is reduced for all the 3D cases, but in different ways:

- 3D façade _ Type 1 Subfamily α: in the hot season the influence is almost null, but in the cold season high reflective materials increase the UTCI.

- 3D façade _ Type 1 Subfamily L: the influence is almost null in both seasons.

- 3D façade _ Type 1 Subfamily d: the influence is low but present in both seasons, with an opposite effect for the two periods.

- 3D façade _ Type 2: in the hot season the influence is almost null, but in the cold season high reflective materials increase the UTCI.

According to the results obtained by the simulations performed at 12:00, the best case is the "3D façade _ Type 1 Subfamily d" for both seasons, the material chosen for the following analysis is the one that resulted best for the hot season application, as it presents the most critical conditions.

In the second step of the analysis, the study of the best case was deepened extending the simulation to the whole day and different subjects. From the simulations, results were found that the comfort can not be evaluated by the mean UTCI value on the grid, especially during the morning for the hot season and the central hours of the day for the cold season, for this particular Case Study. At the same time also a gap in the comfort perception for different subjects is highlighted, which is not just simply a reduction or increase of the UTCI values but presents another evolution of the comfort during the day.

In the last section of the analysis, the script has been applied to study two configurations that do not observe the LEED prescriptions, to study the effects of two borderline cases excluded previously. From this deepening one possible application that raised is on the study of the critical angle of the glazed components and the consequent effect on the comfort conditions. Due to the combination of the orientation of the building and geometry of the façade the specific angle could not be reached for this Case Study.

This demonstrated how the developed script can be applied in any study that requires evaluating the impact of a façade design on the thermal comfort in the urban environment. The workflow here proposed could be applied to the first stages of the design to evaluate the effect of the form-finding ideas combined with different materials, but the geometry could be easily complicated adding other details to evaluate also not only the main geometry but also the impact of mullion, transoms or external shading systems.

It is important to remember that the focus of this work is the thermal comfort of the users in the open area, therefore the evaluation of materials is only linked to the UTCI

results. These materials may not correspond with those that would be optimal for the Urban Heat Island effect. To implement the UHI mitigation in the equation the 3D façade_Type 1 Subfamily α and Subfamily L for which the influence of the material is almost null and a high albedo material can be applied. Another option is to consider applying retroreflective materials, that reflect the incoming beam radiation back to the source (if the retroreflection is three-dimensional and ideal) or at least upwards (if the retroreflection is two-dimensional and/or imperfect)[50].

Possible future development of this framework could be the introduction of other environmental parameters for the evaluation of the design:

- For the indoor, an assessment of the impact of the surface temperatures deriving from each configuration of the modules, on the Indoor Thermal Comfort, and consequently on the energy consumption, would be useful: to achieve this will be required an evolution in the surface temperature computation procedure that now consider a fixed indoor temperature.

- At the same time, for the outdoor, the evaluation of the presence of glare, and consequent creation of visual discomfort spots on the area adjacent to the façade, could complete the workflow.

A

APPENDIX
OUTDOOR THERMAL COMFORT SIMULATION

APPENDIX A

This appendix is focused on the explanation of the workflow to follow to properly apply the Outdoor Comfort evaluating tool developed as a Grasshopper script.

The parametric nature of the tool allows the user to adapt it to different geometries, urban environments, and locations.

The next paragraphs are not intended as a detailed explanation of the components used or created, as the theoretical concepts behind the script have already been exposed in the previous chapters, but as a practical guide for the use of the script resulted from this thesis work. The complete schematic representation of the whole path is here reported:
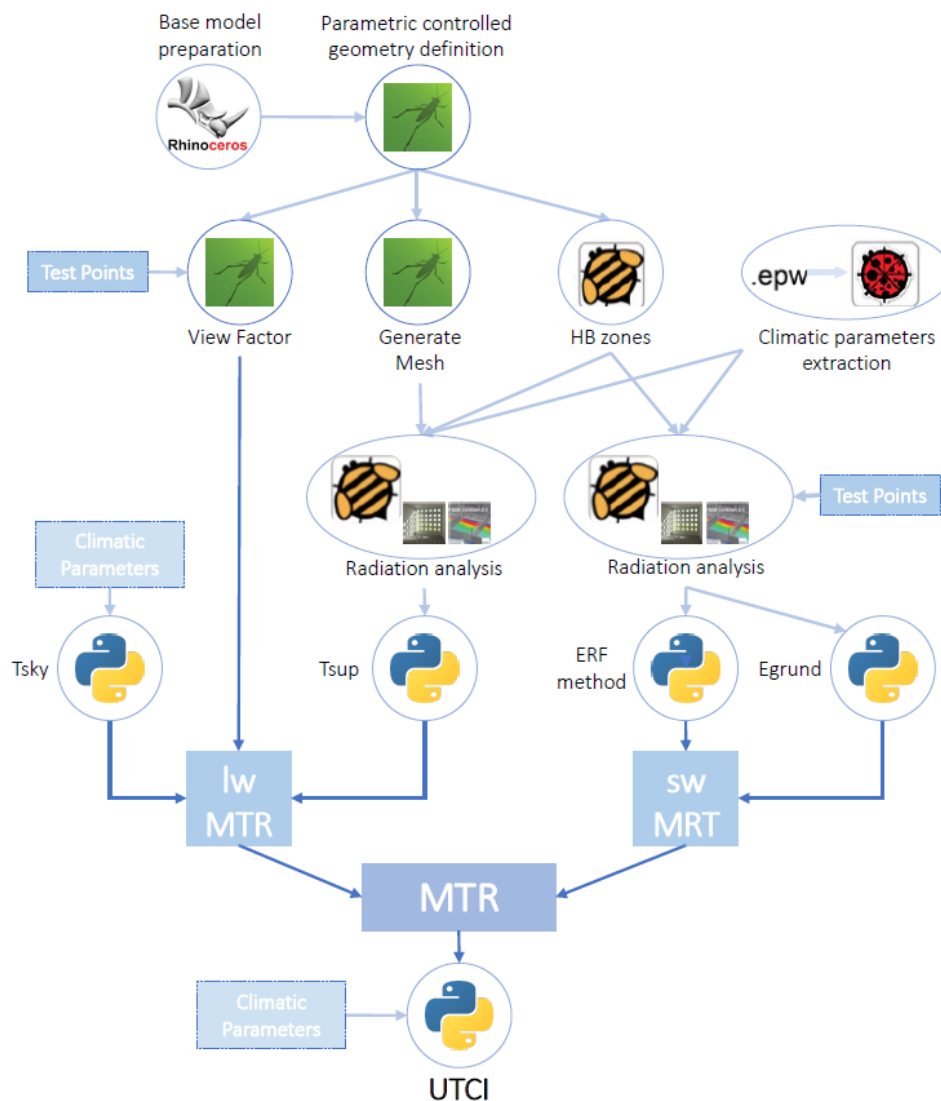
Figure 83 Schematic representation of the Outdoor Thermal Comfort Simulation.

Outdoor Thermal Comfort Simulation

Simulation setting

Geometry definition

The first step of the process is the definition of geometry, both of the urban environment and the subject of the study.

The modelling of the geometry can be done also in the Rhino environment but must be internalized in Grasshopper to proceed with the simulation.

In the specific case of the case study presented in this thesis, the base of the geometry was modelled in Rhino and then internalized in Grasshopper to modify it and add the parametric definition of the façade.
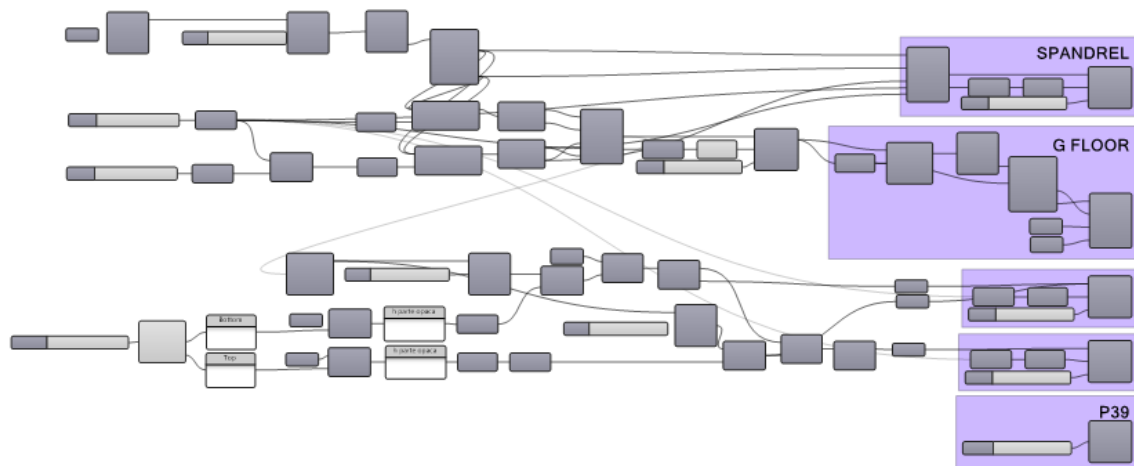
Figure 84 Grasshopper script – Geometry definition.

HB zones definition

Once the geometry has been defined the second step is the creation of the Honeybee zones, divided into the main building, context, and ground areas.

For the definition of the main building, each surface will be considered, and the typology and the Radiance material will be assigned. The surfaces will be then joined again to create the zone. To the ground surface, an Energy+ material will be assigned, but this will not be considered in the Radiation analysis. In the end, the context area is defined with the application of the Radiance material.

The number and type of zones depend on the urban environment considered.
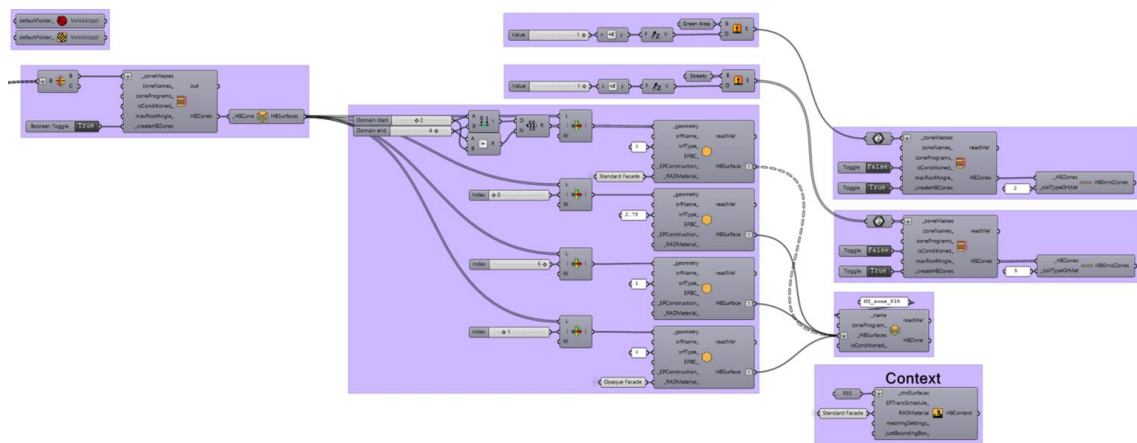
Figure 85 Grasshopper script – HB Zones definition.

Material definition

As anticipated when the zones are defined the Radiance material is assigned to each surface of the envelope.

Following the parametric definition of the primitives for the envelope finishing opaque materials, and consequently the solar absorptance of the envelope.
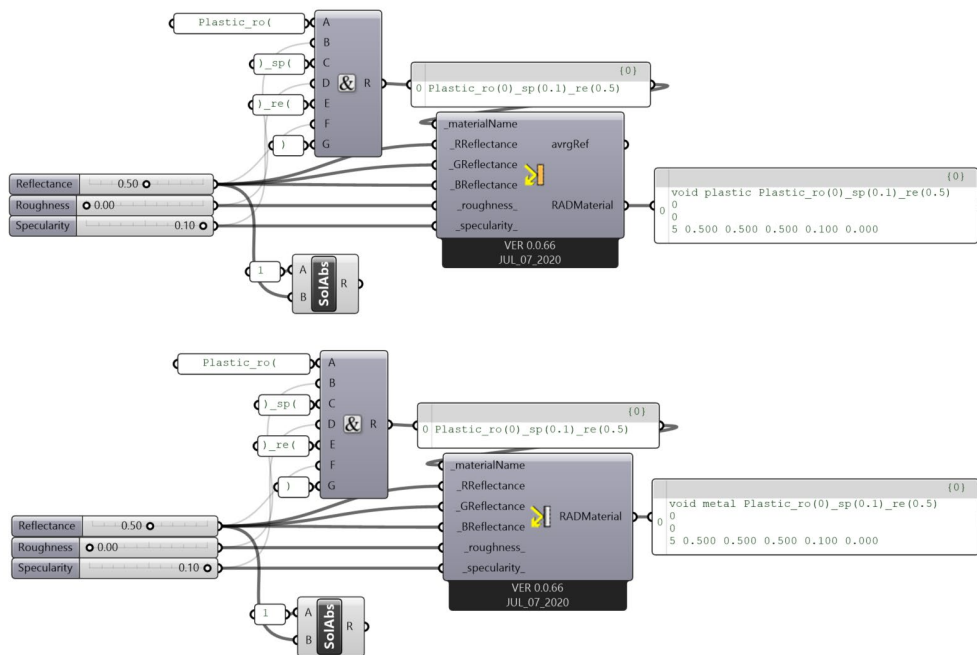
Figure 86 Grasshopper script – Material definition.

Test point Definition

The third step of setting for the simulation is the choice of the Test Points, which means the locations for which the comfort level will be calculated.

In the script developed 2 options are proposed:

- A Polar reference system-based grid (which is the one chosen for the case study),

- A Cartesian reference system-based grid.

Among the points of the grid, it is possible to choose the most relevant points for the specific analysis. Besides the geometric definition of the points, a small Python script-based component has been developed so that choosing from the available list the preferred option the Test Points and the related Mesh are automatically selected.

asshopper script – Test Points definition.
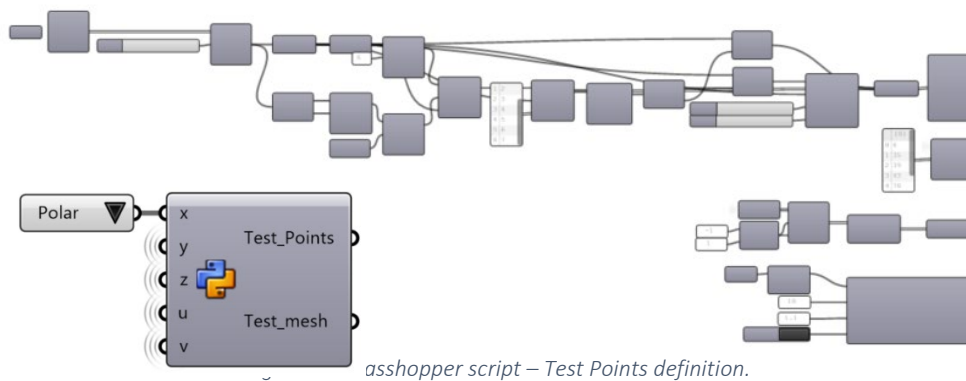
Human body model

Now that the Test Points have been chosen for each of them the human body model must be set. The reference model has been described previously and is based on an ellipsoid. In this case, the human body is considered facing the main building, but the model can be rotated on its axis according to the will of the user.

As for the Test point, a list is provided so that choosing from that the subject of the analysis the model adapts its dimensions automatically.
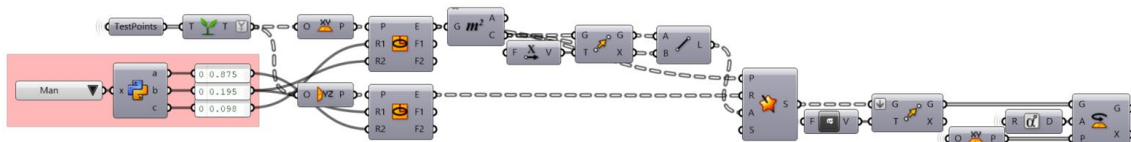
Figure 88 Grasshopper script – Human Body Model definition.

Set the grid on all the context

Lastly, for the calculation of the long wave MRT, and more specifically of the T_{sup}, it is necessary to set a grid of Test Points on all the urban context considered. As mentioned

for the definition of the HB Zones this step is strictly connected with the geometry of the urban context considered.
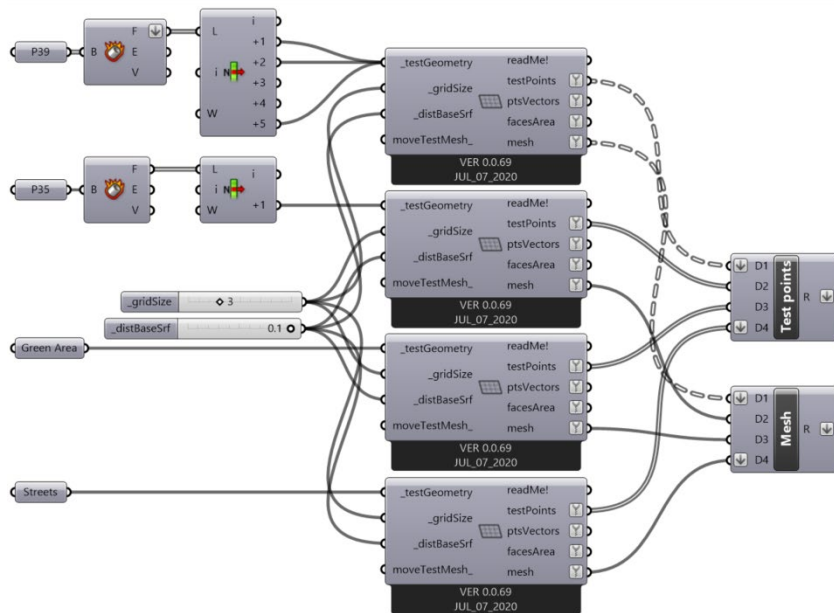
Figure 89 Grasshopper script – Contest Test Point grid definition.

Running the simulation

sw MRT calculation

The first path of the simulation process is the calculation of the short wave MRT, which is the contribution in the MRT calculation of the direct, diffuse, and reflected solar radiation directly on the human body.

Therefore the first step is the calculation of the total incident radiation on the Test Points.

To do that the user should at first generate a cumulative sky, with the *Generate Cumulative Sky* component (that can be used only for radiation analysis). After that, the Rad parameters must be set and both used as input in the *Grid-Based Simulation* component. At this point the Honeybee component *run Daylight Simulation* is used, which allows exporting geometries to rad file, and run daylighting/energy simulation with radiance.

The results, which are in kWh/m^2, are immediately converted in W/m^2 to be able to apply the ERF method.
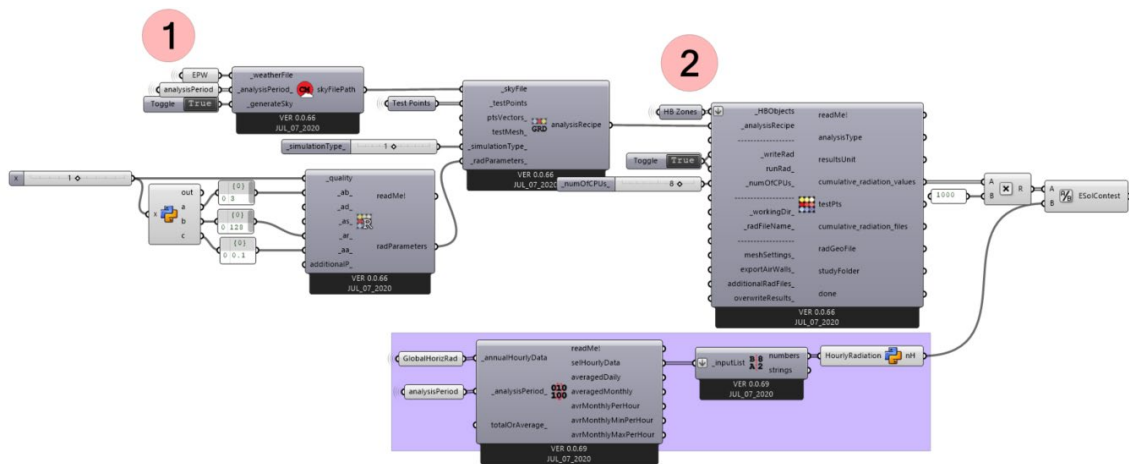
Figure 90 Grasshopper script – Radiation Analysis for the Test Points.

The physics and the assumption behind this method have been explained in the Methodology chapter, the application of it is here reported.

The total incident radiation from the sky and reflected by the buildings is used to find the approximate radiation reflected by the ground, through a generic value of albedo and the calculated view factor for each Test Point.

In this way, the total E_{sol} is calculated and used to apply the Effective Radiant Field method.
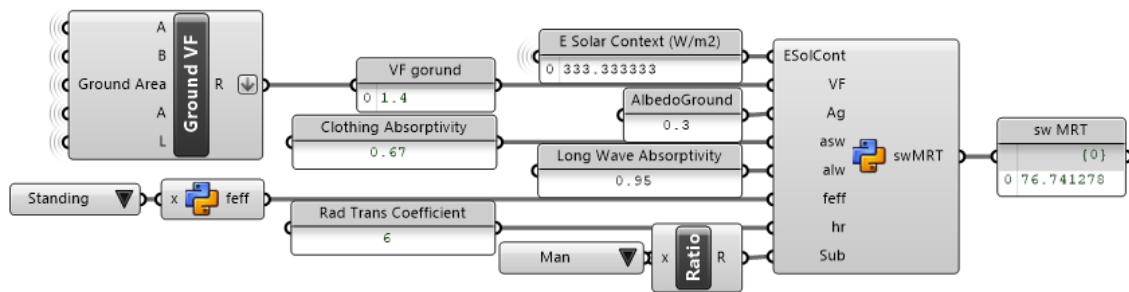
Figure 91 Grasshopper script – ERF method application.

Both for the calculation of the E_{ground} and the sw MRT a Python code was written and implemented in a custom component.

In the ERF method, it is possible to choose the posture of the subject of the analysis, as it influences the portion of the body that is exposed, but the model used in the second part of the script only considers the standing position, therefore, to use the sitting option the ellipsoid model described should be changed.

lw MRT calculation

the first step of this path is analogous to the first stage of the sw MTR calculation, the only difference is the Test Points subject of the simulation, that in this case are disposed on a grid that covers all the context.
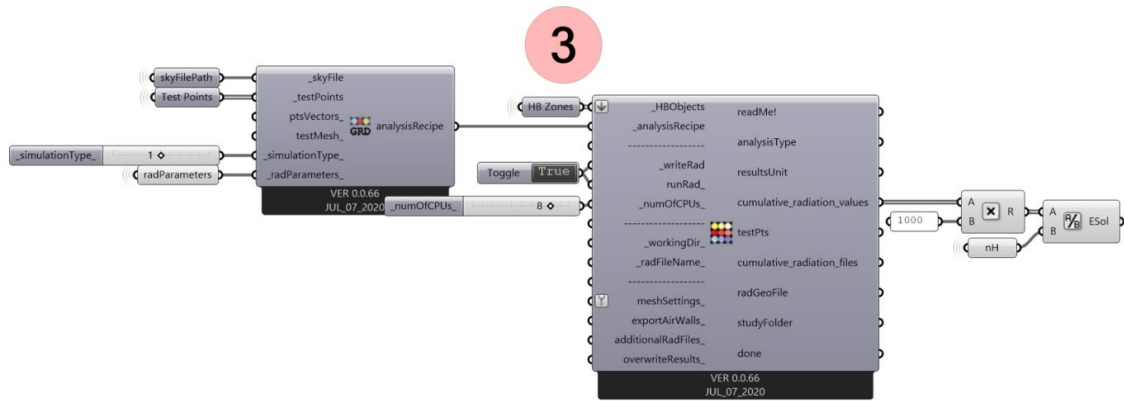
Figure 92 Grasshopper script – Radiation Analysis for the context grid.

The next step is the surface Temperature calculation, but to be able to do that the radiation values resulted from the previous simulation should be divided to assign the correct value and the correct properties to each urban surface.

Once this procedure is completed the user can proceed with the calculation of the Surface Temperatures.

To do that the heat diffusion equation process was written in a python code through the forward Euler method and applied in a custom component.
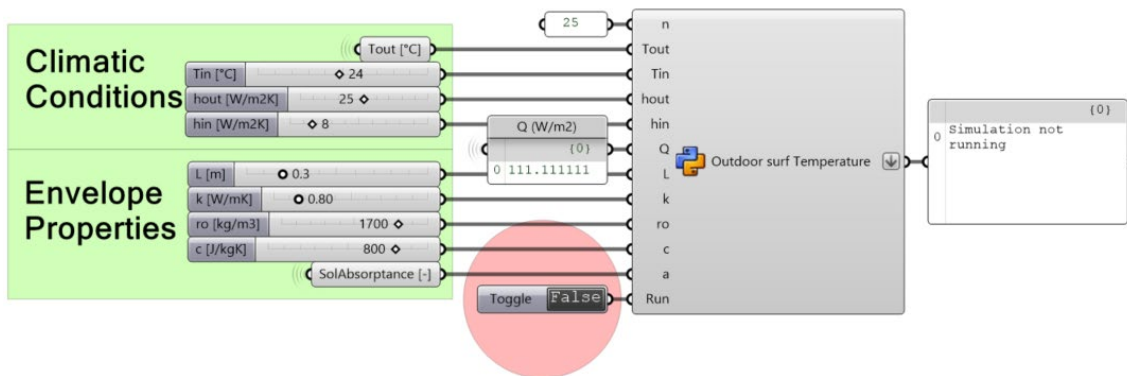
Figure 93 Grasshopper script – Wall Tsup calculation.

When the ground is considered the boundary conditions are different and consequently also the required input.
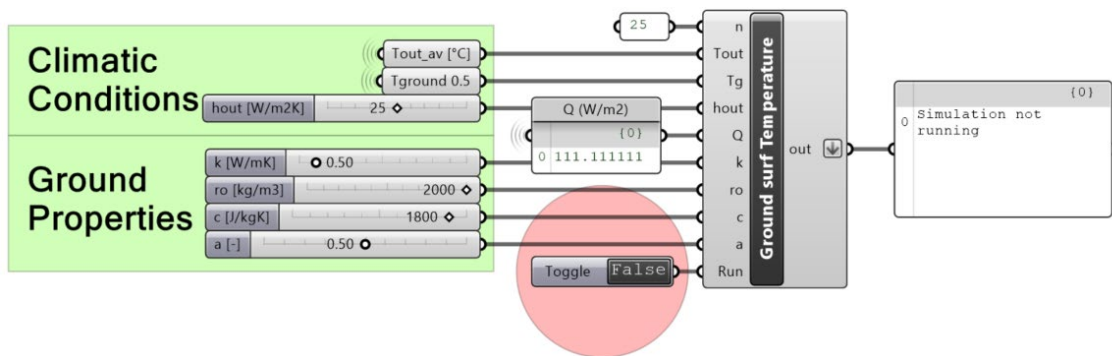
Figure 94 Grasshopper script – Ground T$_{sup}$ calculation.

The other necessary temperature for the lw MRT calculation is the Temperature of the Sky, which is derived from the Horizontal infrared Radiation provided by the EPW.

Again, the theoretical concepts have been translated into Python code to calculate it and applied in a custom component.
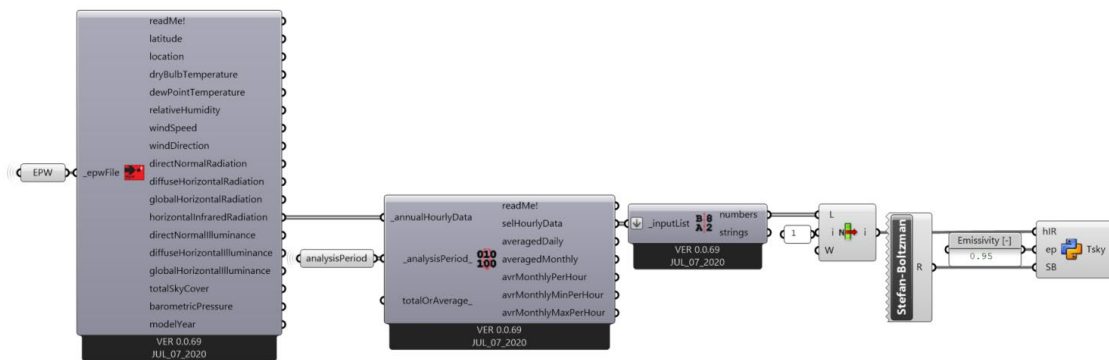
Figure 95 Grasshopper script – Tsky calculation.

The last factor necessary to conclude the path is the calculation of the View Factor.

Starting from the human body model described in the settings paragraph the surrounding surfaces are raytraced with zero bounces and the VF calculated.
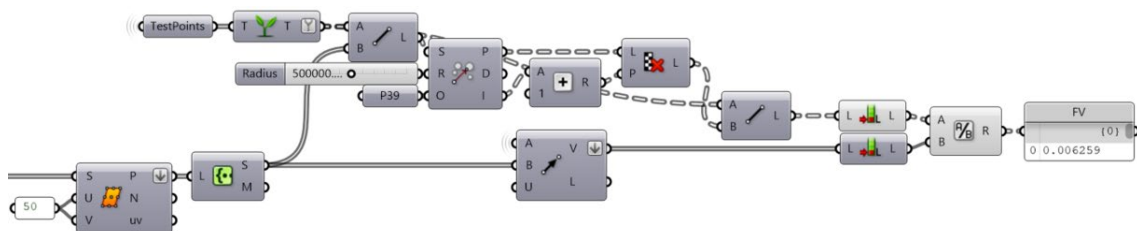
Figure 96 Grasshopper script – View Factor calculation.

Now that all the necessary components are available the lw MRT is calculated:
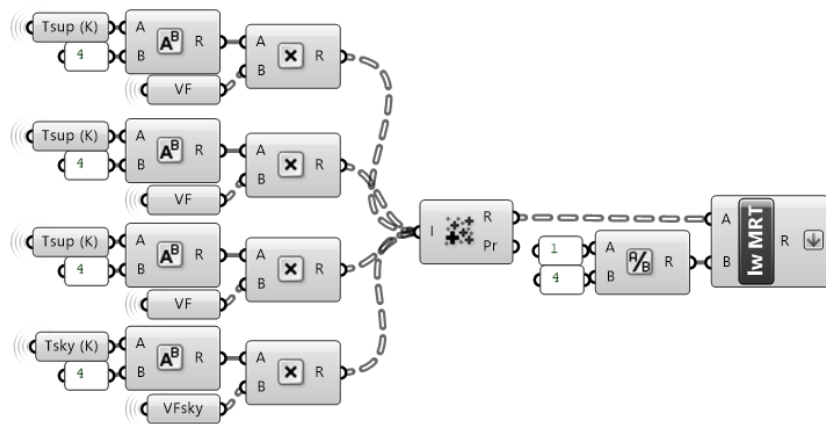
Figure 97 Grasshopper script – lw MRT calculation.

It is important to remember that the input temperature must be in Kelvin, therefore the results must be converted before proceeding with the simulation as the UTCI calculation requires input temperatures in degrees Celsius (In the script this conversion is sone automatically).

UTCI

The last step of the simulation is the UTCI calculation. To proceed with it the necessary inputs are the climatic conditions and the Mean Radiant Temperature, which results from the combination of the long wave and the short wave contributions.

In this stage, the sw and lw MRT are converted to degrees Celsius and summed.

For the UTCI calculation itself, the code has been translated and adapted in the Python programming language from the original Fortran code, available on the UTCI official web page by the COST Action 730, and used to create a new custom component.
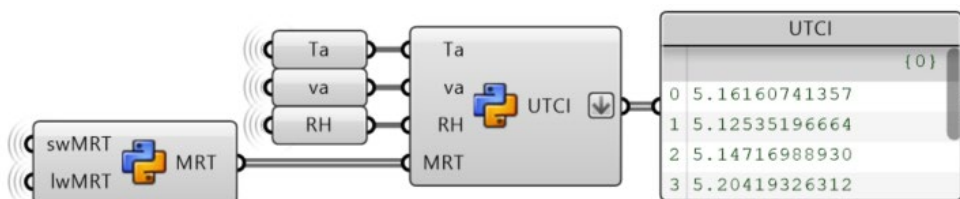
Figure 98 Grasshopper script – UTCI calculation.

B

APPENDIX
PYTHON CODES DEVELOPPED FOR THE
APPLICATION OF THE PHYSICAL MODELS

APPENDIX B

In this section, the Python codes developed for the application of the physical models are reported. These scripts are adapted for the application in the Grasshopper environment through the GhPython component, therefore, the variables are defined as inputs to the component.

ERF Method

```python
"""Inputs:
      ESolCont : sw solar radiant flux from the context - ground excluded (W/m2)
      VF : View Factor of the ground (-)
      Ag : ground albedo (-)
      asw : short wave absorptivity (-)
      alw : long wave absorptivity (-)
      feff : fraction of the body exposed to radiation (-)
      hirr : radiation heat transfer coefficient (W/m2K)
      Sub : ratio between the Man and the subject body model areas (-)
   Output:
       swMRT : short wave mean radiant temperature (°C) """


# ***********************************************************************
#    Ground reflected radiation function, EreflGround(VF, ESolCont, Ag)
# ***********************************************************************
# Function to calculate the sw solar radiant flux reflected by the ground in W/m2
#
# Input parameters
# - ESolCont : sw solar radiant flux from the context - ground excluded (W/m2)
# - VF : View Factor of the ground (-)
# - Ag : ground albedo (-)
# ***********************************************************************

def EreflGround(VF, ESolCont, Ag):

    Erg = VF * ESolCont * Ag

    return Erg


# *************************************************************************
#    Short wave delta MRT function, DTmrt(Esol, asw, alw, feff, hirr, Sub)
# *************************************************************************
# Function to calculate the sw contribution to the total MRT in °C
#
# Input parameters
# - ESol : total sw solar radiant flux (W/m2)
# - asw : short wave absorptivity (-)
# - alw : long wave absorptivity (-)
# - feff : fraction of the body exposed to radiation (-)
# - hirr : radiation heat transfer coefficient (W/m2K)
# - Sub : ratio between the Man and the subject body model areas (-)
# *************************************************************************

def DTmrt(Esol, asw, alw, feff, hirr, Sub):

    D = (Esol * Sub * asw) / (alw * feff * hirr)
```

```python
    return D

# ********************
#    Code application
# ********************

Esol = ESolCont + EreflGround(VF, ESolCont, Ag) # total Esol calculation

swMRT = DTmrt(Esol, asw, alw, feff, hr)
```

Surface Temperatures

Application to a generic wall

```python
"""Inputs:
       n : number of layers (-)
       Tout : outdoor air temperature (°C)
       Tin : indoor air temperature (°C)
       hout : outdoor convective coefficient (W/m2K)
       hin : indoor convective coefficient (W/m2K)
       Q : incident radiation (W/m2)
       L : wall thickness (m)
       k : conductivity (W/mK)
       ro : density (kg/m3)
       c : specific heat capacity (j/kgK)
       a : solar absorbance (-)
       Run : set Boolean to True to run the component
   Output:
        Tsup : surface temperature (°C)"""

# set the required variables

T0 = 0.0
Q = Q*a
dx = L/n
dx2 = dx**2
alpha = k/(ro*c)
den = dx * ro * c

t_final = 120000      # set to reach the steady state condition
dt = 100
len_t = int(t_final/dt)

# *******************************************
#    Vector setting function, creavect(n, val)
# *******************************************

def creavect(n, val):
    vect = []

    for i in range(0,n):
        vect.append(val)

    return (vect)

# Recall the Vector setting function to define the temperature and time vectors

T = creavect(n, T0)
```

```python
dTdt = creavect(n, 0.0)

# *******************
#    Code application
# *******************

if Run == True:

    # Set the procedure to apply the Heat Diffusion Equation

    for j in range (1,len_t):

        Ts1 = T[0]
        Ts2 = T[n-1]

        for i in range (1, n-1):
            dTdt[i] = alpha * (- (T[i] - T[i-1]) / dx2 + (T[i+1] - T[i]) / dx2)

        dTdt[1] = alpha * (- (T[1] - Ts1) / dx2 + (T[2] - T[1]) / dx2)
        dTdt[n-2] = alpha * (- (T[n-2] - T[n-3]) / dx2 + (Ts2 - T[n-2]) / dx2)

        # set boundary conditions

        dTdt[0] =(2 * alpha * (T[1] - Ts1) / dx2) + (2 * hout * (Tout - Ts1) / den) +
        (2 * Q / den)
        dTdt[n-1] = (2 * alpha * (T[n-2] - Ts2) / dx2) + (2 * hin * (Tin - Ts2) /
        den)

         for i in range(0,n):
             T[i] = T[i] + dTdt[i]*dt

    print(float(T[0]))

else:

    print("Simulation not running")
```

Application to the ground

```python
"""Inputs:
        n : number of layers (-)
        Tout : outdoor air temperature (°C)
        Tg : ground temperature at 0.5 m (°C)
        hout : outdoor convective coefficient (W/m2K)
        Q : incident radiation (W/m2)
        k : conductivity (W/mK)
        ro : density (kg/m3)
        c : specific heat capacity (j/kgK)
        a : solar absobance (-)
        Run : set Boolean to True to run the component
    Output:
        Tsup : surface temperature (°C)"""

# set the required variables

T0 = 0.0
L= 0.5
Q = Q*a
dx = L/n
```

```python
dx2 = dx**2
alpha = k/(ro*c)
den = dx * ro * c

t_final = 120000        # set to reach the steady state condition
dt = 100
len_t = int(t_final/dt)

# *********************************************
#     Vector setting function, creavect(n, val)
# *********************************************

def creavect(n, val):
    vect = []

    for i in range(0,n):
        vect.append(val)

    return (vect)

# Recall the Vector setting function to define the time vectors

T = creavect(n, T0)
dTdt = creavect(n, 0.0)

# *******************
#     Code application
# *******************

if Run == True:

    # Set the procedure to apply the Heat Diffusion Equation

    for j in range (1,len_t):

        Ts1 = T[0]

        for i in range (1, n-1):
          dTdt[i] = alpha * (- (T[i] - T[i-1]) / dx2 + (T[i+1] - T[i]) / dx2)

        dTdt[1] = alpha * (- (T[1] - Ts1) / dx2 + (T[2] - T[1]) / dx2)
        dTdt[n-2] = 2*alpha * (- (T[n-2] - T[n-3]) / dx2 + (Tg - T[n-2])
         / dx2) # boundary condition at 0.5m


        # outdoor boundary condition

        dTdt[0] =(2 * alpha * (T[1] - Ts1) / dx2) + (2 * hout * (Tout - Ts1) / den) +
        (2 * Q / den)

        for i in range(0,n):
            T[i] = T[i] + dTdt[i]*dt

    print(T[0])

else:

    print("Simulation not running")
```

UTCI

```python
"""Inputs:
        Ta : air temperature (°C)
        va : wind speed (m/s)
        RH : Relative humidity (%)
        MRT : mean radiant temperature (°C)
    Output:
        UTCI : Universal Thermal Climate Index (°C)"""

# Import libraries

import math

# ***********************************************
#    Saturation vapor pressure function, es(ta)
# ***********************************************
# Function to calculate the saturation vapour pressure over water in hPa
#
# Input parameters
# - Ta = air temperature (°C)
# ***********************************************

def es(ta):

    Tk = ta + 273.15

    g = [-2.8365744E3, -6.028076559E3, 1.954263612E1, -2.737830188E-2, 1.6261698E-5,
7.0229056E-10, -1.8680009E-13, 2.7150305]

    es = 2.7150305 * math.log(Tk)

    for i in range(0, 6):
        es = es + g[i] * Tk ** (i-2)

    es=math.exp(es)*0.01              # *0.01: convert Pa to hPa

    return es

# ***********************************************
#    UTCI function, UTCI_approx(Ta,ehPa,Tmrt,va)
# ***********************************************
# Function to calculate the UTCI in degree Celsius
#
# Input parameters
# - Ta = air temperature (°C)
# - ehPa = water vapour pressure (hPa)
# - Tmrt = mean radiant temperature (°C)
# - va = wind speed (m/s)
# ***********************************************

def UTCI_approx(Ta,RH,Tmrt,va):

        D_Tmrt = Tmrt - Ta
        Pa = ehPa / 10          # vapour pressure in kPa

        # calculate 6th order polynomial as approximation
        UTCI_calc = ( Ta + \
                ( 6.07562052E-01 )    + \
```

```
( -2.27712343E-02 ) * Ta + \
( 8.06470249E-04 ) * Ta*Ta + \
( -1.54271372E-04 ) * Ta*Ta*Ta + \
( -3.24651735E-06 ) * Ta*Ta*Ta*Ta + \
( 7.32602852E-08 ) * Ta*Ta*Ta*Ta*Ta + \
( 1.35959073E-09 ) * Ta*Ta*Ta*Ta*Ta*Ta + \
( -2.25836520E+00 ) * va + \
( 8.80326035E-02 ) * Ta*va + \
( 2.16844454E-03 ) * Ta*Ta*va + \
( -1.53347087E-05 ) * Ta*Ta*Ta*va + \
( -5.72983704E-07 ) * Ta*Ta*Ta*Ta*va + \
( -2.55090145E-09 ) * Ta*Ta*Ta*Ta*Ta*va + \
( -7.51269505E-01 ) * va*va + \
( -4.08350271E-03 ) * Ta*va*va + \
( -5.21670675E-05 ) * Ta*Ta*va*va + \
( 1.94544667E-06 ) * Ta*Ta*Ta*va*va + \
( 1.14099531E-08 ) * Ta*Ta*Ta*Ta*va*va + \
( 1.58137256E-01 ) * va*va*va + \
( -6.57263143E-05 ) * Ta*va*va*va + \
( 2.22697524E-07 ) * Ta*Ta*va*va*va + \
( -4.16117031E-08 ) * Ta*Ta*Ta*va*va*va + \
( -1.27762753E-02 ) * va*va*va*va + \
( 9.66891875E-06 ) * Ta*va*va*va*va + \
( 2.52785852E-09 ) * Ta*Ta*va*va*va*va + \
( 4.56306672E-04 ) * va*va*va*va*va + \
( -1.74202546E-07 ) * Ta*va*va*va*va*va + \
( -5.91491269E-06 ) * va*va*va*va*va*va + \
( 3.98374029E-01 ) * D_Tmrt + \
( 1.83945314E-04 ) * Ta*D_Tmrt + \
( -1.73754510E-04 ) * Ta*Ta*D_Tmrt + \
( -7.60781159E-07 ) * Ta*Ta*Ta*D_Tmrt + \
( 3.77830287E-08 ) * Ta*Ta*Ta*Ta*D_Tmrt + \
( 5.43079673E-10 ) * Ta*Ta*Ta*Ta*Ta*D_Tmrt + \
( -2.00518269E-02 ) * va*D_Tmrt + \
( 8.92859837E-04 ) * Ta*va*D_Tmrt + \
( 3.45433048E-06 ) * Ta*Ta*va*D_Tmrt + \
( -3.77925774E-07 ) * Ta*Ta*Ta*va*D_Tmrt + \
( -1.69699377E-09 ) * Ta*Ta*Ta*Ta*va*D_Tmrt + \
( 1.69992415E-04 ) * va*va*D_Tmrt + \
( -4.99204314E-05 ) * Ta*va*va*D_Tmrt + \
( 2.47417178E-07 ) * Ta*Ta*va*va*D_Tmrt + \
( 1.07596466E-08 ) * Ta*Ta*Ta*va*va*D_Tmrt + \
( 8.49242932E-05 ) * va*va*va*D_Tmrt + \
( 1.35191328E-06 ) * Ta*va*va*va*D_Tmrt + \
( -6.21531254E-09 ) * Ta*Ta*va*va*va*D_Tmrt + \
( -4.99410301E-06 ) * va*va*va*va*D_Tmrt + \
( -1.89489258E-08 ) * Ta*va*va*va*va*D_Tmrt + \
( 8.15300114E-08 ) * va*va*va*va*va*D_Tmrt + \
( 7.55043090E-04 ) * D_Tmrt*D_Tmrt + \
( -5.65095215E-05 ) * Ta*D_Tmrt*D_Tmrt + \
( -4.52166564E-07 ) * Ta*Ta*D_Tmrt*D_Tmrt + \
( 2.46688878E-08 ) * Ta*Ta*Ta*D_Tmrt*D_Tmrt + \
( 2.42674348E-10 ) * Ta*Ta*Ta*Ta*D_Tmrt*D_Tmrt + \
( 1.54547250E-04 ) * va*D_Tmrt*D_Tmrt + \
( 5.24110970E-06 ) * Ta*va*D_Tmrt*D_Tmrt + \
( -8.75874982E-08 ) * Ta*Ta*va*D_Tmrt*D_Tmrt + \
( -1.50743064E-09 ) * Ta*Ta*Ta*va*D_Tmrt*D_Tmrt + \
( -1.56236307E-05 ) * va*va*D_Tmrt*D_Tmrt + \
( -1.33895614E-07 ) * Ta*va*va*D_Tmrt*D_Tmrt + \
( 2.49709824E-09 ) * Ta*Ta*va*va*D_Tmrt*D_Tmrt + \
( 6.51711721E-07 ) * va*va*va*D_Tmrt*D_Tmrt + \
```

```
( 1.94960053E-09 ) * Ta*va*va*va*D_Tmrt*D_Tmrt + \
( -1.00361113E-08 ) * va*va*va*va*D_Tmrt*D_Tmrt + \
( -1.21206673E-05 ) * D_Tmrt*D_Tmrt*D_Tmrt + \
( -2.18203660E-07 ) * Ta*D_Tmrt*D_Tmrt*D_Tmrt + \
( 7.51269482E-09 ) * Ta*Ta*D_Tmrt*D_Tmrt*D_Tmrt + \
( 9.79063848E-11 ) * Ta*Ta*Ta*D_Tmrt*D_Tmrt*D_Tmrt + \
( 1.25006734E-06 ) * va*D_Tmrt*D_Tmrt*D_Tmrt + \
( -1.81584736E-09 ) * Ta*va*D_Tmrt*D_Tmrt*D_Tmrt + \
( -3.52197671E-10 ) * Ta*Ta*va*D_Tmrt*D_Tmrt*D_Tmrt + \
( -3.36514630E-08 ) * va*va*D_Tmrt*D_Tmrt*D_Tmrt + \
( 1.35908359E-10 ) * Ta*va*va*D_Tmrt*D_Tmrt*D_Tmrt + \
( 4.17032620E-10 ) * va*va*va*D_Tmrt*D_Tmrt*D_Tmrt + \
( -1.30369025E-09 ) * D_Tmrt*D_Tmrt*D_Tmrt*D_Tmrt + \
( 4.13908461E-10 ) * Ta*D_Tmrt*D_Tmrt*D_Tmrt*D_Tmrt + \
( 9.22652254E-12 ) * Ta*Ta*D_Tmrt*D_Tmrt*D_Tmrt*D_Tmrt + \
( -5.08220384E-09 ) * va*D_Tmrt*D_Tmrt*D_Tmrt*D_Tmrt + \
( -2.24730961E-11 ) * Ta*va*D_Tmrt*D_Tmrt*D_Tmrt*D_Tmrt + \
( 1.17139133E-10 ) * va*va*D_Tmrt*D_Tmrt*D_Tmrt*D_Tmrt + \
( 6.62154879E-10 ) * D_Tmrt*D_Tmrt*D_Tmrt*D_Tmrt*D_Tmrt + \
( 4.03863260E-13 ) * Ta*D_Tmrt*D_Tmrt*D_Tmrt*D_Tmrt*D_Tmrt + \
( 1.95087203E-12 ) * va*D_Tmrt*D_Tmrt*D_Tmrt*D_Tmrt*D_Tmrt + \
( -4.73602469E-12 ) * D_Tmrt*D_Tmrt*D_Tmrt*D_Tmrt*D_Tmrt*D_Tmrt + \
( 5.12733497E+00 ) * Pa + \
( -3.12788561E-01 ) * Ta*Pa + \
( -1.96701861E-02 ) * Ta*Ta*Pa + \
( 9.99690870E-04 ) * Ta*Ta*Ta*Pa + \
( 9.51738512E-06 ) * Ta*Ta*Ta*Ta*Pa + \
( -4.66426341E-07 ) * Ta*Ta*Ta*Ta*Ta*Pa + \
( 5.48050612E-01 ) * va*Pa + \
( -3.30552823E-03 ) * Ta*va*Pa + \
( -1.64119440E-03 ) * Ta*Ta*va*Pa + \
( -5.16670694E-06 ) * Ta*Ta*Ta*va*Pa + \
( 9.52692432E-07 ) * Ta*Ta*Ta*Ta*va*Pa + \
( -4.29223622E-02 ) * va*va*Pa + \
( 5.00845667E-03 ) * Ta*va*va*Pa + \
( 1.00601257E-06 ) * Ta*Ta*va*va*Pa + \
( -1.81748644E-06 ) * Ta*Ta*Ta*va*va*Pa + \
( -1.25813502E-03 ) * va*va*va*Pa + \
( -1.79330391E-04 ) * Ta*va*va*va*Pa + \
( 2.34994441E-06 ) * Ta*Ta*va*va*va*Pa + \
( 1.29735808E-04 ) * va*va*va*va*Pa + \
( 1.29064870E-06 ) * Ta*va*va*va*va*Pa + \
( -2.28558686E-06 ) * va*va*va*va*va*Pa + \
( -3.69476348E-02 ) * D_Tmrt*Pa + \
( 1.62325322E-03 ) * Ta*D_Tmrt*Pa + \
( -3.14279680E-05 ) * Ta*Ta*D_Tmrt*Pa + \
( 2.59835559E-06 ) * Ta*Ta*Ta*D_Tmrt*Pa + \
( -4.77136523E-08 ) * Ta*Ta*Ta*Ta*D_Tmrt*Pa + \
( 8.64203390E-03 ) * va*D_Tmrt*Pa + \
( -6.87405181E-04 ) * Ta*va*D_Tmrt*Pa + \
( -9.13863872E-06 ) * Ta*Ta*va*D_Tmrt*Pa + \
( 5.15916806E-07 ) * Ta*Ta*Ta*va*D_Tmrt*Pa + \
( -3.59217476E-05 ) * va*va*D_Tmrt*Pa + \
( 3.28696511E-05 ) * Ta*va*va*D_Tmrt*Pa + \
( -7.10542454E-07 ) * Ta*Ta*va*va*D_Tmrt*Pa + \
( -1.24382300E-05 ) * va*va*va*D_Tmrt*Pa + \
( -7.38584400E-09 ) * Ta*va*va*va*D_Tmrt*Pa + \
( 2.20609296E-07 ) * va*va*va*va*D_Tmrt*Pa + \
( -7.32469180E-04 ) * D_Tmrt*D_Tmrt*Pa + \
( -1.87381964E-05 ) * Ta*D_Tmrt*D_Tmrt*Pa + \
( 4.80925239E-06 ) * Ta*Ta*D_Tmrt*D_Tmrt*Pa + \
```

```
( -8.75492040E-08 ) * Ta*Ta*Ta*D_Tmrt*D_Tmrt*Pa + \
( 2.77862930E-05 ) * va*D_Tmrt*D_Tmrt*Pa + \
( -5.06004592E-06 ) * Ta*va*D_Tmrt*D_Tmrt*Pa + \
( 1.14325367E-07 ) * Ta*Ta*va*D_Tmrt*D_Tmrt*Pa + \
( 2.53016723E-06 ) * va*va*D_Tmrt*D_Tmrt*Pa + \
( -1.72857035E-08 ) * Ta*va*va*D_Tmrt*D_Tmrt*Pa + \
( -3.95079398E-08 ) * va*va*va*D_Tmrt*D_Tmrt*Pa + \
( -3.59413173E-07 ) * D_Tmrt*D_Tmrt*D_Tmrt*Pa + \
( 7.04388046E-07 ) * Ta*D_Tmrt*D_Tmrt*D_Tmrt*Pa + \
( -1.89309167E-08 ) * Ta*Ta*D_Tmrt*D_Tmrt*D_Tmrt*Pa + \
( -4.79768731E-07 ) * va*D_Tmrt*D_Tmrt*D_Tmrt*Pa + \
( 7.96079978E-09 ) * Ta*va*D_Tmrt*D_Tmrt*D_Tmrt*Pa + \
( 1.62897058E-09 ) * va*va*D_Tmrt*D_Tmrt*D_Tmrt*Pa + \
( 3.94367674E-08 ) * D_Tmrt*D_Tmrt*D_Tmrt*D_Tmrt*Pa + \
( -1.18566247E-09 ) * Ta*D_Tmrt*D_Tmrt*D_Tmrt*D_Tmrt*Pa + \
( 3.34678041E-10 ) * va*D_Tmrt*D_Tmrt*D_Tmrt*D_Tmrt*Pa + \
( -1.15606447E-10 ) * D_Tmrt*D_Tmrt*D_Tmrt*D_Tmrt*D_Tmrt*Pa + \
( -2.80626406E+00 ) * Pa*Pa + \
( 5.48712484E-01 ) * Ta*Pa*Pa + \
( -3.99428410E-03 ) * Ta*Ta*Pa*Pa + \
( -9.54009191E-04 ) * Ta*Ta*Ta*Pa*Pa + \
( 1.93090978E-05 ) * Ta*Ta*Ta*Ta*Pa*Pa + \
( -3.08806365E-01 ) * va*Pa*Pa + \
( 1.16952364E-02 ) * Ta*va*Pa*Pa + \
( 4.95271903E-04 ) * Ta*Ta*va*Pa*Pa + \
( -1.90710882E-05 ) * Ta*Ta*Ta*va*Pa*Pa + \
( 2.10787756E-03 ) * va*va*Pa*Pa + \
( -6.98445738E-04 ) * Ta*va*va*Pa*Pa + \
( 2.30109073E-05 ) * Ta*Ta*va*va*Pa*Pa + \
( 4.17856590E-04 ) * va*va*va*Pa*Pa + \
( -1.27043871E-05 ) * Ta*va*va*va*Pa*Pa + \
( -3.04620472E-06 ) * va*va*va*va*Pa*Pa + \
( 5.14507424E-02 ) * D_Tmrt*Pa*Pa + \
( -4.32510997E-03 ) * Ta*D_Tmrt*Pa*Pa + \
( 8.99281156E-05 ) * Ta*Ta*D_Tmrt*Pa*Pa + \
( -7.14663943E-07 ) * Ta*Ta*Ta*D_Tmrt*Pa*Pa + \
( -2.66016305E-04 ) * va*D_Tmrt*Pa*Pa + \
( 2.63789586E-04 ) * Ta*va*D_Tmrt*Pa*Pa + \
( -7.01199003E-06 ) * Ta*Ta*va*D_Tmrt*Pa*Pa + \
( -1.06823306E-04 ) * va*va*D_Tmrt*Pa*Pa + \
( 3.61341136E-06 ) * Ta*va*va*D_Tmrt*Pa*Pa + \
( 2.29748967E-07 ) * va*va*va*D_Tmrt*Pa*Pa + \
( 3.04788893E-04 ) * D_Tmrt*D_Tmrt*Pa*Pa + \
( -6.42070836E-05 ) * Ta*D_Tmrt*D_Tmrt*Pa*Pa + \
( 1.16257971E-06 ) * Ta*Ta*D_Tmrt*D_Tmrt*Pa*Pa + \
( 7.68023384E-06 ) * va*D_Tmrt*D_Tmrt*Pa*Pa + \
( -5.47446896E-07 ) * Ta*va*D_Tmrt*D_Tmrt*Pa*Pa + \
( -3.59937910E-08 ) * va*va*D_Tmrt*D_Tmrt*Pa*Pa + \
( -4.36497725E-06 ) * D_Tmrt*D_Tmrt*D_Tmrt*Pa*Pa + \
( 1.68737969E-07 ) * Ta*D_Tmrt*D_Tmrt*D_Tmrt*Pa*Pa + \
( 2.67489271E-08 ) * va*D_Tmrt*D_Tmrt*D_Tmrt*Pa*Pa + \
( 3.23926897E-09 ) * D_Tmrt*D_Tmrt*D_Tmrt*D_Tmrt*Pa*Pa + \
( -3.53874123E-02 ) * Pa*Pa*Pa + \
( -2.21201190E-01 ) * Ta*Pa*Pa*Pa + \
( 1.55126038E-02 ) * Ta*Ta*Pa*Pa*Pa + \
( -2.63917279E-04 ) * Ta*Ta*Ta*Pa*Pa*Pa + \
( 4.53433455E-02 ) * va*Pa*Pa*Pa + \
( -4.32943862E-03 ) * Ta*va*Pa*Pa*Pa + \
( 1.45389826E-04 ) * Ta*Ta*va*Pa*Pa*Pa + \
( 2.17508610E-04 ) * va*va*Pa*Pa*Pa + \
( -6.66724702E-05 ) * Ta*va*va*Pa*Pa*Pa + \
```

```python
                ( 3.33217140E-05 ) * va*va*va*Pa*Pa*Pa + \
                ( -2.26921615E-03 ) * D_Tmrt*Pa*Pa*Pa + \
                ( 3.80261982E-04 ) * Ta*D_Tmrt*Pa*Pa*Pa + \
                ( -5.45314314E-09 ) * Ta*Ta*D_Tmrt*Pa*Pa*Pa + \
                ( -7.96355448E-04 ) * va*D_Tmrt*Pa*Pa*Pa + \
                ( 2.53458034E-05 ) * Ta*va*D_Tmrt*Pa*Pa*Pa + \
                ( -6.31223658E-06 ) * va*va*D_Tmrt*Pa*Pa*Pa + \
                ( 3.02122035E-04 ) * D_Tmrt*D_Tmrt*Pa*Pa*Pa + \
                ( -4.77403547E-06 ) * Ta*D_Tmrt*D_Tmrt*Pa*Pa*Pa + \
                ( 1.73825715E-06 ) * va*D_Tmrt*D_Tmrt*Pa*Pa*Pa + \
                ( -4.09087898E-07 ) * D_Tmrt*D_Tmrt*D_Tmrt*Pa*Pa*Pa + \
                ( 6.14155345E-01 ) * Pa*Pa*Pa*Pa + \
                ( -6.16755931E-02 ) * Ta*Pa*Pa*Pa*Pa + \
                ( 1.33374846E-03 ) * Ta*Ta*Pa*Pa*Pa*Pa + \
                ( 3.55375387E-03 ) * va*Pa*Pa*Pa*Pa + \
                ( -5.13027851E-04 ) * Ta*va*Pa*Pa*Pa*Pa + \
                ( 1.02449757E-04 ) * va*va*Pa*Pa*Pa*Pa + \
                ( -1.48526421E-03 ) * D_Tmrt*Pa*Pa*Pa*Pa + \
                ( -4.11469183E-05 ) * Ta*D_Tmrt*Pa*Pa*Pa*Pa + \
                ( -6.80434415E-06 ) * va*D_Tmrt*Pa*Pa*Pa*Pa + \
                ( -9.77675906E-06 ) * D_Tmrt*D_Tmrt*Pa*Pa*Pa*Pa + \
                ( 8.82773108E-02 ) * Pa*Pa*Pa*Pa*Pa + \
                ( -3.01859306E-03 ) * Ta*Pa*Pa*Pa*Pa*Pa + \
                ( 1.04452989E-03 ) * va*Pa*Pa*Pa*Pa*Pa + \
                ( 2.47090539E-04 ) * D_Tmrt*Pa*Pa*Pa*Pa*Pa + \
                ( 1.48348065E-03 ) * Pa*Pa*Pa*Pa*Pa*Pa
                    )
        print(UTCI_calc)

# *******************
#    Check input data
# *******************

x = float(Ta)
y = float(MRT)
z = float(va)
u = float(RH)

if x >= -50 and x <= 50 :
        Ta = x
else :
        print('Ta out of range')

if y >= (Ta - 30) and y <= (Ta + 70) :
        Tmrt = y
elif y <= (Ta - 30) :
        Tmrt = (Ta - 30)
else :
        Tmrt = (Ta + 70)

if z >= 0.50 and z <= 1.7 :
        va = z
elif y <= 0.50 :
        va = 0.5
else :
        va = 1.7

if u >= 0 and u <= 100 :
    RH = u
    ehPa = es(Ta) * RH / 100        # recall Saturation vapor pressure function
else :
```

```python
        print('RH out of range')



# *******************
#    Code application
# *******************

UTCI_list= []

UTCI = UTCI_list.append(UTCI_approx(Ta,RH,Tmrt,va)) # recall UTCI function
```

BIBLIOGRAPHY

[1]   D. Dernie and J. Gaspari, "Building envelope over-cladding: Impact on energy balance and microclimate," *Buildings*, vol. 5, no. 2, pp. 715–735, 2015, doi: 10.3390/buildings5020715.

[2]   M. Perino, V. Serra, F. Zanghirella, and A. Kindinis, "Rapporto sulle attività della IEA ECBCS Annex 44," 2009.

[3]   M. C. Brito, "Assessing the impact of photovoltaics on rooftops and facades in the urban micro-climate," *Energies*, vol. 13, no. 11, 2020, doi: 10.3390/en13112717.

[4]   A. Synnefa, M. Santamouris, and K. Apostolakis, "On the development, optical properties and thermal performance of cool colored coatings for the urban environment," *Sol. Energy*, vol. 81, no. 4, pp. 488–497, 2007, doi: 10.1016/j.solener.2006.08.005.

[5]   F. Rossi, A. L. Pisello, A. Nicolini, M. Filipponi, and M. Palombo, "Analysis of retro-reflective surfaces for urban heat island mitigation: A new analytical model," *Appl. Energy*, vol. 114, pp. 621–631, 2014, doi: 10.1016/j.apenergy.2013.10.038.

[6]   S. Haddad, R. Paolini, A. Synnefa, and M. Santamouris, "Mitigation of urban overheating in three Australian cities (Darwin, Alice Springs and Western Sydney)," *Engag. Archit. Sci. Meet. Challenges High. Density*, pp. 577–584, 2018.

[7]   T. Karlessi, M. Santamouris, K. Apostolakis, A. Synnefa, and I. Livada, "Development and testing of thermochromic coatings for buildings and urban structures," *Sol. Energy*, vol. 83, no. 4, pp. 538–551, 2009, doi: 10.1016/j.solener.2008.10.005.

[8]   K. Fabbri, J. Gaspari, S. Bartoletti, and E. Antonini, "Effect of facade reflectance on outdoor microclimate: An Italian case study," *Sustain. Cities Soc.*, vol. 54, no. July 2019, 2020, doi: 10.1016/j.scs.2019.101984.

[9]   K. Mehaoued and B. Lartigue, "Influence of a reflective glass façade on surrounding microclimate and building cooling load: Case of an office building in Algiers," *Sustain. Cities Soc.*, vol. 46, no. January, 2019, doi: 10.1016/j.scs.2019.101443.

[10]   M. Taleghani, W. Swan, E. Johansson, and Y. Ji, "Urban cooling: Which façade orientation has the most impact on a microclimate?," *Sustain. Cities Soc.*, vol. 64, 2021, doi: 10.1016/j.scs.2020.102547.

[11]   J. Fox, P. Osmond, and A. Peters, "The effect of building facades on outdoor microclimate-Reflectance recovery from terrestrial multispectral images using a robust empirical line method," *Climate*, vol. 6, no. 3, 2018, doi: 10.3390/cli6030056.

[12]   K. Kalvelage, U. Passe, and M. Dorneich, "Investigating the Impact of Reflective Facades on the Microclimate," no. June, 2015, doi: 10.13140/RG.2.1.4306.1922.

[13]   G. Evola, V. Costanzo, C. Magrì, G. Margani, L. Marletta, and E. Naboni, "A novel comprehensive workflow for modelling outdoor thermal comfort and energy demand in urban canyons: Results and critical issues," *Energy Build.*, vol. 216, p. 109946, 2020, doi: 10.1016/j.enbuild.2020.109946.

[14]   S. Cohen *et al.*, "Mean radiant temperature in urban canyons from solar calculations, climate and surface properties – Theory, validation and 'Mr.T' software," *Build. Environ.*, vol. 178, no. May, p. 106927, 2020, doi: 10.1016/j.buildenv.2020.106927.

[15]   M. H. Elnabawi, N. Hamza, and S. Dudek, "Numerical modelling evaluation for the microclimate of an outdoor urban form in Cairo, Egypt," *HBRC J.*, vol. 11, no. 2, pp. 246–251, 2015, doi: 10.1016/j.hbrcj.2014.03.004.

[16]   Y. C. Chen, T. P. Lin, and A. Matzarakis, "Comparison of mean radiant temperature from field experiment and modelling: a case study in Freiburg, Germany," *Theor. Appl. Climatol.*, vol. 118, no. 3, pp. 535–551, 2014, doi: 10.1007/s00704-013-1081-z.

[17]   Y. Nishi, "Chapter 2: Measurement of Thermal Balance of Man," *Bioeng. Therm. Physiol. Comf.*, pp. 29–39, 1981.

[18]   S. Coccolo, J. Kämpf, J. L. Scartezzini, and D. Pearlmutter, "Outdoor human comfort and thermal stress: A comprehensive review on models and standards," *Urban Clim.*, vol. 18, pp. 33–57, 2016, doi: 10.1016/j.uclim.2016.08.004.

[19]   S. Thorsson, F. Lindberg, I. Eliasson, and B. Holmer, "Different methods for estimating the mean radiant temperature in an outdoor urban setting," *Int. J. Climatol.*, vol. 2029, no. March 2008, pp. 2011–2029, 2008, doi: 10.1002/joc.

[20]   R. Tarek, Z. Pouya, and C. Reinhart, "A Framework for Outdoor Mean Radiant Temperature Simulation: Towards Spatially Resolved Thermal Comfort Mapping in Urban Spaces," vol. 32, no. 3, pp. 14–21, 2017.

[21]   E. Arens, T. Hoyt, X. Zhou, L. Huang, H. Zhang, and S. Schiavon, "Modeling the comfort effects of short-wave solar radiation indoors," *Build. Environ.*, vol. 88, pp. 3–9, 2015, doi: 10.1016/j.buildenv.2014.09.004.

[22]   K. Blazejczyk, "MENEX_2005. The Updated Version of Man-Environment Heat Exchange Model," 2005, [Online]. Available: https://www.igipz.pan.pl/tl_files/igipz/ZGiK/opracowania/indywidualne/blazejczyk/MENEX_2005.pdf.

[23]   ANSI/ASHRAE, "ANSI/ASHRAE Standard 55-2017 : Thermal Environmental Conditions for Human Occupancy," *ASHRAE Inc.*, vol. 2017, p. 66, 2017.

[24]   COST Action 730, "The UNIVERSAL THERMAL CLIMATE INDEX UTCI FOR ASSESSING THE THERMAL ENVIRONMENT OF THE HUMAN BEING." [Online]. Available: www.utci.org.

[25]   M. Barbalace, F. Gugliermetti, F. Lucchese, and F. Bisegna, "Studio per la

valutazione degli effetti della luce sugli esseri umani," 2012.

[26] "Directive 2006/25/EC of the European Parliament and of the Council of 5 April 2006 on the Minimum Health and Safety Requirements regarding the Exposure of Workers to Risks Arising from Physical Agents (Artificial Optical Radiation)," 1989. https://eur-lex.europa.eu/legal-content/EN/TXT/?uri= CELEX%3A02006L0025-20140101 (accessed Jul. 07, 2020).

[27] F. Fantozzi and M. Rocca, "An extensive collection of evaluation indicators to assess occupants' health and comfort in indoor environment," *Atmosphere (Basel).*, vol. 11, no. 1, 2020, doi: 10.3390/atmos11010090.

[28] C. F. Reinhart, J. Mardaljevic, and Z. Rogers, "Dynamic daylight performance metrics for sustainable building design," *LEUKOS - J. Illum. Eng. Soc. North Am.*, vol. 3, no. 1, pp. 7–31, 2006, doi: 10.1582/LEUKOS.2006.03.01.001.

[29] A. Nabil and J. Mardaljevic, "Useful daylight illuminances: A replacement for daylight factors," *Energy Build.*, vol. 38, no. 7, pp. 905–913, 2006, doi: 10.1016/j.enbuild.2006.03.013.

[30] J. Wienold and J. Christoffersen, "Evaluation methods and development of a new glare prediction model for daylight environments with the use of CCD cameras and RADIANCE," no. September 2018, 2006, doi: 10.1016/j.enbuild.2006.03.017.

[31] A. Tsagrassoulis, Aris, Kontadakis, Antonis and Roetzel, "Comparing climate based daylight modelling with daylight factor assessment - implications for architects," *Archit. Sci. Assoc. Int. Conf. (49th 2015 Melbourne, Vic.)*, no. April 2016, pp. 1097–1106, 2015, [Online]. Available: http://dro.deakin.edu.au/view/DU:30080331.

[32] "LEED rating sistem," 2020. https://www.usgbc.org/leed (accessed Jul. 09, 2020).

[33] I. E. S. D. M. Committee, "IES Spatial Daylight Autonomy (sDA) and Annual Sunlight Exposure (ASE), Daylight Metrics Committee. Approved Method IES LM-83-12," *Illum. Eng. Soc. North Am.*, 2012.

[34] U.S. Green Building Council, "LEED v4.1 BUILDING DESIGN AND CONSTRUCTION," pp. 45–59, 2019, doi: 10.1007/978-94-009-5652-0_4.

[35] J. Hu, W. Place, and A. M. Ardakan, "Using diva for assessing climate-based leed daylight credit," *43rd ASES Natl. Sol. Conf. 2014, Sol. 2014, Incl. 39th Natl. Passiv. Sol. Conf. 2nd Meet. Young Emerg. Prof. Renew. Energy*, vol. 1, pp. 674–679, 2014.

[36] S. J. Allen, "The radiofrequency radiation dosimetry handbook: Reminiscences," *Bioelectromagnetics*, vol. 20, no. SUPPL. 4, pp. 9–11, 1999, doi: 10.1002/(SICI)1521-186X(1999)20:4+<9::AID-BEM3>3.0.CO;2-J.

[37] A. Bamba, W. Joseph, G. Vermeeren, A. Thielens, E. Tanghe, and L. Martens, "A formula for human average whole-body SARwbunder diffuse fields exposure in the GHz region," *Phys. Med. Biol.*, vol. 59, no. 23, pp. 7435–7456, 2014, doi: 10.1088/0031-9155/59/23/7435.

[38]   G. Jendritzky, G. Havenith, P. Weihs, and E. Batchvarova, "Towards a Universal Thermal Climate Index UTCI for assessing the thermal environment of the human being," *Final Rep. COST Action 730*, p. 10, 2009, [Online]. Available: http://www.utci.org/cost/documents.php.

[39]   B. Hardy, "ITS-90 FORMULATIONS FOR VAPOR PRESSURE, FROSTPOINT TEMPERATURE, DEWPOINT TEMPERATURE, AND ENHANCEMENT FACTORS IN THE RANGE −100 TO +100 C Bob Hardy," *Proc. Third Int. Symp. Humidity Moisture*, no. April, pp. 1–8, 1998.

[40]   U.S. Green Building Council, "LEED v4.1 BUILDING DESIGN AND CONSTRUCTION," 2020. doi: 10.1088/978-0-7503-3259-0ch3.

[41]   C. F. Reinhart and M. Andersen, "Development and validation of a Radiance model for a translucent panel," *Energy Build.*, vol. 38, no. 7, pp. 890–904, 2006, doi: 10.1016/j.enbuild.2006.03.006.

[42]   "Material Properties," 2021. https://www.engineeringtoolbox.com/material-properties-t_24.html (accessed Feb. 09, 2021).

[43]   S. Crone, "Radiance users manual," *Glass*, no. November, 1992.

[44]   U. Gent, S. Verbruggen, and I. S. O. S. Order, "TECHNICAL REPORT ISO / TR Energy performance of buildings — Overall energy performance assessment procedures — environmental input parameters for," vol. 2018, 2018.

[45]   G. Antonutto and A. McNeil, "Radiance Primer."

[46]   M. Pesenti, G. Masera, and F. Fiorito, "Exploration of Adaptive Origami Shading Concepts through Integrated Dynamic Simulations," *J. Archit. Eng.*, vol. 24, no. 4, Dec. 2018, doi: 10.1061/(ASCE)AE.1943-5568.0000323.

[47]   G. Lobaccaro, F. Fiorito, G. Masera, and T. Poli, "District geometry simulation: A study for the optimization of solar façades in urban canopy layers," *Energy Procedia*, vol. 30, pp. 1163–1172, 2012, doi: 10.1016/j.egypro.2012.11.129.

[48]   M. Manni *et al.*, "Development and validation of a Monte Carlo-based numerical model for solar analyses in urban canyon configurations," *Build. Environ.*, vol. 170, no. December 2019, p. 106638, 2020, doi: 10.1016/j.buildenv.2019.106638.

[49]   R. D. Judkoff *et al.*, "Standard method of test for the evaluation of building energy analysis computer programs," *ASHRAE Stand.*, vol. 8400, no. 140.2004, 2004.

[50]   R. Levinson, S. Chen, J. Slack, H. Goudey, T. Harima, and P. Berdahl, "Design, characterization, and fabrication of solar-retroreflective cool-wall materials," *Sol. Energy Mater. Sol. Cells*, vol. 206, no. July 2019, p. 110117, 2020, doi: 10.1016/j.solmat.2019.110117.